UNIVERSITÀ
DEGLI STUDI
FIRENZE

DOTTORATO DI RICERCA IN

GESTIONE SOSTENIBILE DELLE RISORSE AGRARIE FORESTALI E ALIMENTARI

Curriculum: ECONOMIA, PIANIFICAZIONE FORESTALE E SCIENZE DEL LEGNO

CICLO XXXI

COORDINATORE Prof.ssa Susanna Nocentini

LiDAR REMOTE SENSING FOR FORESTRY APPLICATIONS

Settore Scientifico Disciplinare AGR/05

Dottorando

Dott. (*Del Perugia Barbara)*

Tutore

Prof. (*Travaglini Davide)*

Coordinatore

Prof. (*Nocentini Susanna)*

Anni 2016/2018

This is for **my family**:

my parents Roberto e Lucia, my sister Olga and my husband-to-be Lorenzo

who have supported me during this journey.

Thank you for always believing in me, even when I doubt.

Thank you for allowing and for following me along my dreams.

I couldn't be luckier**.**

Table of contents

1. Abstract

LiDAR is a new approach for sustainable forest management. 3D remote sensing technologies are rapidly evolving and becoming more accurate and precise. This thesis is aimed to use LiDAR data to derive qualitative and quantitative information on forest resources useful for forest inventory applications. This thesis is a work carried out at different stages to examine the innovative uses of the LiDAR technology at a large scale (classification of species in a forest) and gradually to a more detailed scale (determination of single-tree attribute). The thesis is a collection of five papers.

A first study was carried out to assess the combination of multi-source remote sensing data (LiDAR and multispectral) data from two different ALS platform (helicopter and UAV) for the classification of main tree species in a Mediterranean forest. Two supervised classifiers were tested: Random Forest (RF) and k-NN (Paper I).

Then a study in *Pine radiata* plantation in Australia was conducted. The state-of-the-art LiDAR sensor Riegl VUX-1LR was tested by flight altitude and flight path to investigate how the accuracy on tree detection, tree height and DBH (Diameter at Breast Height) estimation is affected (Paper II).

A comparison between the Riegl VUX-1LR dataset and a below canopy UAS dataset for the estimation of diameter and tree position was also performed (Paper III).

An in-depth study about the possibility of the VUX1-LR dataset for the automatic detection of the trunk's diameter in the point cloud and the evaluation of the accuracy with two different methods (Circle fitting and Hough transform) was realized (Paper IV).

Finally, a Hand-Held Mobile Laser Scanning, the ZEB1, was tested. Five tree-level attributes were evaluated by scan path density in a Mediterranean forest (Paper V).

The new technologies and tools were tested for improving the data collection, work efficiency and quality of forest information that can be used to take sustainable forest management decisions.

Keywords: LiDAR, Remote Sensing, Airborne Laser Scanner, Terrestrial Laser Scanner, Unmanned Aerial Vehicle, Hand-held Laser Scanner, Forestry, Forestry inventories, forest management

2. Introduction

2.1 LiDAR in Forestry

In recent years, the use of LiDAR technology has grown exponentially since it has a high-precision acquisition capability of a large amount of information in small time intervals. LiDAR is the acronym for "Light Detection And Ranging", and it is the term that is used to describe the remote sensing technology which allows to determine the distance of an object or a surface using a laser pulse (active sensor). The working principle of the laser scanning system is based on the emission of a laser pulse from a platform (aerial, terrestrial or orbital) with a high repetition frequency, the return time of the laser pulses between the platform and the object is measured by the sensor and allows to estimate the distance between the sensor itself and the object (McCormick and Leavor, 2013; Michez et al., 2016).

Laser scanning technology plays an important role in forest inventory, as it allows accurate three-dimensional information capturing in a fast and environmentally-friendly way (Yang et al., 2016), and its use can produce substantial cost reductions when compared with traditional forest surveys (Hyyppä et al., 2012).

Since the first studies in the 80s, LiDAR technology was implemented on a wide variety of platforms (e.g., aerial platform, ground platform, mobile terrestrial platform, personal and handheld platform) depending on the different study objectives (mapping, resource inventory, ecological monitoring) and investigation scale (local, regional, national). A summary of the classification of laser scanning based on different platforms was presented by Liang et al. (2016), which distinguished between Airborne Laser Scanning (ALS), Terrestrial Laser Scanning (TLS), Mobile Laser Scanners (MLS) and Personal Laser Scanning (PLS). Moreover, Bosse et al. (2012) introduced the definition for the Hand-Held Mobile Laser Scanning (HMLS).

ALS has found wide use in the forest sector. ALS includes all data collected from aerial platforms, such as airplanes, helicopters, and drones. ALS consists of three complementary technologies: a laser to measure the distance to the target; an inertial navigation system (INS) or inertial measurement unit (IMU) to record the pitch, roll and yaw of the platform; and a kinematic global satellite positioning system (GPS) to record position (Wulder et al., 2012). The collected data are expressed as 3D points, characterized by spatial coordinates (X, Y and Z) that correspond to the surfaces of the objects present on the territory: vegetation, buildings and infrastructures, etc.

The first applications of LiDAR technology in the forest sector were aimed at estimating the height of the trees (Næsset, 1997a; Næsset and Økland, 2002) and then used such information as a base for the estimation of other forest variables such as wood volume (Nilsson, 1996; Næsset, 1997b; Magnussen and Boudewyn, 1998; Naesset and Gobakken, 2005; Corona and Fattorini, 2008) and biomass (van Aardt et al., 2006).

The tendency is to use ALS data as standard practice for National Forest Inventory, like in some countries in Europe (Næsset et al., 2004; Magnussen et al., 2018, Torresan et al., 2017), in Oceania (Beets et al., 2010; Watt et al., 2013 a & b), in USA (McRoberts and Tomppo, 2007) and in Asia (He et al., 2017).

ALS data alone or combined with spectral data, have been used to assess species diversity (Ozdemir and Donoghue, 2013) and species composition (Abdollahnejad et al., 2017; Cho e t al., 2012; Dalponte et al., 2013; Dechesne et al., 2017). Tree species diversity and composition are important information to study forest ecosystems, to assess forest resilience and vulnerability and to estimate the forest's economic value (Abdollahnejad et al., 2017; Nevalainen et al., 2017).

Moreover, ALS data have been use to assess the vertical stratification of forest vegetation (Zimble et al., 2003; Ferraz et al., 2012) and more recently to assess forest structural diversity (Mura et al., 2015; Valbuena et al., 2016; Bottalico et al., 2017; Teobaldelli et al., 2017), to classify silvicultural systems (Bottalico et al., 2014) and to assess forest disturbances such as windthrow damages (Chirici et al., 2017).

ALS acquisition density is usually in the range of 1 to 10 points/m^2 depending on the flight parameters (e.g., altitude, scanner configuration, etc). However, current ALS technology can collect more dense point clouds and at a more reasonable price than older sensors, in particular with light-weight LiDAR systems mounted on Small Unmanned Aerial Vehicles (UAV). For instance, Wallace et al. (2014) using the Ibeo LUX laser scanner produced point clouds with up to 50 points/m^2. Jaakkola et al. (2010) integrated an Ibeo Lux and Sick LMS151 profile scanner that produced point clouds with 100 to 1500 points/m^2. Brede et al. (2017), using the LiDAR sensor Riegl VUX-1 obtained a point density of 140 points/m^2 for a single flight line and an average plot density of ~3000 points/m^2, which was successfully used to detect single tree attributes.

The use of ALS has revolutionized the ability to collect forest inventory data over large areas. However, for accurate measurements of structural parameters and for model calibration field plots are still needed (Liang and Hyyppä, 2013; Ryding et al., 2015).

Field data can be collected with traditional instruments (e.g., calliper and hypsometer) or using new techniques based on LiDAR scanning systems (Liang et al., 2016; Giannetti et al., 2018). Terrestrial Laser Scanning (TLS) has been largely studied for detailed small-area surveys having a typical radius for a high-density scan of less than a few tens of meters. TLS is a scanning system mounted on a tripod, used in many fields, such as architecture, civil engineering, archaeology and cultural heritage, and robotics (Holopainen et al., 2013; Zlot et al., 2014).

The major advantage of using TLS in forest inventories lies in its capability to document the forest automatically and in millimeter-level detail (Liang et al., 2016). TLS three-dimensional scan can be acquired in three different way: single-scan, multi-scan and multi-single-scan (Liang et al., 2014; Michez et al., 2016). These three methods differ mainly for the reduction of shadow areas in the scan (Liang et al., 2016), while the acquisition time increase from single- to multi-scan approach. TLS has been used to assess forest inventory parameters such as DBH (Liang and Hyyppä, 2013; Kankare et al., 2015; Cabo et al., 2018), tree position (Bienert et al., 2006; Murphy et al., 2010), tree height (Giannetti et al., 2018) and to determine high-quality tree attributes that are important but are not directly measurable, such as individual-tree stem volume (Thies et al. 2004; Astrup et al., 2014). Further, the obtained data has been used for full-tree structural modelling (Raumonen et al. 2013, de Conto et al., 2017). The accuracy of DBH estimates based on TLS was demonstrated to be acceptable with RMSE within 1-2 cm, while larger errors were obtained for tree heights with RMSE in the range 0.8-6.5 m, as tree tops are usually shadowed by other trees (Liang et al., 2016; Giannetti et al., 2018).

TLS is a promising technique for forest inventory. However, TLS has not yet become an integrated part of operational procedures in forest inventories because of the time needed for data processing due to the difficulties in the automation of point cloud analysis to automatically derive tree attributes (Holopainen et al., 2013; Astrup et al., 2014).

DBH is one of the most important parameters required for forest inventory, and it is usually measured with callipers or DBH tapes at 1.30m height. Several studies have been carried out to assess DBH from TLS point clouds using different methods, such as cylindrical or circular least squares fitting methods (Hopkinson et al., 2004; Henning and Radtke, 2006; Koreň et al., 2017) and Hough transform for circle fitting (Hough, 1962; de Conto et al., 2017). However, only few studies have tested ALS point clouds for DBH estimation (Brede et al., 2017; Dalponte et al., 2018; Krisanski et al., 2018).

Laser scanning has been put on moving platforms to build Mobile Laser Scanning (MLS) system, a modification of ALS, with a laser scanner, a GPS receiver, an IMU and preferably cameras. MLS is used

for short distances (Holopainen et al., 2013) but allow to investigate larger areas compared to TLS technique (Liang et al., 2014; Ryding et al., 2015). The use of a moving platform is limited in forest ecosystems, it may not provide spatially continuous mapping and does not match with the non-destructive nature of LiDAR data acquisition (Bauwens et al., 2016). Moreover, the accuracy of MLS point clouds is usually lower than multi-scan TLS data, due to the low GNSS signal detection under forest cover (Forsman et al., 2016; Bauwens et al., 2016). That is the reason why MLS systems are currently predominant in urban mapping studies (Holopainen et al., 2013; Yang et al., 2013). To overcome the moving limitation of MLS, the Finnish Geodetic Institute created a backpack type MLS system, where the scanning and positioning systems were on the operator's back rather than on a vehicle platform (Liang et al., 2014), leading to the concept of personal laser scanning (PLS). Even if PLS allow for a rapid data collection in various terrain condition, the quality of data remain lower compared to TLS data because of the positioning error (Liang et al., 2014). This led to a new instrument introduced by Bosse et al. (2012): the ZEB1, a Hand-Held Mobile Laser Scanning that use the movement of the operator as a platform. Like PLS this system minimizes occlusion effects since the movement through the plot results in a theoretically unlimited number of scan-positions; unlike MLS, forest cover is no longer a limitation, as HMLS does not need satellite positioning (GNSS) (Bauwens et al., 2016). A first study with HMLS ZEB1 was carried out by Ryding et al. (2015). The aim of the study was to evaluate the potential of HMLS for forest surveys and the results were promising: being a faster approach on complex topography and returning a more detailed point cloud compared to TLS survey. Bauwens et al. (2016) conducted a second study to assess and compare the ZEB1-HMLS and TLS approaches for the estimation of forest parameters in a wide range of forest types, considering topography and forest structure. This study confirmed the advantages of HMLS over TLS to detect the principal forest parameters but also pointed out a limitation of the instrument for the assessment of forest height. However, only few studies have tested the ZEB 1 instrument in the Mediterranean environment (Giannetti et al., 2018) and no studies have been carried out to examine the relationships between walking scan paths and accuracy of forest variables estimations.

2.2 Objectives

This research work addresses the use of LiDAR data to derive qualitative and quantitative information on forest resources useful for forest inventory applications. The thesis aims at contributing to reduce the gap in research in LiDAR applications, such as: increasing the accuracy of tree species classification in Mediterranean forests, testing the potential of very dense ALS point clouds for single-tree attribute estimation, investigating the effects of scan density on single-tree attribute estimation by hand-held mobile laser scanning.

The thesis is a collection of five papers:

Paper I - Classification of dominant forest tree species by multi-source very high-resolution remote sensing data.

"In this study we compared the use of multispectral and point cloud based data taken from conventional (helicopter) and unconventional (UAV) remote sensing platforms to classify dominant forest tree species in Mediterranean environment. Two supervised classifiers were tested: Random Forest (RF) and k-NN. Several combinations of data sources were adopted for both helicopter and UAV data: RGB, NIR, NDVI and point cloud alone, and all data sources. The overall goal was to investigate how the combination of multi-source remote sensing data is helpful to increase the accuracy of forest tree species classification in the Mediterranean region."

Del Perugia B., Travaglini D., Barbati A., Barzagli A., Giannetti F., Lasserre B., Nocentini S., Santopuoli G., Chirici G. (2018)

Paper II - Optimal acquisition specifications for the Riegl VUX-1LR over a Pinus radiata plantation.

"In this study, the Riegl VUX-1 long range LiDAR sensor mounted on a helicopter was tested for the acquisition of very dense point clouds over a Pinus radiata plantation (Tumut, NSW – Australia). The specific objectives of the study were: (I) to investigate the effects of different flight altitudes (30m, 60m, 90m above ground level) on tree height and DBH estimation, and count of peaks; (II) to investigate the effects of different flight paths on DBH estimation. The dataset used to assess single-tree attributes was validated with field data."

Del Perugia B., Travaglini D., Chirici G., Gonzalez Aracil S. (2018)

Paper III - Below Canopy UAS Photogrammetry for Stem Measurement in a Radiata Pine Plantation.

"This paper describes the application of a UAS flown below the forest canopy as an efficient and effective approach for stem measurement in areas where the canopy is difficult to penetrate, and as a potential solution to measuring trees in areas of dense undergrowth. This study aims to investigate the accuracy of sub-canopy UAS photogrammetry relative to aerial laser scanning and manual stem measurement in terms of ability to extract the DBH and position measurements of the stems."

Krisanskia S., Del Perugia B., Sadegh Taskhiria M., Turnera P. (2018)

Paper IV - Automatic detection of diameter in an ultra-dense point cloud.

"In this study we tested the VUX-1LR database with two different methods for the estimation of DBH in the ALS point cloud. We compared the use of the software Dendrocloud, with two circle-fitting methods, and the R package TreeLS based on Hugh Transform. The estimations of the diameters were validated with field data."

Del Perugia B., Travaglini D., Chirici G., Gonzalez Aracil S. (2018)

Paper V - Influence of scan density on single-tree attributes estimation by hand-held mobile laser scanning.

"In this study, our objective was to investigate the influence of walking scan path density on single-tree attributes estimation by HMLS. The following tree-level attributes were considered: number of trees, tree position (TP), DBH, tree height (TH) and crown base height (CBH). Using a single-tree scan approach as reference data set, we compared the estimates of single-tree attributes obtained by point clouds acquired walking along straight lines drawn with two different scan line densities."

Del Perugia B., Travaglini D., Giannetti F., Chirici G. (2018)

The specific objectives of the papers are:

- to investigate how the combination of multi-source remote sensing data (LiDAR and multispectral) is helpful to increase the accuracy of the classification of dominant forest tree species in Mediterranean forests (Paper I);
- to test the optimal acquisition specifications (flight altitude and flight path) for the Riegl VUX-1LR to assess tree heights and DBH in a *Pinus radiata* plantation in Australia (Paper II);
- to assess the accuracy of below canopy UAS and ALS Riegl VUX-1LR for the estimation of diameters and tree position (Paper III);

- to test the performances of two different methodologies for the automatically detection and estimation of trunk's diameter in the ALS point cloud (Paper IV);
- to investigate the influence of walking scan path density on single-tree attributes estimation by ZEB1 HMLS (Paper V).

References

Abdollahnejad A., Panagiotidis D., Joybari S.S., Surový P. (2017) Prediction of Dominant Forest Tree Species Using QuickBird and Environmental Data. doi: 10.3390/f8020042

Astrup, R., Ducey, M.J., Granhus, A., Ritter, T., von Lüpke, N. (2014) Approaches for estimating stand-level volume using terrestrial laser scanning in a single-scan mode. Can. J. For. Res. 44, 666–676. http://dx.doi.org/10.1139/cjfr-2013-0535.

Bauwens S., Bartholomeus H., Calders K., Lejeune P. (2016) Forest Inventory with Terrestrial LiDAR: A Comparison of Static and Hand-Held Mobile Laser Scanning. Forests, 7(6), 127; doi:10.3390/f7060127

Beets P. N., Brandon A., Fraser B. V., Goulding C. J., Lane P. M., Stephens P. R. (2010) National forest inventories: New Zealand. In E. Tomppo, T. Gschwantner, M. Lawrence, & R. E. McRoberts (Eds.), National forest inventories — Pathways for common reporting (pp. 391–410) Springer.

Bienert A., Scheller S., Keane E., Mullooly G., Mohan F. (2006). Application of terrestrial laser scanners for the determination of forest inventory parameters. Int. Arch. Photogramm., Remote Sens. Spatial Inform. Sci. 36.

Bottalico F., Travaglini D., Chirici G., Marchetti M., Marchi E., Nocentini S., Corona P. (2014) Classifying silvicultural systems (coppices vs. high forests) in mediterranean oak forests by airborne laser scanning data. Eur J Remote Sens 47:437–460. doi: 10.5721/EuJRS20144725

Bottalico F., Chirici G., Giannini R., Mele S., Mura M., Puxeddu M., McRoberts R., Valbuena R., Travaglini D. (2017) Modeling Mediterranean forest structure using airborne laser scanning data International Journal of Applied Earth Observation and Geoinformation Volume 57, doi: 10.1016/j.jag.2016.12.013

Bosse M., Zlot R., Flick P. (2012) Zebedee: Design of a spring-mounted 3-d range sensor with application to mobile mapping. IEEE Trans. Robot, 28, 1104–1119.

Brede B., Lau A., Bartholomeus H., Kooistra L. (2017) Comparing RIEGL RiCOPTER UAV LiDAR Derived Canopy Height and DBH with Terrestrial LiDAR. Sensors, 17(10), p.2371.

Cabo C., Ordóñez C., López-Sánchez C., Armesto J. (2018) Automatic dendrometry: Tree detection, tree height and diameter estimation using terrestrial laser scanning. Int J Appl Earth Obs Geoinformation 69 (2018) 164–174

Chirici G., Bottalico F., Giannetti F., Rossi F., Del Perugia B., Travaglini D., Nocentini S., Kutchartt E, Marchi E., Foderi C., Fioravanti F., Fattorini L., Guariglia A., Ciancio O., Bottai L., E. McRoberts R., Næsset E., Corona P., Gozzini B. (2017) Assessing forest windthrow damage using single-date, post-event airborne laser scanning data. Forestry: An International Journal of Forest Research. https://doi.org/10.1093/forestry/cpx029

Cho M.A., Mathieu R., Asner G.P., Naidoo L., van Aardt J., Ramoelo A., Debba P., Wessels K., Main R., Smit I.P.J., Erasmus B. (2012) Mapping tree species composition in South African savannas using an integrated airborne spectral and Lidar system. Remote Sensing of Environment, 125: 214-226. doi: http://dx.doi.org/10.1016/j.rse.2012.07.010

Corona P., Fattorini L. (2008) Area-based lidar-assisted estimation of forest standing volume. Canadian Journal of Forest Research, 38(11), 2911–2916. doi:10.1139/X08-122

Dalponte M., Ørka H.O., Gobakken T., Gianelle D., Næsset E. (2013) Tree species classification in boreal forests with hyperspectral data. IEEE Trans. Geosci. Remote Sens. 51 (5), 2632–2645.

Dalponte M, Frizzera, L, Ørka, H.O, Gobakken, T, Næsset, E, Gianelle, D. (2018) Predicting stem diameters and aboveground biomass of individual trees using remote sensing data. Ecological Indicators, 85: 367-376. doi: 10.1016/j.ecolind.2017.10.066

Dechesne C., Mallet C., Le Bris A., Gouet-Brunet V. (2017) Semantic segmentation of forest stands of pure species combining airborne lidar data and very high resolution multispectral imagery ISPRS Journal of Photogrammetry and Remote Sensing 126 129–145 Doi: 10.1016/j.isprsjprs.2017.02.011

de Conto T., Olofsson k., Bastos Görgensc E., Estraviz Rodriguezd L. C., Almeidad G. (2017) Performance of stem denoising and stem modelling algorithms on single tree point clouds from terrestrial laser scanning. Computers and Electronics in Agriculture 143 165–176

Del Perugia B., Travaglini D., Barbati A., Barzagli A., Giannetti F., Lasserre B., Nocentini S., Santopuoli G., Chirici G. (2018a) Classification of dominant forest tree species by multi-source very high-resolution remote sensing data

Del Perugia B., Travaglini D., Chirici G., Gonzalez Aracil S. (2018b) Optimal acquisition specifications for the Riegl VUX-1LR over a Pinus radiata plantation.

Del Perugia B., Travaglini D., Chirici G., Gonzalez Aracil S. (2018c) Automatic detection of diameter in a ultra-dense point cloud.

Del Perugia B., Travaglini D., Giannetti F., Chirici G. (2018d) Influence of scan density on single-tree attributes estimation by hand-held mobile laser scanning

Ferraz A., Bretar F., Jacquemoud S., Gonçalves G., Pereira L., Tomé M., Soares P. (2012) 3-D mapping of a multi-layered Mediterranean forest using ALS data. Remote Sensing of Environment, 121: 210-223. doi: http://dx.doi.org/10.1016/j.rse.2012.01.020.

Forsman M., Holmgren J., Olofsson K. (2016) Tree Stem Diameter Estimation from Mobile Laser Scanning Using Line-Wise Intensity-Based Clustering Forests 7 (9), 206

Giannetti F., Puletti N., Quatrini V., Travaglini D., Bottalico F., Corona P., Chirici G. (2018) Integrating terrestrial and airborne laser scanning for the assessment of single tree attributes in Mediterranean forest stands. European Journal of Remote Sensing, 51:1, 795-807, DOI: 10.1080/22797254.2018.1482733

He Y., Song, Z., Liu Z. (2017) Updating Highway Asset Inventory Using Airborne LiDAR. Measurement. 104. 132-141. 10.1016/j.measurement.2017.03.026.

Henning J.G., Radtke P.J. (2006) Detailed stem measurements of standing trees from ground-based scanning LiDAR. For. Sci. 52, 67–80

Hyyppä J, Holopainen M, Olsson H. (2012) Laser scanning in forests. Remote Sens. 4, 2919–2922.

Holopainen M., Kankare V., Vastaranta M., Liang X., Lin Y., Vaaja M., Yub X. (2013) Tree mapping using airborne, terrestrial and mobile laser scanning – A case study in a heterogeneous urban forest. Urban Forestry & Urban Greening Volume 12, Issue 4, 2013, Pages 546–553

Hopkinson C., Chasmer L., Young-Pow C., Treitz P. (2004) Assessing forest metrics with a ground-based scanning lidar. Can. J. For. Res. 34 (3), 573–583.

Hough P.V.C. (1962) Method and means for recognizing complex patterns, U.S. Patent 3,069,654, 18 Dec 1962

Jaakkola A., Hyyppä J., Kukko A., Yu X., Kaartinen H., Lehtomäki M., Lin Y. (2010) A low-cost multi-sensoral mobile mapping system and its feasibility for tree measurements. ISPRS J. Photogramm. Remote Sens.,65, 514–522.

Kankare V., Liang X., Vastarant M., Yu X., Holopainen M., Hyyppä J. (2015) Diameter distribution estimation with laser scanning based multisource single tree inventory. ISPRS Journal of Photogrammetry and Remote Sensing Volume 108, October 2015, Pages 161-171

Krisanski S., Del Perugia B., Sadegh Taskhiria M., Turnera P. (2018) Below Canopy UAS Photogrammetry for Stem Measurement in a Radiata Pine Plantation. SPIE Remote Sensing conference in Berlin (September, 2018). Krisanski S., Del Perugia B., Sadegh Taskhiria M., Turnera P., (2018) Below-canopy UAS photogrammetry for stem measurement in radiata pine plantation. Proc. SPIE 10783, Remote Sensing for Agriculture, Ecosystems, and Hydrology XX, 1078309 (10 October 2018); doi: 10.1117/12.2325480

Koreň M., Mokroš M., Bucha T. (2017) Accuracy of tree diameter estimation from terrestrial laser scanning by circle-fitting methods. Int. J. Appl. Earth Obs. Geoinf. 63, 122–128.

Liang X., Hyyppä J. (2013) Automatic stem mapping by merging several terrestrial laser scans at the feature and decision levels. SensorS, 13, 1614–1634.

Liang X., Kukko A., Kaartinen H. (2014) Possibilities of a personal laser scanning system for forest mapping and ecosystem services. Sensors, vol. 14, pp. 1228–1248

Liang X., Kankare V., Hyyppä J., Wang Y., Kukko A., Haggrén H., Yu X., Kaartinen H., Jaakkola A., Guan F., Holopainen M., Vastaranta M. (2016) Terrestrial laser scanning in forest inventories. ISPRS Journal of Photogrammetry and Remote Sensing 115, 63–77. doi:10.1016/j.isprsjprs.2016.01.006

Magnussen S., Boudewyn P. (1998) Derivations of stand heights from airborne laser scanner data with canopy-based quantile estimators. Can. J. For. Res. 1998;28:1016-1031.

Magnussen S., Nord-Larsen T., Riis-Nielsen T. (2018) Lidar supported estimators of wood volume and aboveground biomass from the Danish national forest inventory (2012–2016). Remote Sensing of Environment 211, pp. 146–153. DOI: 10.1016/j.rse.2018.04.015

McCormick M.P., Leavor K.R. (2013) Active lidar remote sensing. In: Lenoble J., Remer L., Tanre D. (eds) Aerosol Remote Sensing. Springer, Berlin, Heidelberg

McRoberts R., Tomppo E. (2007) Remote sensing support for national forest inventories. Remote Sensing of Environment 110 (2007) 412–419.

Michez A., Bauwens S., Bonnet S., Lejeune P. (2016) Characterization of Forests with LiDAR Technology Land Surface Remote Sensing in Agriculture and Forest, 331-362

Mura M., McRoberts R.E., Chirici G., Marchetti M. (2015) Estimating and mapping forest structural diversity using airborne laser scanning data. Remote Sensing of Environment, 170: 133–142. doi:10.1016/j.rse.2015.09.016.

Murphy G.E., Acuna M.A., Dumbrell I. (2010) Tree value and log product yield determination in radiata pine (Pinus radiata) plantations in Australia: comparisons of terrestrial laser scanning with a forest inventory system and manual measurements. Can. J. For. Res. 40, 2223–2233. http://dx.doi.org/10.1139/X10-171.

Næsset E. (1997a) Determination of mean tree height of forest stands using airborne laser scanner data. ISPRS Journal of Photogrammetry and Remote Sensing 52:49-56.

Næsset E. (1997b) Estimating Timber Volume of Forest Stands Using Airborne Laser Scanner Data. Remote Sensing of Environment, 61: 246-253. doi: http://dx.doi.org/10.1016/S0034-4257(97)00041-2

Næsset E., Økland T. (2002) Estimating tree height and tree crown properties using airborne scanning laser in a boreal nature reserve, Remote Sensing of Environment, 79 (1):105– 115.

Næsset E. (2004) Practical large-scale forest stand inventory using a small-footprint airborne scanning laser. Scandinavian Journal of Forest Research, 19(2), 164-179, doi:Doi 10.1080/02827580310019257.

Næsset E., Gobakken T. (2005) Estimating forest growth using canopy metrics derived from airborne laser scanner data. Remote Sensing of Environment, 96(3-4): 453-465.

Nevalainen O., Honkavaara E., Tuominen S., Viljanen N., Hakala T., Yu X., Hyyppä J., Saari H., Pölönen I., Imai N., Tommaselli A. (2017) Individual Tree Detection and Classification with UAV-Based Photogrammetric Point Clouds and Hyperspectral Imaging. Remote sensing, 9, 185. doi: 10.3390/rs9030185

Nilsson M. (1996) Estimation of tree heights and stand volume using an airborne LiDAR system. Remote Sensing of Environment, 56: 1-7.

Ozdemir I., Donoghue D. N. M. (2013) Modelling tree size diversity from airborne laser scanning using canopy height models with image texture measures, Forest Ecology and Management, Volume 295, 1 May 2013, Pages 28-37, ISSN 0378-1127, http://dx.doi.org/10.1016/j.foreco.2012.12.044

Raumonen P., Kaasalainen M., Akerblom M., Kaasalainen S., Kaartinen H., Vastaranta M., Holopainen M., Disney M., Lewis P. (2013) Fast automatic precision tree models from terrestrial laser scanner data. Remote Sens. 5(2): 491–520. doi:10.3390/rs5020491.

Ryding J., Williams E., Smith M., Eichhorn M. (2015) Assessing handheld mobile laser scanners for forest surveys. Remote Sens. 7

Teobaldelli M., Cona F., Saulino l., Migliozzi a., D'Urso G., Manna P., Saracino A. (2017) Detection of diversity and stand parameters in Mediterranean forests using leaf-off discrete return LiDAR data Remote Sens. 192 doi:10.1016/j.rse.2017.02.008

Thies M., Pfeifer N., Winterhalder D., Gorte B.G.H. (2004) Three-dimensional reconstruction of stems for assessment of taper, sweep and lean based on laser scanning of standing trees. Scand. J. For. Res. 19(6): 571–581. doi:10.1080/02827580410019562.

Torresan C., Berton A., Carotenuto F., Di Gennaro S. F., Gioli B., Matese A., Miglietta F., Vagnoli C., Zaldei C., Wallace L. (2017) Forestry applications of UAVs in Europe: a review, International Journal of Remote Sensing, 38:8-10, 2427-2447, DOI: 10.1080/01431161.2016.1252477

Valbuena R., Eerikäinen K., Packalen P., Maltamo M. (2016) Gini coefficient predictions from airborne lidar remote sensingdisplay the effect of management intensity on forest structure. Ecological Indicators, 60:574-585.

van Aardt J.A.N., Wynne R.H., Oderwald R.G. (2006) Forest volume and biomass estimation using small-footprint lidar-distributional parameters on a per-segment basis. Forest Science, 52: 636-649.

Wallace L., Lucieer A., Watson C.S. (2014) Evaluating Tree Detection and Segmentation Routines on Very High Resolution UAV LiDAR Data. IEEE Trans. on Geoscience and Remote Sensing, 52(12).

Watt M. S., Adams T., Aracil S. G., Marshall H., Watt P. (2013a) The influence of LiDAR pulse density and plot size on the accuracy of New Zealand plantation stand volume equations. New Zealand Journal of Forestry Science, 43(1), 15.

Watt P., Watt M. S. (2013b) Development of a national model of Pinus radiata stand volume from LiDAR metrics for New Zealand. International Journal of Remote Sensing

Wulder M. A., White J. C., Nelson R. F., Næsset E., Ørka H. O., Coops N. C., Hilker T., Bater C. W., Gobakken T. (2012) Lidar sampling for large-area forest characterization: A review. Remote Sensing of Environment, 121, 196–209.

Yang B., Fang L., Li J. (2013) Semi-automated extraction and delineation of 3D roads of street scene from mobile laser scanning point clouds. ISPRS J. Photogramm. Remote Sens. 79, 80–93.

Yang B., Dai W., Dong Z., Liu Y. (2016) Automatic Forest Mapping at Individual Tree Levels from Terrestrial Laser Scanning Point Clouds with a Hierarchical Minimum Cut Method. Remote Sens. 8, 372.

Zimble D.A., Evans D.L., Carlson G.C., Parker R.C., Grado S.C., Gerard P.D. (2003) Characterizing vertical forest structure using small-footprint airborne Lidar. Remote Sensing of Environment, 87: 171-182

Zlot R., Bosse M., Greenop K., Jarzab Z., Juckes E., Roberts J. (2014) Efficiently capturing large, complex cultural heritage sites with a handheld mobile 3D laser mapping system. Journal of Cultural Heritage, 15(6), 670–678.

3. Papers

Paper I

Classification of dominant forest tree species by multi-source very high resolution remote sensing data

Del Perugia B.[1*], Travaglini D.[1], Barbati A.[2], Barzagli A.[1], Giannetti F.[1], Lasserre B.[3], Nocentini S.[1], Santopuoli G.[3], Chirici G.[1]

[1] Dipartimento di Gestione dei Sistemi Agrari, Alimentari e Forestali, Università degli Studi di Firenze, via San Bonaventura, 13 – 50145 Firenze, Italy, e-mail: barbara.delperugia@unifi.it, davide.travaglini@unifi.it, andrea.barzagli@unifi.it, francesca.giannetti@unifi.it, susanna.nocentini@unifi.it, gherardo.chirici@unifi.it

[2] Dipartimento per la Innovazione nei Sistemi Biologici, Agroalimentari e Forestali, Università degli Studi della Tuscia, via S. Camillo de Lellis – 01100 Viterbo, Italy, e-mail: barbati.sisfor@unitus.it

[3] Dipartimento di Bioscienze e Territorio, Università degli Studi del Molise, e-mail: lasserre@unimol.it, giovanni.santopuoli@unimol.it

* Corresponding author: barbara.delperugia@unifi.it

Abstract

In this study we compared the use of multispectral and point cloud based data taken from conventional (helicopter) and unconventional (UAV) remote sensing platforms to classify dominant forest tree species in Mediterranean environment. The work was carried out in the Apennine Mountain, central Italy. The study area was 275 ha large and hosted forest stands dominated by seven tree species, both coniferous and broadleaf, plus two mixed formations, for a total of nine classes. Airborne laser scanning (ALS) data with a point density of 10 pts/m^2 and multispectral data (RGB and NIR) with 20 cm spatial resolution were taken using a helicopter. Multispectral data (RGB and NIR) with 10 cm spatial resolution were also acquired using a fixed wing UAV. Structure from Motion and photogrammetric algorithms were used to obtain 3D point clouds from UAV, with a point density of 20-40 pts/m^2. We divided the study area into a grid of quadrats of side 23 m and each quadrat was assigned to a dominant forest tree species class by visual inspection of remote sensing data. For each

quadrat, helicopter and UAV's data were used to extract both multispectral features and point cloud-derived metrics. For classification purposes, the quadrats were divided into training sites (35%) and test sites (65%). Two supervised classifiers were tested: Random Forest (RF) and k-NN. Several combinations of data sources were adopted for both helicopter and UAV data: RGB, NIR, NDVI and point cloud alone, and all data sources. The accuracy of the supervised classifications was assessed against 2 increased by 29% and 50%, respectively, when helicopter instead of UAV data were used. OA and KIA increased up to 83% and 0.777, respectively, when forest categories (coniferous, broadleaf and mixed) instead of forest tree species were considered.

Keywords: indicators, tree species composition, UAV, drone, RGB, NIR, Lidar, random forest, k-NN

1. Introduction

For proper management of forest resources, reliable, up-to-date and detailed spatial information on forest structure and composition is required. Such information is also needed to quantify and monitor the European Sustainable Forest Management indicators (SFM) (Barbati et al., 2013). In addition, tree species composition is important to study forest ecosystems, to assess forest resilience and vulnerability and to estimate the forest's economic value (Abdollahnejad et al., 2017; Nevalainen et al., 2017).

Forest tree species composition is usually classified using largely subjective methods based upon ground-based visual observations by a surveyor. However, such approaches are time consuming and can suffer from a lack of consistency between surveyors.

Airborne remote sensing platforms equipped with multispectral and/or laser scanning sensors provide very high spatial resolution data useful for forest classification and for the quantification of the SFM indicators. Small Unmanned Aerial Vehicle (UAV) is a rapidly evolving technology, offering new possibilities to carry out such remote sensing tasks.

For land cover classification with remote sensing data, it is desirable to use multi-source data in order to extract as much information as possible. Remote sensing-assisted classification of tree species and land cover has been increased in the last decades, as it is prompted by a wide variety of applications from forest management, such as resource inventories (European Environmental Agency, 2007; Maselli et al., 2014) and conservation sectors, including wildlife habitat mapping, biodiversity

assessment and monitoring (Jansson and Angelstam, 1999; Corona et al., 2011; Shang and Chisholm, 2014,), but also as function of the increased availability of airborne hyperspectral and LiDAR data (Fassnacht et al., 2016).

Several studies on tree species classification were conducted in temperate forest ecosystems, followed by studies in boreal ecosystems and tropical forests (Fassnacht et al., 2016), while few studies were carried out in Savannah systems (Ludwig et al., 2016). Regarding the temperate forest ecosystem's studies, most of them were conducted in North America (USA and Canada) and in Central and Northern Europe (Chan and Paelinckx, 2008; Gislason et al., 2006; Nevalainen et al., 2017), especially in Scandinavia, while the Mediterranean forests were less investigated (Rodriguez-Galiano et al., 2012; Puletti et al., 2016).

Most studies used multispectral and hyperspectral data (Chan and Paelinckx, 2008; Fassnacht et al., 2016; Dechesne et al., 2017; Nevalainen et al., 2017), which range from moderate spatial resolution like Landsat and Hyperion satellites (Gislason et al., 2006; Rodriguez-Galiano et al., 2012; Puletti et al., 2016), to high and very-high spatial resolution systems, like IKONOS, Google-Earth images and airborne sensors (Ludwig et al., 2016; Fu et al., 2017). Several studies combined more sensors type (Dalponte et al., 2014; Pelletier, 2016), like an active system (LiDAR) with a passive optical system (airborne multispectral and hyperspectral systems); in addition, some studies investigated the combination of multiple data sources, for example auxiliary (environmental) data for prediction of tree species (Gislason et al., 2006; Abdollahneiad et al., 2017). UAV platforms have been used for mapping forest categories such as coniferous and broadleaf forests (Fassnacht et al., 2016). However, only a few studies made use of UAV to classify forest tree species (Nevalainen et al., 2017), and to the best of the authors' knowledge the classification of forest tree species in Mediterranean forests using data from UAVs has not yet been studied.

For multi-source data a convenient multivariate statistical model is in general not available, thus the conventional parametric statistical techniques that have been successfully used in remote sensing data analysis are not appropriate (Gislason et al., 2006). Supervised classifiers are widely used since they are more robust than model-based approaches (Niemeyer et al., 2014). These classifiers are able to learn the characteristics of target classes from training samples and to identify these learned characteristics in the unclassified data (Belgiu et Dra, 2016). The Random Forest (RF) classifier is a reliable classification that uses predictions derived from an ensemble of decision trees (Breiman, 2001), while the k-Nearest Neighborn (k-NN) method is one of the simplest and most popular data-

mining algorithms for classification and regression based on multidimensional distance search (Hudak et al., 2007; McRoberts, 2009).

Remote sensing-assisted classification of forest tree species is a field of research widely explored, with different types of sensor data, more or less accessible by local forest managers. Indeed, UAV's flight with multispectral sensor can be an easier available data source, that has a lower cost compared to the purchase of remote sensing images or airborne/helicopter flight.

Since UAV applications in Mediterranean environments have been less investigated for forest classification purposes, the objective of this study is to compare the use of very high spatial resolution multispectral images and point cloud data acquired by conventional and unconventional remote sensing platforms to classify dominant forest tree species in Mediterranean forests using two classifiers: RF and k-NN. The overall goal is to investigate how the combination of multi-source remote sensing data (i.e., spectral data and point clouds) is helpful to increase the accuracy of forest tree species classification in the Mediterranean region.

2. Materials and method

2.1. Study area

The work was carried out in Central Italy (Tuscany Region), in the public forest district of Rincine, about 40 km east from the city of Florence. The area is dominated by lithotypes belonging to the group of the Macigno (Miocene inf. - Oligocene). The morphology is gentle and uneven, with poorly carved valleys, and almost 50% of the surface is in the slope class 30-50%. The climate is characterized by Mediterranean-type rainfall and can be referred to humid (B1) region sensu Thornthwaite. Data recorded by Consuma (1040 m a.s.l.) meteorological station show a monthly rainfall distribution with a maximum in November (163 mm) and a minimum in July (58 mm). The average annual temperature is 9.2 °C; the hottest months are July and August (17.8 °C), the coldest month is January (1.5 °C). The Apennine deciduous montane forest is a temperate broadleaf and mixed forests biome. The district of Rincine is characterized by extensive broadleaf forests (47%) dominated by sweet chestnut, European beech and deciduous Quercus ssp. (eg., downy oak and turkey oak); where the stands are not pure, there are broadleaf mixed forests composed mainly by Fraxinus ssp., Carpinus ssp., Ostrya ssp., Alnus ssp. and Acer ssp.; 36% of the forest district is covered by coniferous species introduced

for reforestation purposes: black pine and Douglas fir. Non-forest area is covered by agricultural crops and pastures.

The study area extends over 275 ha (Figure 1). Elevation ranges between 520 m and 890 m a.s.l. The forest cover of the Apennine Mountain can be very complex and challenging to classify. Relief complexity and high anthropogenic influence results in a very heterogeneous forest landscape, which makes it possible that seven dominant forest tree species plus two mixed classes can be distinguished in the study area.

A summary of the extensions of the main forest species in the area is given in Table 1.

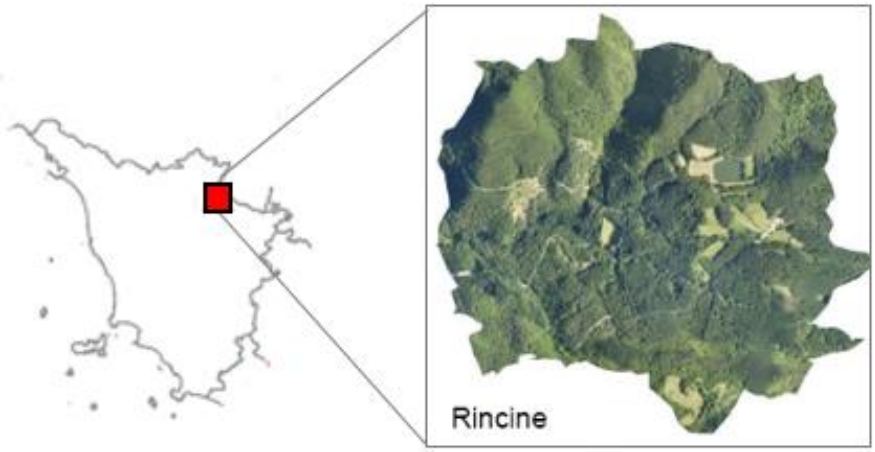

Figure 1. Location of the study area.

Species	Hectares
Douglas fir	73.7
Broadleaf mixed forest	54.8
Turkey oak	44.3
Black pine	40.8
Sweet chestnut	29.4
Downy oak	5.2
European beech	2.7
European alder	2.2
Non-forest	22.1
Total	275.2

Table 1. Area (in hectares) of main forest species.

2.2. Data

2.2.1. Remotely sensed data from helicopter

Between the 4th and 8th of May 2015 a flight was carried out by GEOCART society using an Eurocopter AS350 B3 equipped with a Riegl LMS-Q680i laser scanner and a Digicam H39 red, green, blue (RGB) and near infrared (NIR) optical instrument.

A full-waveform airborne laser scanner (ALS) data was registered and discretized to a point density of 10 pts/m^2 (the emission was of 4.4 pulse for m^2). The maximum laser scanning angle was 60° resulting in an average SWAT of 1100 m, the pulse frequency was 300 kHz with 80 lines per second and 2500 lines per line. The wavelength used was 1550 nm. Standard pre-processing with LAStools software was used to remove noise in the ALS data and echoes were classified as ground/non-ground. From this data, a Digital Terrain Model (DTM) with a spatial resolution of 1m was produced. The DTM was used to normalize the heights of non-ground points in order to convert heights above sea level into relative heights above the ground.

Digital orthophotos with 20cm spatial resolution were taken with a pair of cameras, an RGB camera which works in the blue (400-540 nm), green (480-600 nm) and red (580-600 nm) wavelengths, and a color infrared (CIR) camera which works in the green (500-620 nm), red (580-800 nm) and NIR (800-1000 nm) wavelengths. From the digital orthophotos, the Normalized Difference Vegetation Index (NDVI) with a spatial resolution of 20cm was obtained using the red and NIR bands.

The flight parameters are summarized in Table 2.

Platform	Helicopter		UAV	
Camera	Digicam RGB	Digicam CIR	Sony WX RGB	Canon S110 NIR
Flight altitude above ground level (m)	1100	1100	145	145
Red (nm)	580-600	580-800	660	625
Green (nm)	480-600	500-620	520	550
Blue (nm)	400-540	-	450	-
NIR (nm)	-	800-1000	-	850
Overlap (%)	60	60	80	90
Sidelap (%)	30	30	75	85
Image dimension	7216 × 5412	7216 × 5412	4608 × 3456	4000 × 3000
Estimated ground sampling distance (m)	0.150	0.150	0.050	0.042

Table 2. Parameters used during the helicopter and UAV acquisitions with different cameras.

2.2.2. Remotely sensed data from unmanned aerial veichle

We used the fixed wing UAV eBee by senseFly to collect multispectral data over the study area. A flight campaign was performed in 2016 between July 26th and July 29th.

eBee is a fully autonomous UAV to capture high-resolution aerial photos that can be transformed into accurate orthomosaics and 3D models. eBee is equipped with multispectral sensors and a Global Navigation Satellite System (GNSS) to provide rough positioning.

In this study we used two types of sensors: a Canon S110 NIR camera and a Sony WX RGB camera as the payload. The Canon S110 NIR takes pictures of 12.1 megapixel in the green (550 nm), red (625 nm), and NIR (850 nm) wavelengths, while the Sony WX RGB takes pictures of 18.2 megapixel in the blue (450 nm), green (520 nm) and red (660 nm) wavelengths. Software eMotion 2 version 2.4.2 was used to simulate, to plan and to monitor the flights. The flight parameters we used are summarized in Table 2.

To cover all the study area, 4 RGB (506 images) and 5 NIR (682 images) flights were carried out, respectively. Before the flights, 12 Ground Control Points (GCPs: 50×50 cm targets with a black and white checkerboard pattern) were placed on the ground in open spaces and distributed throughout the study area. The x,y coordinates of each GCP was collected using a Trimble Geo 7X receiver, data collection lasted for approximately 15 min for each target with a 2-sec logging rate. The recorded coordinates were post-processed using Pathfinder software with correction data from the nearest ground base station, with a positional standard deviations for northing, easting, and height of 0.7 cm, 0.5 cm, and 1.4 cm, respectively. For each camera, the blocks of images were pre-processed using the Agisoft PhotoScan software to create a 3D point cloud. Agisoft Photoscan combines Structure from Motion (SfM) and photogrammetric algorithms for 3D reconstruction from unorder but overlapping imagery (Agisoft LLC, 2017). GCPs were used to improve the estimates of the camera position and orientation, allowing for more accurate model reconstruction. After the optimization of the camera position a dense 3D point cloud and a DSM were computed by Agisoft Photoscan. The DSM was then used to orthorectify the UAV images. The results of the images pre-processing produced two dense 3D point clouds (RGB and NIR) with a point density ranging between 20 and 40 pts/m^2, two DSMs with a 50 cm spatial resolution and two ortophotos (RGB and NIR) with a 10 cm spatial resolution. From the digital orthophotos, the NDVI was calculated using the red and NIR bands with a spatial resolution of 10 cm. The ALS-derived DTM was used to normalize the UAV photogrammetric point clouds.

2.2.3. Auxiliary data

Auxiliary data on forest tree species composition were obtained by categorical map and forest inventory plots. In particular, a forest types map (scale 1: 10,000) in vector data format enclosed to the forest management plan of the forest district of Rincine was acquired. This map was created by ground observation and visual inspection of aerial images taken in 2005 (DREAM, 2005). A local forest inventory was carried out in the study area between June and November 2016. A sample of 50 inventory plots was selected using the one per stratum stratified sampling scheme (Fattorini et al., 2015). To do this, the study area was divided into a grid of quadrats of side 23 m, corresponding to the size of the inventory plots (529 m^2). The study area was partitioned into 50 strata of the same size, and one sample plot (i.e., one quadrat) was independently and uniformly selected in each stratum. In each plot, all trees with diameter at breast height > 2.5 cm were inventoried. For each tree the species was noted and the diameter was measured in the field using a calliper. The x,y coordinates of the plot centre were collected using the Trimble Juno 3B receiver with a positional error of 2-5 m.

2.3. Classification of dominant forest tree species

We used the grid of quadrats of the forest inventory sampling scheme as spatial reference for the classification of the forest tree species. Thus, our minimum mapping unit corresponded to a quadrat of side 23 m. Each quadrat of the grid was classified into forest and non-forest by visual inspection of the digital orthophotos taken from helicopter. Non-forest quadrats were excluded from the analysis. The remaining 4800 quadrats were used as reference for classification.

A two levels hierarchical classification system was adopted. The first level (Level 1) refers to the classification of dominant forest tree species and consists of nine classes, seven pure and two mixed classes; the second level (Level 2) refers to the classification of forest categories and consists of three classes, two pure and one mixed class (Table 3).

Code	Species/category	Level 1 9 classes	Level 2 3 classes
1	Sweet chestnut	X	
2	Turkey oak	X	
3	Douglas fir	X	
4	European beech	X	
5	Coniferous and broadleaf mixed forest	X	X
6	Broadleaf mixed forest	X	
7	European alder	X	
8	Black pine	X	
9	Downy oak	X	
10	Coniferous		X
11	Broadleaf		X

Table 3. Two levels hierarchical classification system.

2.3.1. Classification by photointerpretation

Each quadrat of the forest inventory grid was classified into one class of Level 1 and Level 2 of the hierarchical classification system by visual inspection of digital orthophotos taken from helicopter and UAV, using the forest types map as auxiliary information. Mixed classes were considered when individual species did not account for at least 75% of crown cover.

2.3.2. Classification by semiautomatic methods

The semiautomatic classification was carried out using the multi-source very high resolution remote sensing data acquired by multiple platforms. For each quadrat, helicopter and UAV's remote sensing data were used to extract both multispectral features and point cloud-derived metrics. QGIS software vers. 2.14.13 (http://www.qgis.org/) was used to extract multispectral features from RGB, NIR and NDVI images. LAStool (https://rapidlasso.com/lastools/) and R 3.4.1 statistical software (https://www.r-project.org/) were used to compute point cloud-derived metrics from the helicopter's Lidar point cloud and the UAV's photogrammetric point cloud. Specifically, for each quadrat 10 multispectral features (e.g., min, max, mean, standard deviation) were extracted from each RGB, NIR and NDVI image, and 57 metrics (e.g., percentiles, textural and density metrics) were computed from the Lidar and the UAV photogrammetric point clouds. A total of 107 variables were extracted from each platform. The list of multispectral features and point cloud-derived metrics

extracted from the helicopter and UAV's data is reported in Table 4. Several combinations of data sources were tested for both helicopter and UAV data: RGB, NIR, NDVI and point cloud alone, and all data sources.

For classification purposes, the quadrats were divided into training sites and test sites with the following percentage breakdown: 35% training and 65% test (Table 5). Two supervised classifiers were tested: RF and k-NN.

Plataform	Data source	N bands	Variables	Tot
Helicopter	RGB	3	Sum, mean, median, sd, min, max, range, minority, majority, variety (count of distinct)	30
	NIR	1	Sum, mean, median, sd, min, max, range, minority, majority, variety (count of distinct)	10
	NDVI	1	Sum, mean, median, sd, min, max, range, minority, majority, variety (count of distinct)	10
	Point cloud	-	Textural metrics (Mean and Sd of "mean", "variance", "homogeneity", "contrast", "dissimilarity", "entropy", "second_moment" of dsm pixel), density of pixel point (10-90), z_standard, intensity_standard, all, sum, mean, min, max, sd, skewness, kurtosis, p01, p05, p10, p20, p25, p30, p40, p50, p60, p70, p75, p80, p90, p95, p99, b10, b20, b30, b30, b40, b50, b60, b70, b80, b90	57
	All data		All variables listed above	107
UAV	RGB	3	Sum, mean, median, sd, min, max, range, minority, majority, variety (count of distinct)	30
	NIR	1	Sum, mean, median, sd, min, max, range, minority, majority, variety (count of distinct)	10
	NDVI	1	Sum, mean, median, sd, min, max, range, minority, majority, variety (count of distinct)	10
	Point cloud	-	Textural metrics (Mean and Sd of "mean", "variance", "homogeneity", "contrast", "dissimilarity", "entropy", "second_moment" of dsm pixel), density of pixel point (10-90), z_standard, intensity_standard, all, sum, mean, min, max, sd, skewness, kurtosis, p01, p05, p10, p20, p25, p30, p40, p50, p60, p70, p75, p80, p90, p95, p99, b10, b20, b30, b30, b40, b50, b60, b70, b80, b90	57
	All data		All variables listed above	107

Table 4. List of variables extracted from helicopter and UAV data.

Species	Leve 1 9 classes			Level 2 3 classes		
Code	Quadrats	Training	Test	Quadrats	Training	Test
	Num.	%	%	Num.	%	%
1	464	37	63	-	-	-
2	575	44	56	-	-	-
3	1239	33	67	-	-	-
4	48	40	60	-	-	-
5	306	29	71	306	29	71
6	1290	31	69	-	-	-
7	43	47	53	-	-	-
8	789	39	61	-	-	-
9	46	39	61	-	-	-
10	-	-	-	2028	35	65
11	-	-	-	2466	36	64
Total	4800	35	65	4800	35	65

Table 5. Percentage of training sites and test sites divided by level. Code represent the species (see Table 3) and for each level are report the number of cell (Cell N) classify by species.

2.3.2.1. Random forest

RF is a learning method that combines *K* binary CART trees (Classification And Regression Trees) to make a prediction (Breiman, 2001). The trees are created by using a subset of training samples obtained from bootstrapping (an equiprobable selection technique with replacement) (Belgiu et Dra, 2016). Each tree is built by performing an individual learning algorithm that splits the input variable set into subsets based on an attribute value test (for instance, the Gini coefficient) (Pelletier et al., 2016). An internal cross-validation technique of the samples which are used to train the trees is performed. The error for estimating how well the RF model performs is known as the out-of-bag (OOB) error (Breiman, 2001). RF is a suitable tool to handle the amount of data provided by the Lidar and multispectral images.

There are many commercial and open source implementations for RF model development; in this study we used the *randomForest package* within the statistical software R 3.4.1. (Rodriguez-Galiano

et al., 2012; Ghosha et al., 2014; Belgiu et Dra, 2016; Nevalainen et al., 2017). RF trees are built without pruning by randomly selecting at each node a subset of input variables (parameter denoted by m or mtry). The computational complexity of the algorithm is reduced by restraining *m*, and the correlation between the trees decreases. In this way the classification result is less variable and more reliable (Pelletier et al., 2016). Another parameter that needs to be set in order to produce the forest trees is *ntree*, the number of decision trees to be generated. Some authors have highlighted that the classification accuracy is less sensitive to *ntree* than to the *m* parameter (Kulkarni et al., 2012; Ghosh et al., 2014). Because previous studies suggested to set *m* to the square root of the number of input variables (Liaw and Wiener, 2002; Gislason et al., 2006), we decided to verify this with some tests using the *randomForest package* and the *e1071 package*, which is used for setting the best parameter of RF based on the tune method. The results of such control confirmed that the optimal parameters for our study was $m = \sqrt{p}$, where *p* is the number of input variables considered. *Ntree* was set to 500 since the errors stabilized before this number of classification trees was achieved. Since RF is robust to non-informative variables (Ludwig et al., 2016) no further feature selection was needed. We used the following parameterization for the RF model: *m* = 12, *ntree* = 500.

2.3.2.2. k-Nearest Neighbour

The k-NN algorithm present in the *caret package* was used. Given a quadrat to be classified, k-NN identifies the most similar k quadrats in the multidimensional space with *n* variables and assigns the quadrat to be classified the most frequent class among the most similar k. The *caret package* uses the resampling procedure across tuning parameters to choose the optimal value of k. According to McRoberts (2009), a value of k ranging between 1 and 20 is the best option for using the k-NN algorithm. In our study, the optimal k value for k-NN algorithm was k = 5 using helicopter data and k = 9 using UAV data.

2.3.3. Accuracy assessment

The accuracy of the classification by photointerpretation was assessed using the forest inventory plots (50 quadrats) as ground truth. To do this, each plot was assigned to one class of the hierarchical classification system on the bases of the dominant tree species at plot level, identified using the relative basal area proportion out of total plot basal area. Mixed classes were considered when individual species did not account for at least 75% of relative basal area proportion. The accuracy of

the classification by semiautomatic methods (RF and k-NN) was assessed using the test sites as ground truth.

We used four indices to assess the accuracy of the classification: overall accuracy (OA), producer's accuracy (PA), user's accuracy (UA) and kappa index of agreement (KIA). OA quantifies the percentage of quadrats classified correctly according to ground truth. PA quantifies how accurate the map is from the perspective of the producer; i.e. a given map class PA quantifies the percentage of quadrats that are labelled correctly on the map. UA classifies how accurate the map is from the perspective the user; i.e. number of quadrats correctly identified in a given map class out of the number of ground truth assigned to that map class. KIA reflects the difference between actual agreement and the agreement expected by chance: KIA = (OA-c)/(1-c), where c is the overall probability of random agreement.

3. Results

The OA of the classification by photointerpretation was 92% for dominant forest tree species and 96% for forest categories.

The OA and KIA of the classification by RF and k-NN are presented in Table 6. The RF algorithm had a slightly higher performance compared to k-NN algorithm for classification of both dominant forest tree species (Level 1) and forest categories (Level 2).

Helicopter								
	Level 1 9 classes				Level 2 3 classes			
	RF		k-NN		RF		k-NN	
	OA (%)	KIA	OA (%)	KIA	OA (%)	KIA	OA (%)	KIA
All data	70.5	0.628	67.3	0.589	83.4	0.777	82.3	0.732
RGB	64.7	0.553	60.4	0.488	82.2	0.673	80.3	0.608
NIR	46.7	0.318	44.1	0.286	73.6	0.504	72.5	0.445
NDVI	43.8	0.281	42.1	0.264	68.0	0.381	67.1	0.346
Point cloud	62.5	0.523	58.5	0.472	78.5	0.652	77.5	0.600
UAV								
	Level 1 9 classes				Level 2 3 classes			
	RF		k-NN		RF		k-NN	
	OA (%)	KIA	OA (%)	KIA	OA (%)	KIA	OA (%)	KIA
All data	54.7	0.419	50.0	0.376	72.6	0.561	72.0	0.479
RGB	46.0	0.303	39.9	0.233	69.1	0.473	64.5	0.255
NIR	37.7	0.207	37.7	0.207	66.4	0.350	66.7	0.269
NDVI	31.9	0.125	29.6	0.102	58.1	0.163	57.3	0.140
Point cloud	47.4	0.329	45.8	0.316	66.1	0.275	66.9	0.406

Table 6. Overall accuracy (OA) and Kappa Index of Agreement (KIA) of the classification by thematic level and by data sources (helicopter and UAV).

Using source variable individually for classification of dominant forest tree species by RF, the OA ranges between 43.8% and 64.7% using data from helicopter and between 31.9% and 47.4% using data from UAV. RGB images were the best data source among the variables taken by helicopter, while point cloud was the best data source among the variables taken by UAV. The best OA was obtained by RF using all multi-source variables taken by helicopter, OA = 70.5%.

As expected, the accuracy of the classification increased when forest categories where considered. Using source variable individually by RF, the OA ranges between 68% and 82.2% using data from helicopter and between 58.1% and 69.1% using data from UAV. RGB images were the best data

sources. The best OA for classification of forest categories was obtained again by RF using all multi-source variables taken by helicopter, OA = 83.4%.

Table 7 shows producer's accuracy (PA) and user's accuracy (UA) of the best classification obtained by RF algorithm. For dominant forest tree species, the UA was > 70% for five out of nine species: turkey oak, Douglas fir, European alder, Black pine and Downy oak. The worst result was for Coniferous and broadleaf mixed forest class. PA was > 70% for Douglas fir, Black pine and the Broadleaf mixed forest class. Regarding the forest categories classification, UA and PA were greater than 70% for pure classes of Coniferous and Broadleaf.

Level 1 **9 classes**									
Code	1	2	3	4	5	6	7	8	9
UA (%)	62.4	89.2	93.9	40.0	32.8	64.6	100.0	82.0	100.0
PA (%)	64.9	51.1	70.7	6.9	55.8	85.2	26.1	75.1	14.3
Level 2 **3 classes**									
Code	5	10	11						
UA (%)	31.5	91.9	87.2						
PA (%)	44.2	75.7	95.1						

Table 7. User's accuracy (UA) and producer's accuracy (PA) by RF classification using multi-source data from helicopter. For species codes see Table 3.

Figure 2 shows the spatially explicit distribution of the dominant forest tree species in the study area obtained with RF algorithm using multi-source data from helicopter.

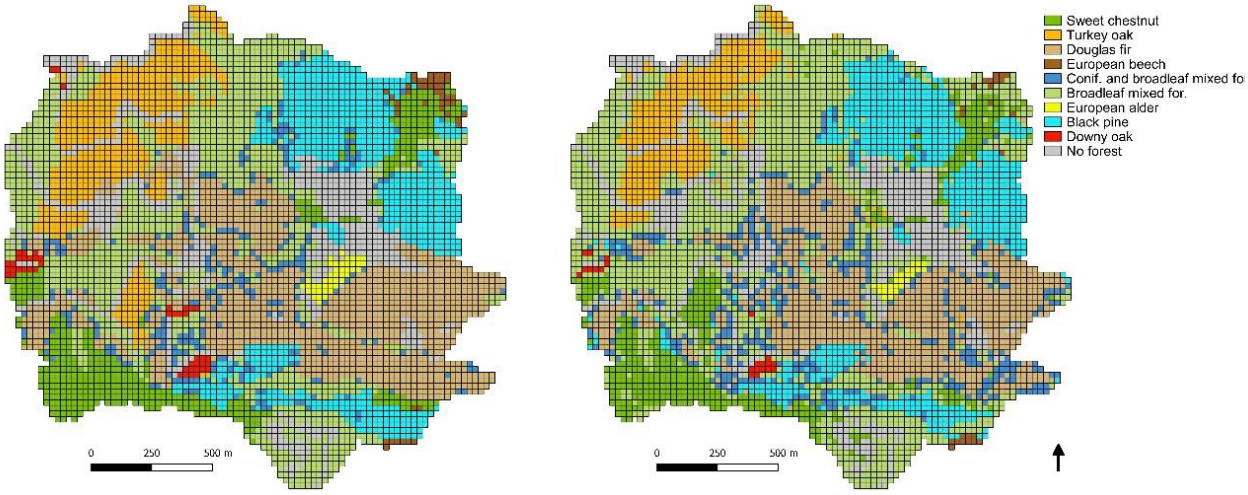

(a) (b)

Figure 2. Spatial distribution of dominant forest tree species by photointerpretation (a) and by classification with Random Forest algorithm using multi-source data from helicopter (b).

4. Discussion

We classified the forest composition according to the dominant forest tree species in a Mediterranean study area characterized by a high species diversity comparing two classifiers, RF and k-NN, and the use of multispectral and point cloud data acquired by two platforms, UAV and helicopter.

In our study, the most depending variables were the group of RGB for the helicopter data and the photogrammetric point cloud group for UAV data. However, our results confirm that the combination of multi-source remote sensing data is helpful to increase the accuracy of the classification. When multispectral variables were combined with point cloud-based metrics for the classification of dominant forest tree species the OA increased by 9% using data from helicopter and by 15% using data from UAV.

The best OA for the classification of nine dominant forest tree species was 71% using the RF algorithm and the data acquired by helicopter. The results reported by other authors for tree species classification in boreal forests are higher than those we obtained in the Mediterranean environment, where the number of species to be classified is usually higher. Nevalainen et al. (2017) in Finland used UAV-based photogrammetry and hyperspectral imaging to classify four tree species in boreal forests

with RF algorithm, achieving an OA = 95%. Alonzo et al. (2018) in an Alaskan boreal forest used structural and spectra (RGB) data from a UAV point cloud to identify canopy-dominant forest species at the individual crown scale of four tree species and one shrub class with 85% accuracy using a canonical discriminant classifier. However, our results are similar to those of other authors who have attempted to classify more plant species. Dechesne et al. (2017) in France, lead a study on segmentation and classification of forest stands of pure species combining airborne lidar data and very high resolution multispectral imagery; the OA of the RF classification-based map created with object-based was 73% in a study area with six vegetation types (mainly tree species). Abdollahnejad et al. (2017) in Iran predicted seven dominant forest tree species using very high resolution multispectral satellite images and environmental data with 64% accuracy using RF algorithm. Komárek et al. (2018), in an arboretum in Czech Republic for the classification of fifteen plant species reached a OA = 69% using Support Vector Machine algorithm with object-based classification and visible (i.e. RGB), multispectral, and thermal data acquired by UAV.

For the classification of three forest categories the best result was obtained using multi-source data from helicopter with RF, which gave 83% overall accuracies. Puletti et al. (2016) in the Apennines mountain used RF to classify coniferous and broadleaf with hyperspectral images from Hyperion satellite obtaining an OA of 94%.

The relatively poor performances of the data provided by the UAV compared to the data acquired by helicopter are probably due to the acquisition period, early May for the helicopter and end of July for UAV. In our study area the disparity in forest tree phenology is at the maximum during early spring and late autumn. Lisein et al. (2015) found that the end of leaf flushing was the most efficient single-date time window to achieve an optimal species discrimination. Therefore, multispectral information provided by helicopter allowed us a better discrimination between dominant forest species compared to multispectral data provided by UAV (Figure 3).

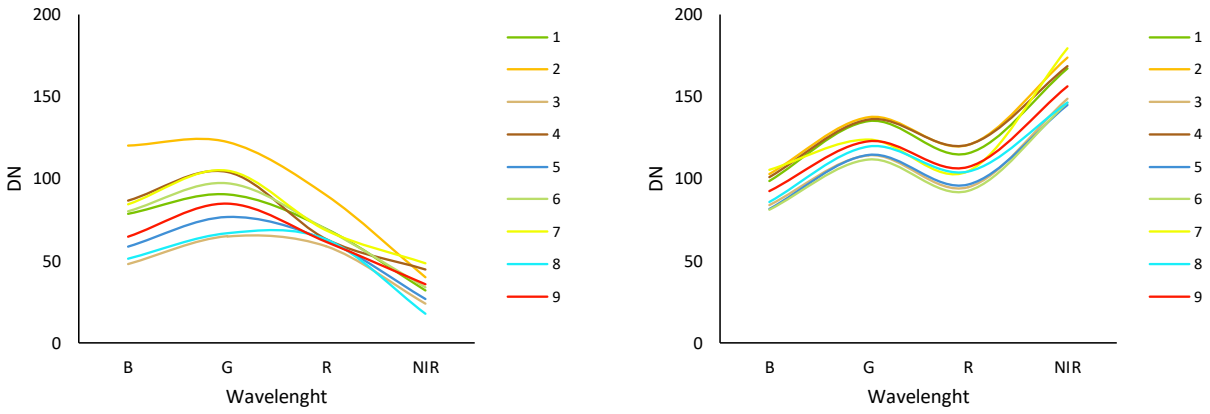

(a) (b)

Figure 3. Spectral signatures of dominant forest tree species in the visible and NIR wavelengths captured by helicopter on May 2015 (a) and by UAV on July 2016 (b). For species codes see Table 3.

5. Conclusions

This study proves the contribution of very high spatial resolution multispectral images and point cloud data for classification of dominant forest tree species in Mediterranean environment. The combination of spectral features with height, textural and density metrics increase classification accuracy when compared to spectral data only. The Random Forest algorithm provided slightly higher performances compared to k-NN algorithm for classification of forest tree species. The best overall accuracy was achieved with Random Forest by combining multispectral information and point cloud data acquired by helicopter. The multi-source data taken by UAVs were less effective for classification compared to helicopter data, as UAV flights were performed in a time window not optimal for species discrimination. Nevertheless, UAV technology provides detailed information for forestry purposes, with costs of acquisition lower than conventional platforms making multitemporal surveys largely affordable. Further researches are needed to investigate if the use of UAV multitemporal imagery can contribute to improve the accuracy of classification of dominant tree species in Mediterranean forests.

Acknowledgments

Work carried out under the FRESh LIFE14 ENV/IT/000414 project: “Demonstrating Remote Sensing integration in sustainable forest management”.

References

Abdollahnejad A., Panagiotidis D., Joybari S. S., Surový P. (2017) Prediction of Dominant Forest Tree Species Using QuickBird and Environmental Data. doi: 10.3390/f8020042

Alonzo M., Andersen H. E., Morton D. C., Cook B. D. (2018) Quantifying Boreal Forest Structure and Composition Using UAV Structure from Motion. Forests, 9, 119. doi: 10.3390/f9030119.

Barbati A., Marchetti M., Chirici G., Corona P. (2013) Forest Ecology and Management European Forest Types and Forest Europe SFM indicators : Tools for monitoring progress on forest biodiversity conservation. For Ecol Manage. doi: 10.1016/j.foreco.2013.07.004

Belgiu M., Dra L. (2016) ISPRS Journal of Photogrammetry and Remote Sensing Random forest in remote sensing: A review of applications and future directions ˇ gut. 114:24–31. doi: 10.1016/j.isprsjprs.2016.01.011

Breiman L. E. O. (2001) Random Forests. Machine Learning, 45, 5–32.

Corona P., Chirici G., McRoberts R., Winter S., Barbati A. (2011) Contribution of large-scale forest inventories to biodiversity assessment and monitoring. Forest Ecology and Management Volume 262, Issue 11, Pages 2061-2069 Doi: 10.1016/j.foreco.2011.08.044

Chan J. C. W., Paelinckx D. (2008) Evaluation of Random Forest and Adaboost tree-based ensemble classification and spectral band selection for ecotope mapping using airborne hyperspectral imagery. Remote Sensing of Environment 112 2999–3011 doi:10.1016/j.rse.2008.02.011

Dalponte M., Ørka H. O., Gobakken T., Gianelle D., Næsset E. (2013) Tree species classification in boreal forests with hyperspectral data. IEEE Trans. Geosci. Remote Sens. 51 (5), 2632–2645.

Dechesne C., Mallet C., Le Bris A., Gouet-Brunet V. (2017) Semantic segmentation of forest stands of pure species combining airborne lidar data and very high resolution multispectral imagery ISPRS Journal of Photogrammetry and Remote Sensing 126 129–145 Doi: 10.1016/j.isprsjprs.2017.02.011

DREAM (2005) Piano di gestione del complesso forestale regionale "Rincine".

European Environmental Agency (2007) European Forest Types: Categories and Types for Sustainable Forest Management Reporting and Policy. (No. EEA Terchnical Report No 9/2006). EEA, Copenhagen Retrieved from http://www.env-edu.gr/Documents/European%20forest%20types.pdf

Fassnacht F. E., Latifi H., Stereńczak K., Modzelewska A., Lefsky M., Waser L., Straub C., Ghosh A. (2016) Remote Sensing of Environment, 186, 64–87. Doi: 10.1016/j.rse.2016.08.013

Fu B., Wang Y., Campbell A., Lia Y., Zhanga B., Yind S., Xinga Z., Jina X. (2017) Comparison of object-based and pixel-based Random Forestalgorithm for wetland vegetation mapping using high spatialresolution GF-1 and SAR data. Ecological Indicators 73, 105–117 doi: 10.1016/j.ecolind.2016.09.029

Ghosh A., Ewald F., Joshi P.K., Koch B. (2014) International Journal of Applied Earth Observation and Geoinformation A framework for mapping tree species combining hyperspectral and LiDAR data: Role of selected classifiers and sensor across three spatial scales. Int J Appl Earth Obs Geoinf 26:49–63. doi: 10.1016/j.jag.2013.05.017

Gislason P. O., Benediktsson J. A., Sveinsson J. R. (2006) Random Forests for land cover classification. Pattern Recognition Letters 27 (2006) 294–300 doi: 10.1016/j.patrec.2005.08.011

Hudak A., Crookston N. L., Evans J. S., Hall D. E., Falkowski M. J. (2007) Nearest neighbor imputation of species-level, plot-scale forest structure attributes from LiDAR data. Remote Sensing of Environment 112 (2008) 2232–2245 doi:10.1016/j.rse.2007.10.009

Komárek J., Klouček T., Prošek J. (2018) The potential of Unmanned Aerial Systems: A tool towards precision classification of hard-to-distinguish vegetation types? Int J Appl Earth Obs Geoinformation, 71: 9-19. doi: 10.1016/j.jag.2018.05.003.

Kulkarni V. Y., Sinha P. K., Classifiers A. E. (2012) Pruning of Random Forest Classifiers: A Survey and Future Directions. Data Science & Engineering (ICDSE) 64–68 Doi:10.1109/ICDSE.2012.6282329

Jansson G., Angelstam P. (1999) Threshold levels of habitat composition for the presence of long-tailed tit (Aegithalos audatus) in a boreal landscape. Landsc. Ecol. 14, 283–290.

Liaw A., Wiener M. (2002) Classification and Regression by randomForest. R News, Vol. 2, No. 3. (2002), pp. 18-22.

Lisein J., Michez A., Claessens H., Lejeune P. (2015) Discrimination of Deciduous Tree Species from Time Series of Unmanned Aerial System Imagery. PLoS ONE 10(11): e0141006. doi:10.1371/journal.pone.0141006.

Ludwig A., Meyer H., Nauss T. (2016) International Journal of Applied Earth Observation and Geoinformation Automatic classification of Google Earth images for a larger scale monitoring of bush encroachment in South Africa. Int J Appl Earth Obs Geoinf 50:89–94. doi: 10.1016/j.jag.2016.03.003

Maselli F., Chiesi M., Mura M., Marchetti M., Corona P., Chirici G. (2014) Combination of optical and LiDAR satellite imagery with forest inventory data to improve wall-to-wall assessment of growing stock in Italy. International Journal of Applied Earth Observation and Geoinformation Volume 26, February 2014, Pages 377-386. Doi: 10.1016/j.jag.2013.09.001

McRoberts R. (2009) Diagnostic tools for nearest neighbors techniques when used with satellite imagery. Remote Sens Environ 113:489–499. doi: 10.1016/j.rse.2008.06.015

Nevalainen O., Honkavaara E., Tuominen S., Viljanen N., Hakala T., Yu X., Hyyppä J., Saari H., Pölönen I., Imai N., Tommaselli A. (2017) Individual Tree Detection and Classification with UAV-Based Photogrammetric Point Clouds and Hyperspectral Imaging. Remote sensing, 9, 185. doi: 10.3390/rs9030185

Niemeyer J., Rottensteiner F., Soergel U. (2014) ISPRS Journal of Photogrammetry and Remote Sensing Contextual classification of lidar data and building object detection in urban areas. ISPRS J Photogramm Remote Sens 87:152–165. doi: 10.1016/j.isprsjprs.2013.11.001

Pelletier C., Valero S., Inglada J., Champion N., Dedieu G. (2016) Remote Sensing of Environment Assessing the robustness of Random Forests to map land cover with high resolution satellite image time series over large areas. Remote Sens Environ 187:156–168. doi: 10.1016/j.rse.2016.10.010

Puletti N., Camarretta N., Corona P. (2016) Evaluating EO1-Hyperion capability for mapping conifer and broadleaved forests, European Journal of Remote Sensing, 49:1, 157-169, DOI: 10.5721/EuJRS20164909

Rodriguez-Galiano V. F., Ghimire B., Rogan J., Chica-Olmo M., Rigol-Sanchez J. P. (2012) An assessment of the effectiveness of a random forest classifier for land-cover classification. ISPRS Journal of Photogrammetry and Remote Sensing 67, 93–104. doi:10.1016/j.isprsjprs.2011.11.002

Shang X., Chisholm L. A. (2014) Classification of Australian native Forest species using hyperspectral remote sensing and machine-learning classification algorithms. IEEE J. Sel. Top. in Appl. Earth Obs. Remote Sens. 7 (6), 2481–2489

Paper II

Optimal acquisition specifications for the Riegl VUX-1LR over a *Pinus radiata* plantation

Barbara Del Perugia[1*], Davide Travaglini[1], Gherardo Chirici[1], Susana Gonzalez Aracil[2]

[1] geoLAB Laboratory of Forest Geomatics - Department of Agricultural, Food and Forestry Systems - University of Florence

[2] Interpine Group Ltd, 99 Sala Street, Rotorua, New Zealand; susana.gonzalez@interpine.nz

*Corresponding Author: barbara.delperugia@unifi.it

Abstract

The present study has tested the Riegl VUX-1 long range LiDAR sensor over a *Pinus radiata* plantation to investigate the effects of flight altitude and flight path on tree detection, tree height and DBH estimation. High density LiDAR point clouds were collected at three different heights above the ground (30m, 60m, 90m). The flight path was tested in four different configurations. Individual tree detection was performed with local maxima detection method. Diameter detection was performed with a combination of the Hough transformation stem denoising method and the Random Sample Consensus (RANSAC) technique for the circle fitting procedure directly in the point cloud. The dataset used to assess forest attributes was validated with field data. All flight altitudes produced acceptable results for tree height, with values of R^2 and RMSE between 0.53-0.59 and 1.61-1.73m, respectively. The best result of DBH estimation in horizontal cross slices was produced at 60m height, with $R^2 > 0.82$ and RMSE < 0.03m. The 60m point cloud was further analysed with different flight configurations. Our results show that a single flight direction with flight line spacing of 15 m (14 flight lines for plot) is enough for the automatic estimation of diameters in the point cloud (R^2=0.78 RMSE < 0.04m).

Keywords: Airborne Laser Scanning, ALS, LiDAR, forest inventory, point cloud, VUX-1LR LiDAR, Radiata pine plantation

1. Introduction

Light Detection and Ranging (LiDAR) has been widely applied in forest inventory to assess forest variables. The purpose of most of this studies is to use Airborne Laser Scanning (ALS) data as standard practice for National Forest Inventory, like in some countries in Europe (Næsset et al., 2004a; Magnussen et al., 2018), in Oceania (Beets et al., 2010; Watt et al., 2013; Watt and Watt, 2013), in USA (McRoberts and Tomppo, 2007) and in Asia (He et al., 2017).

The inventory methodology currently in use is a LiDAR based plot-imputation approach. Tree measurements are collected manually across a number of sample plots to estimate stand and compartment variables. There are several tasks currently performed manually in inventory assessments, including diameter and height measurements, branch size estimation, sweep estimation and stem quality assessments. Several studies (Næsset, 2002; Hyyppä et al., 2012; Corona et al., 2012) have documented the efficient use of ALS data to provide accurate predictions of forest structural attributes, such as forest height (Næsset, 1997; Næsset and Økland, 2002) and growing stock volume (Bottalico et al., 2017). Because ALS survey can cover large areas, ALS can serve as means to up-scale plot measurements to the landscape level.

ALS data can also be used for Individual Tree Detection (ITD) studies (Akay et al., 2009; Vastaranta et al., 2012). ITD and software routines are being developed to perform single tree detection, estimations of single tree attributes such as Diameter at Breast Height (DBH) (Brede et al., 2017; Dalponte et al., 2018) and counting on the point cloud based on tree segmentation methods (Lamprecht et al., 2015; Ayrey et al., 2017). One of the most common is watershed segmentation method (Beucher et Lantuéjoul, 1979), which delineate adjacent individual tree crowns by inverted the local maxima ridges detected in the Canopy Height Model (CHM). This method has been tested in several type of forest stands and has been implemented with variations that allow to detect overlapping trees (Reitberger et al., 2009; Koch et al., 2014; Duncanson et al., 2014). Local maxima segmentation method identifies as peaks of trees in the CHM when the LiDAR total height value of the pixel is greater than all surrounding neighbours in a certain search radius. These peaks are used as reference points to delineate the tree crown (Solberg et al., 2006; Véga and Durrieu, 2011). Li et al. (2012), developed a segmentation algorithm that assign LiDAR points to a single tree based on a distance threshold from the local maxima. Ayrey et al. (2017) presented a new tree segmentation algorithm that slices the point cloud in one meter layers and isolated the trees in each layer.

ALS acquisition density is usually in the range of 1 to 10 points/m^2 depending on flight altitude and scanner configuration. However, current ALS technology can collect more dense point clouds and at a more reasonable price than older sensors, in particular with light-weight LiDAR systems mounted on Unmanned Aerial Vehicles (UAV). For instance, Wallace et al. (2012) using the Ibeo LUX laser scanner produced point clouds with up to 50 points/m^2. Jaakkola et al. (2010) integrating an Ibeo Lux and Sick LMS151 profile scanner produced point clouds with 100 to 1500 points/m^2. Brede et al. (2017) using the VUX-1UAV sensor obtained a point density of 140 points/m^2 for a single flight line and an average plot density of ~3000 points/m^2, which was successfully used to detect single tree attributes.

These high density ALS point clouds are being evaluated for their suitability not only for ITD applications but also for tree-level on screen visual assessments and 3D reconstruction modelling in a Virtual Reality (VR) environment. VR is a 3D human computer interface technology that enables users to be immersed in a computer generated virtual environment. The aerially-acquired LiDAR 3D point clouds can be imported into a VR system and tools, currently under development, will allow foresters to interactively measure stem and tree structure (Chinthammit et al., 2005; Widjojo et al., 2017). Remote forest measurement has safety benefits and enables a larger sample to be collected by eliminating time travelling to the forest and within the stand. The Trans-Tasman forestry industries are interested in the development of both ITD software and VR LiDAR tools to get more reliable, effective and cost efficient resource information.

However, for an effective ALS data acquisition is important to set an appropriate flight plan over the area of interest. Næsset (2004b) investigated the effects of different flying altitudes on biophysical stand properties estimated from ALS data with low point density (1 point/m^2). Due to the increase of the point cloud density provided by modern LiDAR sensors, determine the best flight altitude and flight path (number of flight lines and distance between the flight lines) over the forest canopy is important to make more effective the cost of acquisition and to widen the survey to the entire forest. To our knowledge, no studies have been conducted to determine the best flight altitude and flight path for the acquisition of high dense ALS point clouds.

In this study, the Riegl VUX-1 long range LiDAR sensor mounted on a helicopter has been tested at three different flight altitudes and four different flight path configurations to identify the optimal specifications for the acquisition of high dense point clouds over a Pinus radiata plantation for automatic estimation of tree parameters.

The specific objectives of the study were:

- to investigate the effects of different flight altitudes (30m, 60m, 90m above ground level) on total tree height (Ht) and DBH estimation, and count of peaks;
- to investigate the effects of different flight paths on DBH estimation.

2. Dataset description

2.1 Study Area

The study was carried out in the Carabost State Forest, which is managed by Forestry Corporation of New South Wales (FCNSW) (Figure 1).

Figure 1: On the left the location of Tumut, NSW, Australia. On the right the map of the location of each study sites (boxes) and plots (circle), forest management units are outlined in grey.

Two stand areas of four ha (200x200m) were selected targeting a similar range forest structure within the *Pinus radiata* forest. Both stands, hereafter Site 1 and Site 2 are mature and pruned and thinned in the same years (Table 1).

Site	Age	Compartment/Stand Id	Pruned	Last Thinning	Stocked Area (m^3)
1	23	455/1	2004	2017 (*T2)	61.51
2	23	454/1	2004	2017 (*T2)	33.97

Table 1: Description of the two *Pinus radiata* stands measured. *T2 indicate second thinning.

The sensor calibration was done by the provider before data acquisition. The survey consisted of three flights over the sites. The flight altitudes were chosen as close as possible to the canopy (from

now on 30m), at 60m and at 90m above ground level (AGL). The flight speed was set at 5m/s or 10 knots. The frequency was set at 400kHz.The sensor potentially can scan with a Field Of View (FOV) of 330°, but in this study the scanner was set up on the front of the helicopter in a fix position, with a fix open angle around 170° for not to scan the helicopter itself. Flight lines were set at 15m apart (flight line spacing) with 27 flight lines per flight altitude. These parameters led to the acquisition of high dense point clouds. The average pulse density of a single flight line was 224 pulse/m^2 at 30m height, 121 pulse/m^2 at 60m height and 86 pulse/m^2 at 90m height.

The flight plan performed with the VUX1-LR sensor is reported in Figure 2. Flight lines were acquired from east to west (EW) and from north to south (NS). In Site 1, the pattern at 60m was done at a 45 angle from northeast to southwest (NESW) and from northwest to southeast (NWSE).

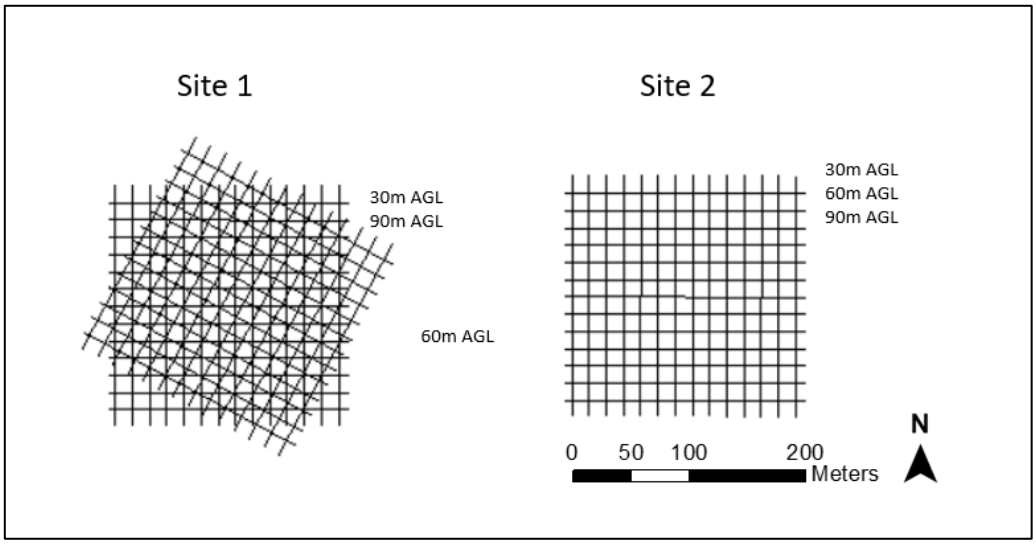

Figure 2: Flight plan. Flight lines were acquired from north to south end from east to west. In Site 1, flight lines at 60m AGL were acquired from northeast to southwest and from northwest to southeast

2.3 Ground Control Points

Before the flights, to match the point cloud with the field data, 10 high reflective Ground Control Points (GCP) (five for each site) were positioned on the ground in open spaces (Brede et al., 2017) and geo-located with a high-grade GPS (Trimble® Geo 7X with the same antenna used for the plot centre collection).

GCPs consisted of two equally sized closed cell foam panes (50 cm x 50 cm with a base of 80 cm), covered with high retro-reflective tape, connected via piano hinges. When set up the panes form a 110° angle between them, which makes them look like tents.

The positioning error of the GPS was computed and the GNSS location was fixed for the subsequent LiDAR analysis. The resulting average horizontal precision for GCP was 0.72 m with an average standard deviation of 0.0008 m. For the plot centre (CP) the average horizontal precision was 0.56 m with an average standard deviation of 0.0008 m.

2.4 Ground-based data

Fieldworks were carried out in the study area during the same week of the helicopter acquisition. The field data were collected with Juniper Allegro 2 field computer using the software PLOTSAFE (2007) developed by Silmetra Ltd, Tokoroa, New Zealand. Five plots were established with a radius of 13.82m (=0.06 ha), three plots in Site 1 and two in Site 2. A wooden pole with a reflective polystyrene ball on top was positioned in the centre of each plot. The x and y coordinates of the plot centre were collected using a Trimble® Geo 7X receiver connected to an external high quality GNSS antenna, with a positional error of 5-50 cm. Each tree was marked with a unique identifier (TreeId). For each, tree the location was collected through the measurement of bearing and distance from the plot centre, respectively with a Suunto Kb-14 compass and a Haglof VL5 Vertex. In the case of leaning trees, the stem location and the tree top location over a meter apart were annotated. The species was noted, the DBH was measured using a DBH tape and the height (H) was measured with the Vertex. Trees with a bifurcation in the trunk (fork) were also noted. According to the PLOTSAFE protocol, diameters and heights were collected using the following rules. The diameter was measured at 1.30 m above the ground, the collecting point may be shifted up or down a maximum of 10 cm to remove the effect of the swelling. If a move of more than 10 cm was required, the diameter measurements were taken equidistant above and below the breast height and averaged. The tolerance for the diameter measurement was 5 mm up to a diameter of 500 mm and 10 mm for diameter over 500 mm. The height was measured at a distance similar to the height of the tree. For leaning tree, Ht was taken 90° from the leaning direction. The tolerance for total tree height measurement was 0.5 m up to a tree height of 20 m, 1 m for tree height between 20 m and 30 m and 1.5 m for tree height over 30 m. Table 3 shows a summary of the statistics for the field DBH and the tree height measured in the plots.

Plot	Tree N	DBH minimum	DBH maximum	DBH mean	DBH sd	Ht minimum	Ht maximum	Ht mean	Ht sd
1	15	28.2	46.8	36.08	4.66	25.3	30.6	27.75	1.69
2	15	25.1	49.1	37.54	5.35	22.4	28.7	26.49	1.64
3	12	27.7	48	37.52	6.08	18	27.9	24.84	2.77
4	15	25.9	48	39.29	7.55	22	30.6	27.79	2.54
5	17	31.1	46.1	38.24	4.26	27	31	29.49	1

Table 3: Summary statistics of field data by plots. Minimum, maximum, mean and standard deviation of DBH and total tree height (Ht). DBH is reported in cm and Ht is reported in m.

The collected field data was processed and used as a reference data for the validation of the VUX-1LR datasets. The count of the forks was considered as the number of "field peaks". Through a procedure written in the statistical software R (version 3.4.1), stem maps were produced for each plot using both the stem and tree top positions.

3.Methods

3.1 Processing VUX-1LR Data

The raw LiDAR dataset was divided by site, height and direction of acquisition. The individual trajectory lines were generated as a shapefile from the helicopter flight path. Each trajectory line was given an identification number in the attribute table (Point Source Id). The raw ALS data points were then classified with LAStools (version 14 September 2017- rapidlasso GmbH) as ground and non-ground. The data was de-noise using LAStools, that classifies as noise the isolated points (3 or fewer) in a grid of cells of size 0.5 meter.

The quality of the VUX-1LR dataset and the derived products were checked using LAStools and QTModeler software. The overlap of flights lines and the ground coverage were checked to be sure the area of interest was properly covered by the LiDAR survey. To be able to process the point cloud, the data was divided in tiles of 30m x 30m. LAStools was used to normalize the heights of non-ground points in order to convert heights above sea level into relative heights above the ground. The normalized dataset was clipped by plot and separated by flight altitudes.

3.2 Individual tree analysis

Height analysis and stem analysis were carried out to investigate the effects of different flight altitudes on the count of peaks and estimations of tree heights and tree diameters compared to field measurements.

3.2.1 Height analysis

For the height analysis a CHM-based approach was used. For each flight altitude, a 0.3m resolution CHM was produced using a pit free algorithm developed by Khosravipour (2015).

The potential tree tops, 'peaks' (Gonzalez Aracil et al., 2015), were identified with FUSION software (version 3.42 - USDA Forest Service) using the CanopyMaxima tool, which is based on a local maxima detection method (McGaughey, 2015). Duplicated and overlapping peaks (distance between peaks <30cm) were cleaned, and peaks with a height less than 10m were discarded. The peaks detected at different flight altitudes were automatically counted with R software (version 3.4.1 - CRAN-R).

The field TreeId was assigned to the cleaned peaks with an automatic procedure developed in this study, using R software. Peaks were matched with the field tree top based on Euclidean distance and difference of height between field data and peak H value. The number of peaks identified with the local maxima detection method was compared with the number of trees and number of peaks counted in the field. The coefficient of determination (R^2) and the Root Mean Squared Error (RMSE) among the tree heights estimated with different flight altitudes and field measurements were computed.

3.2.2 DBH Estimation

To analyse how the different flight altitudes affected the detection of the DBH, the normalized point cloud was sliced into horizontal cross-sections. The slices were produced between 1m and 1.5m height above the ground. Given the high density of the dataset only the last return points were kept in the slices.

First a visual check of the different sliced point clouds was carried out. Then a software routine, developed in this study with R software, was used to test the three datasets acquired at different heights.

To isolate the trunk sections in the sliced point cloud an automatic clustering procedure based on point density aggregation was applied. The point distribution was transformed in a raster of intensity. The estimation of intensity of a point was calculated with the R package *spatstat* by applying kernel

smoothing algorithm based on Berman and Diggle (1989) method. The density information was transformed in contours of equal value, similar to those used to represent slope and altitude. The contours levels were converted into polygons, the clusters. The cluster polygons were used to clip the sliced point cloud, then the same group identification number (Cluster Id) was assigned to all points of a spatial cluster. Clusters with areas greater than $3m^2$ (value established based on field observations and visual inspection of the point clouds) were discarded to clean the majority of the noise present in the plots due to low branches or low vegetation. The remaining clusters were visually checked with the field position of the trees, to ensure that correctly represent the stems.

An existing R package known as TreeLS (de Conto, 2017) was used to estimate the DBH. TreeLS package was designed for Terrestrial Laser Scanner (TLS) point clouds that are usually denser than ALS. The functions process individual tree points clouds from TLS datasets, focusing on stem isolation algorithms. The automatically diameter detection was performed combining the Hough transformation stem denoising method and the Random Sample Consensus (RANSAC) technique for the circle fitting procedure directly in the point cloud (de Conto, 2017). The DBH estimated with TreeLS were compared with the field measurements and R^2 and RMSE were computed.

To match the automatic diameter detection with the reference data the Euclidian distance between the centre of the clustered trunks and the field tree location was computed, then the attributes TreeId and DBH of the field dataset were assigned to the clusters.

3.3 Flight path

To investigate how the flight path affected the quality of the data for DBH estimation the point cloud at 60m was further analysed. Each site was covered with 27 individual flight lines from two directions. The coverage of the single flight lines over the plots was checked with LAStools.

Four flight path configurations, differed in the number of flight lines and flight line spacing distance, were tested on the horizontal cross-section between 1m and 1.5m AGL. For each configuration, a visual check of the trunks section and the DBH estimation with TreeLS method were performed.

The following flight path configurations were tested (Figure 3):

All flight lines from both directions (27 flight lines - 15m flight line spacing);

All flight lines from one direction (13-14 flight lines - 15m flight line spacing);

Flight lines taken in odd order according to the flight line number from one direction (6-7 flight lines - 30m flight line spacing);

The centre flight line crossing a plot and the alternate flight line either side (3 flight lines - 30m flight line spacing).

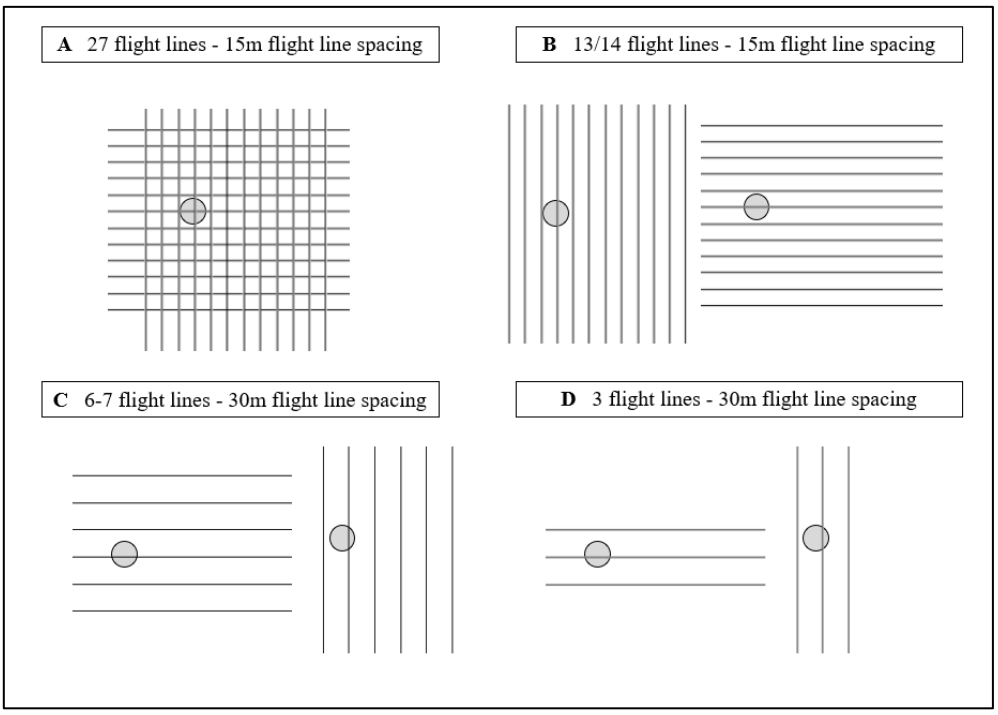

Figure 3 – Example of the four flight path configurations, the circle represents a theorical plot.

However, the theoretical flight plan designed to have a very narrow flight line spacing (15m) was difficult to be followed by the helicopter pilot and therefore the resulting flight path not always respected the 15m flight line spacing.

Since the actual flight plan presented some flight lines less than 10m apart, we tested the effect of a narrower flight line spacing, approximately 10m. Two extra plots, from here on virtual plots (not measured in the field) were created in those location. The flight path configurations tested for the virtual plot were A_2, B_2 and D_2 (flight line spacing constant) (workflow reported in Figure 4).

The DBH used as reference data for the virtual plots were manually measured in ArcMap by drawing polygons in the 0.5m sliced point cloud with a fix scale of 1:25, then DBH were derived from the polygon perimeters.

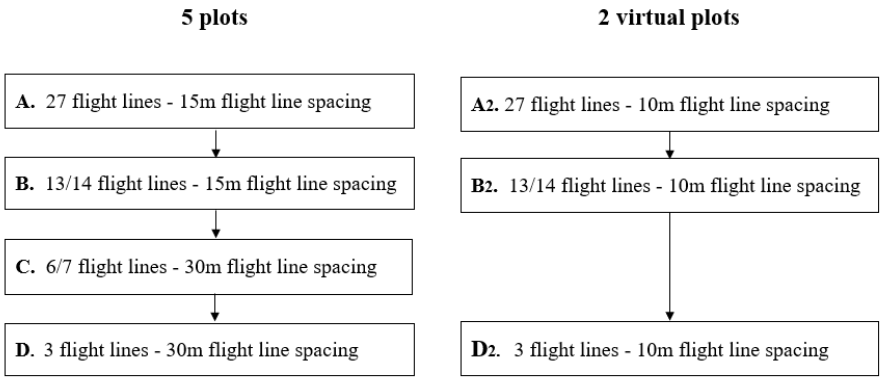

Figure 4 - Workflow diagram showing the flight path configurations examined.

4. Results

The pulse repetition frequency of the VUX-1LR set at 400kHz resulted powerful enough to penetrate the vegetation and coming back to the sensor with up to 7 returns. The pulse density of a single flight line was between 100 and 400 pulses/m^2. The dataset for this campaign has reached a pulse density between 6,000 and 8,000 pulses/m^2 and a return density of over 11,000 returns/m^2 for site with the combination of the three flight altitudes. An example of the point cloud is reported in Figure 5.

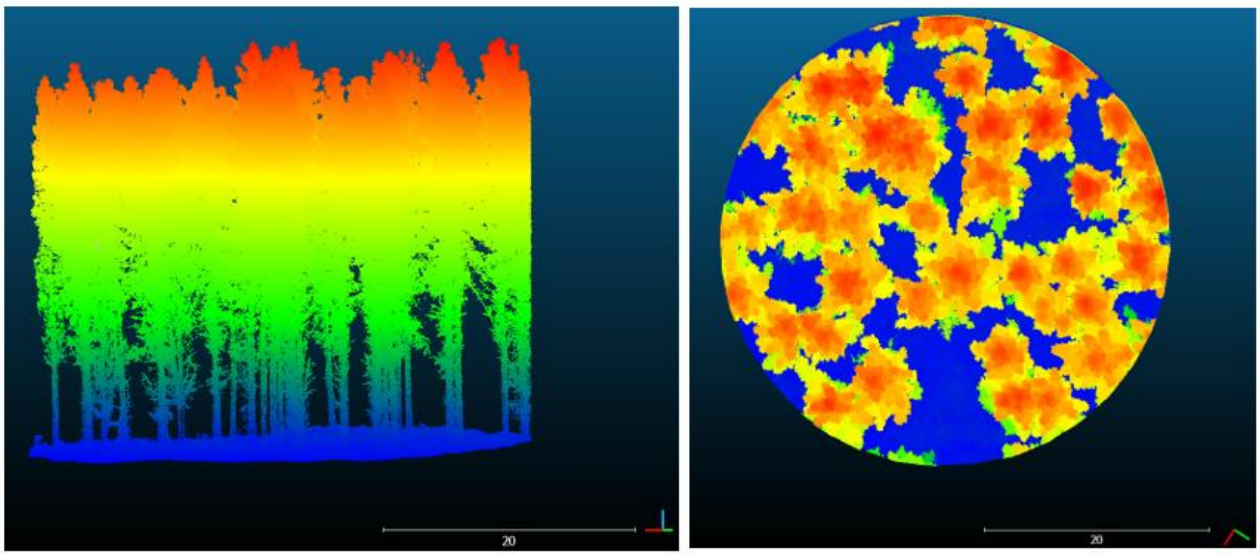

Figure 5 – Example of the point cloud of Plot 5, Site 2 captured at 60m of altitude.

Changing the altitude above ground has direct impact on the spacing between the scanned points. Increasing the flying altitude, without changing other parameters, will amplify the spacing the points

that will decrease the point density. The pulse and point density was very high in all the three surveys. A summary of the pulse and return density by flight altitudes and plot is reported in Table 4. Point spacing varied between 0.01m at 30m AGL and 0.03m at 90m AGL.

Flying at the same speed at different height impact also the Field Of View (FOV), that get smaller with the increasing of the flight altitude. The min/max FOV varied between -86/82° at 30m AGL and -69/74° at 90m AGL.

	30m		60m		90m	
Plot	Returns	Pulse	Returns	Pulse	Returns	Pulse
1	5,004.85	2,750.33	3,323.87	1,857.39	2,263.7	1,310.58
2	5,808.23	3,296.73	4,015.06	2,341.05	2,892.34	1,729.96
3	5,249.44	2,962.99	3,200.08	1,845.85	2,159.94	1,316.35
4	6,341.1	3,578.16	3,854.25	2,198.83	3,340.61	1,957.24
5	7,161.69	3,877.27	5,037.96	2,754.89	3,656.28	2,030.11

Table 4 – Summary of returns and pulse density by flight altitude and plot. Unit of measurement returns/m^2 and pulses/m^2.

Furthermore, with at a higher altitude the laser pulse signal generated by the sensor will have to travel further and the laser signal will spread with distance according to the sensor's beam divergence, growing the footprint on the ground. The beam divergence was calculated for the three altitudes, the VUX-1LR beam divergence is 0.5m/rad that corresponds to an increase of 50 mm of beam diameter per 100 m distance (RIEGL, 2017). Therefore, the beam footprint on the ground was 1.5cm for 30m AGL, 3cm for 60m AGL and 4.5cm for 90m AGL.

4.1.1 Individual Tree Height Analysis

Figures 6 shows the CHM's computed at different flight altitudes by site.

All the flight altitudes returned positive results; only the 30m AGL survey present some canopy artefacts in the CHM, this is because less pulses hits the top of the trees.

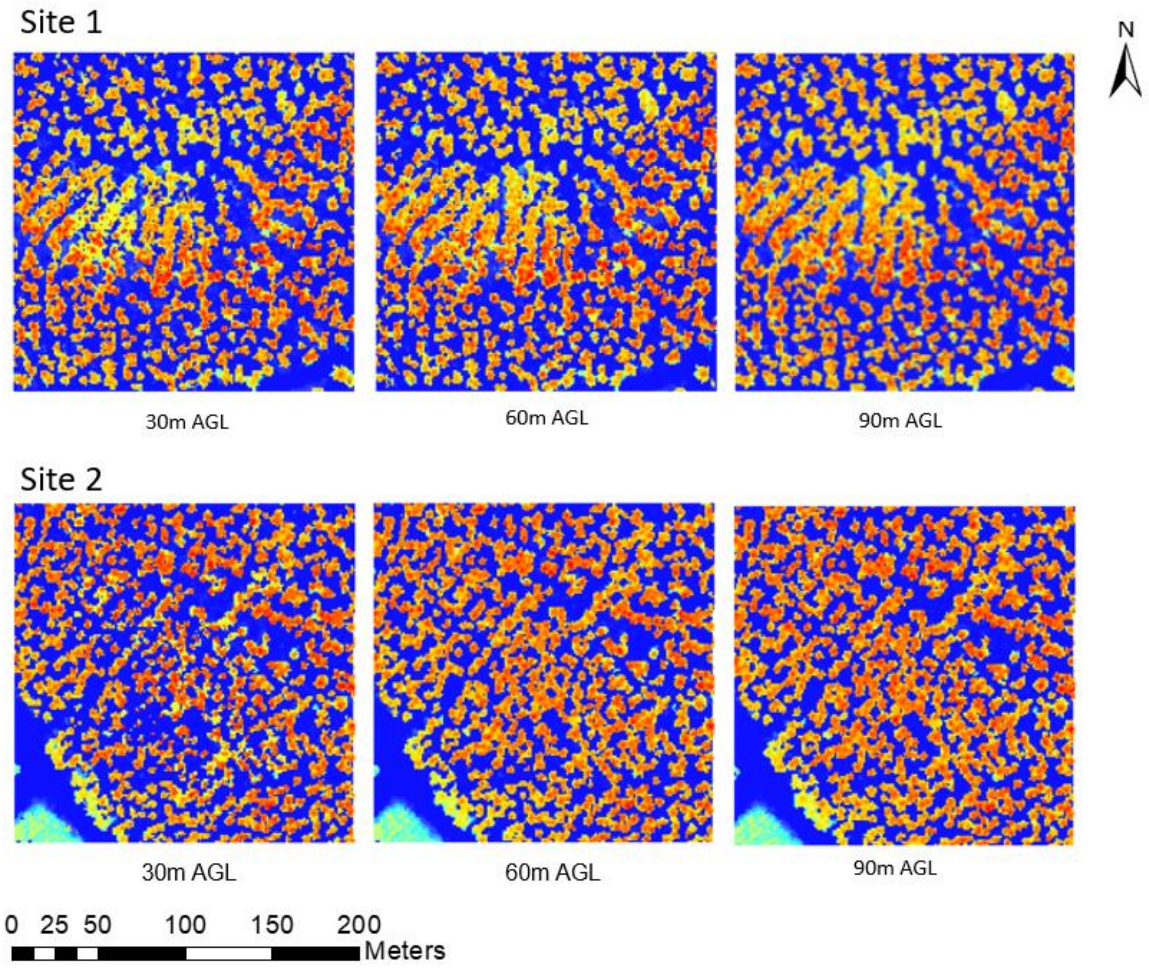

Figure 6 - The CHM of Site 1 and 2, at 30m (left image), 60m (central image) and 90m (right image).

According to the PLOTSAFE protocol, in each plot the forks were counted. This count was considered as the number of "field peaks". The cleaned LiDAR detected peaks at different flight altitude were intersected with the plot boundaries to count how many were detected (Figure 7). All the three flights returned a good estimation of the peaks, the 30m AGL resulted the closest one, but the difference between the peaks count at different AGL is not significant.

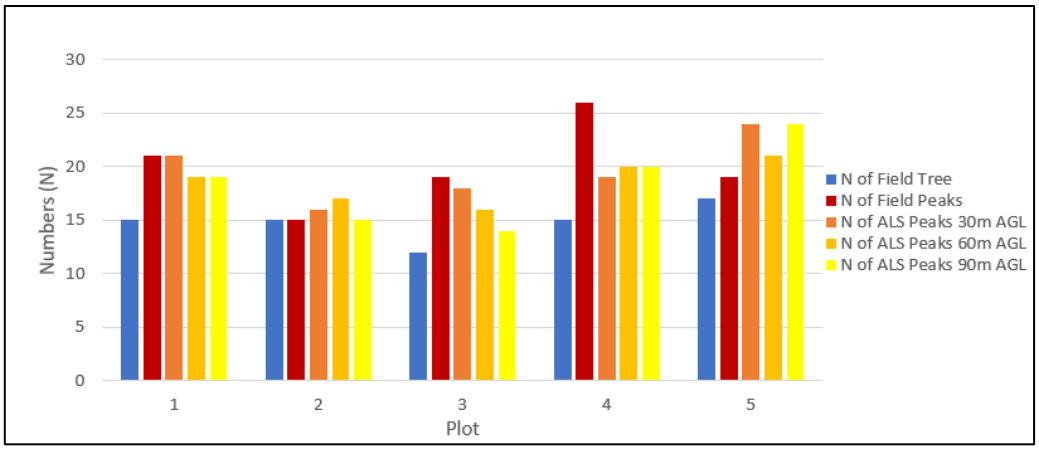

Figure 7 - Comparison of number of trees and number of peaks counted in the field with the number of peaks detected with Fusion at different flight altitude.

With the automatic TreeId identification procedure based on minimum Euclidean distance and minimum total height difference, all field tree tops were assigned to the closest peaks by flight altitude of survey.

An analysis of the peaks from all the flight altitudes combined was performed to investigate which altitude returns the closest match between peaks and tree tops in terms of minimum Euclidean distance and minimum total height difference. Of 74 field trees, the 30m CHM produced the closest match between peaks and tree tops on 31 occasions, the 60m CHM produced the closest match on 28 occasions and the 90m CHM produced the closest match on 15 occasions.

For each plot the maximum and mean tree height detected at different flight altitude was compared with the field data (Table 5). All flight altitudes produced acceptable results for maximum tree height: field data = 31.00m, 30m AGL = 30.60m, 60m AGL = 30.70m and 90m AGL = 30.65m. The mean tree height for the field data was 27.31m, while the mean for the 30m, 60m and 90m resulted 27.17m, 27.15m and 27.40m, respectively.

Plot	Hf max	Hf mean	H max30	H mean30	H max60	H mean60	H max90	H mean90
1	30.6	27.75	30.21	27.15	30.7	27.32	30.65	27.46
2	28.7	26.41	29.71	27.36	30.54	26.78	30.32	27.65
3	27.9	24.84	27.46	25.01	27.5	24.93	28.29	25.34
4	30.6	27.44	29.45	26.74	29.37	27.09	29.84	27.38
5	31	29.33	30.6	28.93	30.65	28.94	30.3	28.62
All	**31**	**27.31**	**30.6**	**27.17**	**30.7**	**27.15**	**30.65**	**27.4**

Table 5 – Maximum and mean tree height (H) (in meter) for each flight altitude compared with field data (Hf).

The regression between the field Ht and the correspondent peak Ht for each flight altitude is presented in Figure 8. The R^2 (0.530 for the 30m AGL, 0.587 for the 60m AGL and 0.581 for the 90m AGL) and RMSE (1.73m for the 30m AGL, 1.61m for the 60m AGL and 1.63m for the 90m AGL) show that similar results were achieved with the three flight altitudes. The 60m flight was slightly more accurate than the others.

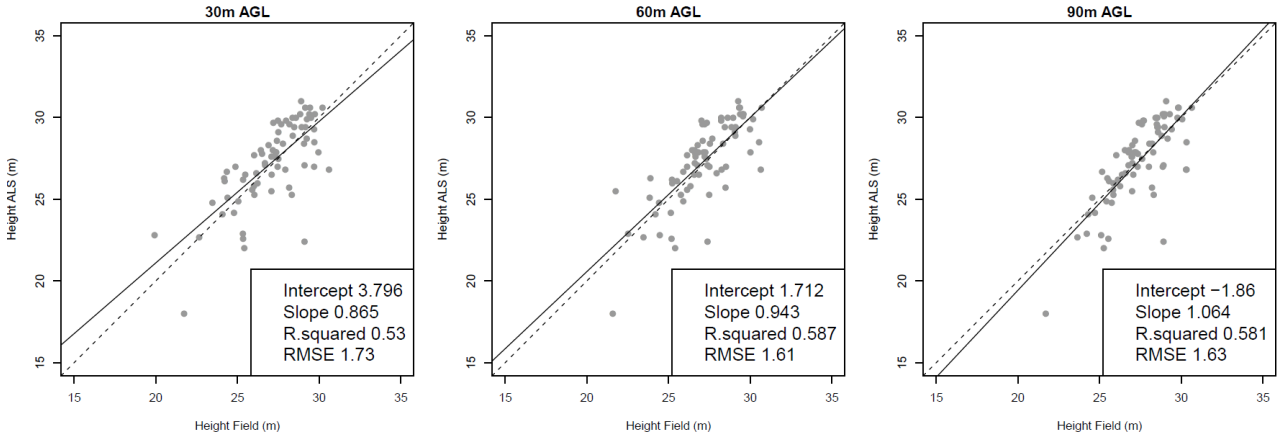

Figure 8 – Field height vs ALS Height for each flight altitude. Dashed line represent the 1:1 line, continuous line represent the fitted line.

4.1.2 DBH Estimation

A visual check of the horizontal cross-sections of the point clouds captured at different flight altitudes was carried out. The 90m AGL point cloud was found to be unacceptable at capturing DBH accurately. The 30m AGL point cloud was affected by an offset in the trunks that lead to a misdetection of the diameter with automatic procedures. The 60m AGL point cloud returned in almost all instances a full

trunk circumference, that allowed the estimation of the DHB with the automatic procedure (Figure 9).

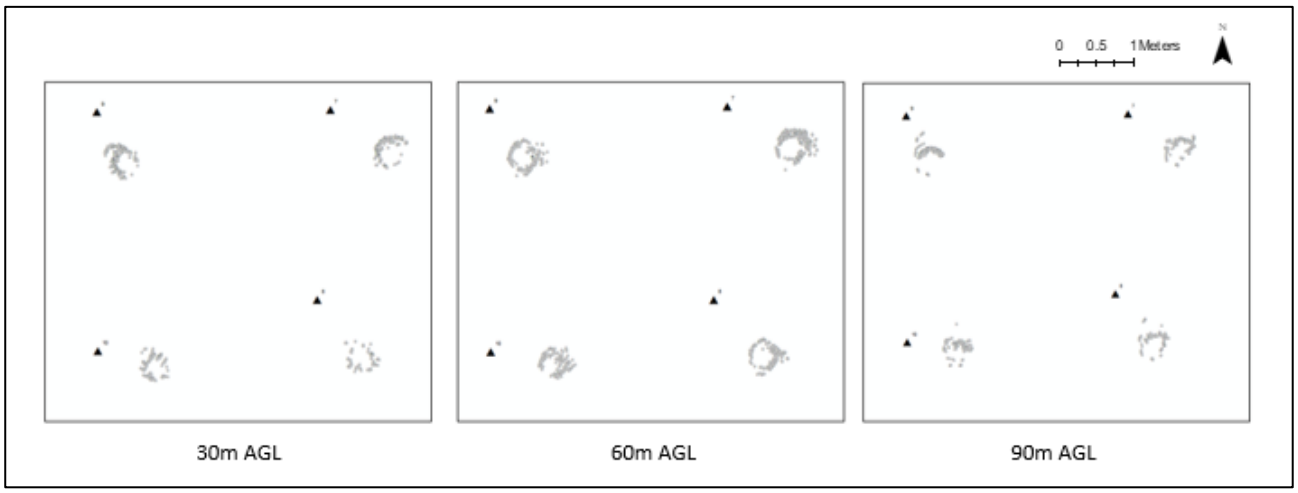

Figure 9 - Example of stem detection at different flight altitudes in Site 1, Plot 1 (TreeId 7-10). The first box on the left represent the trunk's point cloud at 30m AGL, the central one is the 60m AGL point cloud and the right box is the 90m AGL point cloud.

The 0.5m slices acquired at different flight altitudes were analysed with the R package TreeLS. In both Plots 2 and 3 one tree was not detected due to dense low vegetation. The DBH estimated with TreeLS were compared with field measurements. The resulting R^2 and RMSE are presented in Table 6. The horizontal cross slices of the 60m height dataset provided the better accuracy with $R^2 > 0.82$ for four out of five plots and RMSE < 3.6cm in all cases.

	R^2			RMSE		
Plot	30m	60m	90m	30m	60m	90m
1	0.819	0.894	0.537	1.8	1.8	3.5
2*	0.682	0.832	0.661	2.2	1.6	2.3
3*	0.885	0.899	0.502	1.7	1.6	4.2
4	0.782	0.822	0.712	3.7	3.6	3.1
5	0.458	0.671	0.334	3.7	2.4	3.7
All	0.725	**0.824**	0.549	3.7	**3.6**	4.2

Table 6 – Results of DBH estimation with TreeLS for the horizontal cross slice between 1m and 1.5m for the five plots. RMSE in cm. * Indicate one diameter was not automatically detected due to low vegetation noise.

4.2 Flight path

The flight path is presented in figure 10, the theoretical flight line spacing (15m) was very narrow, and the resulting flight line spacing oscillates between 4m and 26m in the two sites.

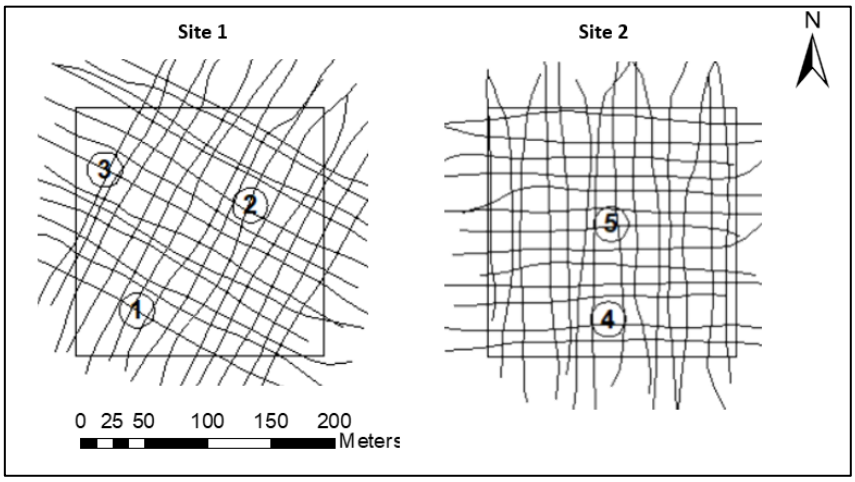

Figure 10 – Helicopter flight plan for Site 1 and Site 2 at 60m AGL. Plots represented with circle.

The point source of the points covering the plot was checked with LAStools and it was found that all the 27 flight lines for each site contributed to the plot point cloud.

The flight path configurations were tested with the TreeLS R package for DBH estimation. The results are reported in Table 7 for the five plots (configurations A, B, C, D) and in Table 8 for the two virtual plots (configurations A_2, B_2, D_2).

For the five plots, configurations A and B provided a good fit between the DBH estimated from the point clouds and the corresponding field reference data. Configuration B had a lower accuracy compared to configuration A.

Configuration C allowed the estimation of the diameters on 64% of trunks (28 trees over 74 were not detected). Configuration D resulted insufficient to detect most of the trunks and the diameters were estimated for few stems.

	A		B			C		
Plot	R^2	RMSE	R^2	RMSE	Not Det	R^2	RMSE	Not Det
1	0.89	1.8	0.78	2.1		0.95	2.4	6
2	0.83	1.6	0.83	1.4	1	0.60	2.8	6
3	0.90	1.6	0.86	2.1	1	*NA*	*NA*	9
4	0.82	3.6	0.83	4.5		0.61	5.4	3
5	0.67	2.4	0.63	1.8		0.44	2.9	4

Table 7 - R^2 and RMSE in cm, obtained with TreeLS diameter detection for configuration A, B and C for the five plots. "Not Det" represent the number of not detected trees.

The virtual plots were analysed with configurations A_2, B_2 and D_2 without changing the flight line spacing (10m). With configurations A_2 and B_2 was possible to detect the circumference of trunks, while configuration D_2 was affected by a consistent loss of points and only few trunks were completely detected. The accuracies were lower than the ones for the five plots because the reference diameters, which were measured manually in the point cloud using ArcMap, were affected by a subjective error. Moreover, Virtual Plot 1 (VP1) was characterized by a high presence of low vegetation. Anyway, configuration A_2 and B_2 resulted optimal for trunk detection and DBH estimation (Table 8). These results confirm that flight line spacing influences the accuracy in trunk detection.

	A_2		B_2		
Plot	R2	RMSE	R2	RMSE	Not Det
VP1	0.56	3.3	0.54	4.0	2
VP2	0.75	2.6	0.66	3.0	1

Table 8 - R^2 and RMSE in cm, obtained with TreeLS diameter detection for configuration A_2, B_2 for the two virtual plots. "Not Det" represent the number of trees not detected.

The visual assessment of the horizontal cross-sections showed that configuration A returned most full trunk circumferences. The mis-estimation of the diameter of a few trunks was due to the low vegetation noise that added points to the circumference (i.e. Plot 2).

To investigate if a single direction of flight was sufficient to detect trunks, configuration B was tested. All plots with configuration B returned most of the full trunks in at least one of the two directions. The single directions investigated were NWSE, SWNE, NS and EW. Because plots 1 and 3 were located near the site boundary the flight lines coverage was not complete in one quarter site of the plots. That's affected the detection of diameters. In Plot 1 the trunks were well detected with the NWSE point cloud, while in plots 2 and 3 the trunks were well detected with the SWNE point cloud. Plots 4 and 5 resulted well detected in both the single directions (EW, NS). The results of configuration B proved that potentially any single flight direction was enough to detect the full trunk.

To analyse how the flight line spacing affected the quality of the data, alternate trajectories lines were selected, configuration C. The flight line spacing was increased to 30m theoretical flight line spacing, but the actual range for all plots resulted between 21m and 38m. With this configuration it was still possible to detect some complete trunk circumferences, but often parts of the trunk circumference were missing.

Using Configuration D, only three flight lines for each plot were tested, the most central flight line along with one flight line 30m either side. The results of this configuration show that there were few points to detect the trunk circumferences, both visually and automatically. This confirms the contribution of all flight lines to the single plot point cloud.

An example of circumference detection in the trunk's point cloud with the TreeLS software is reported in Figure 11. The trunk (Plot 1 TreeId 9) was successfully estimated with configuration A, B and C.

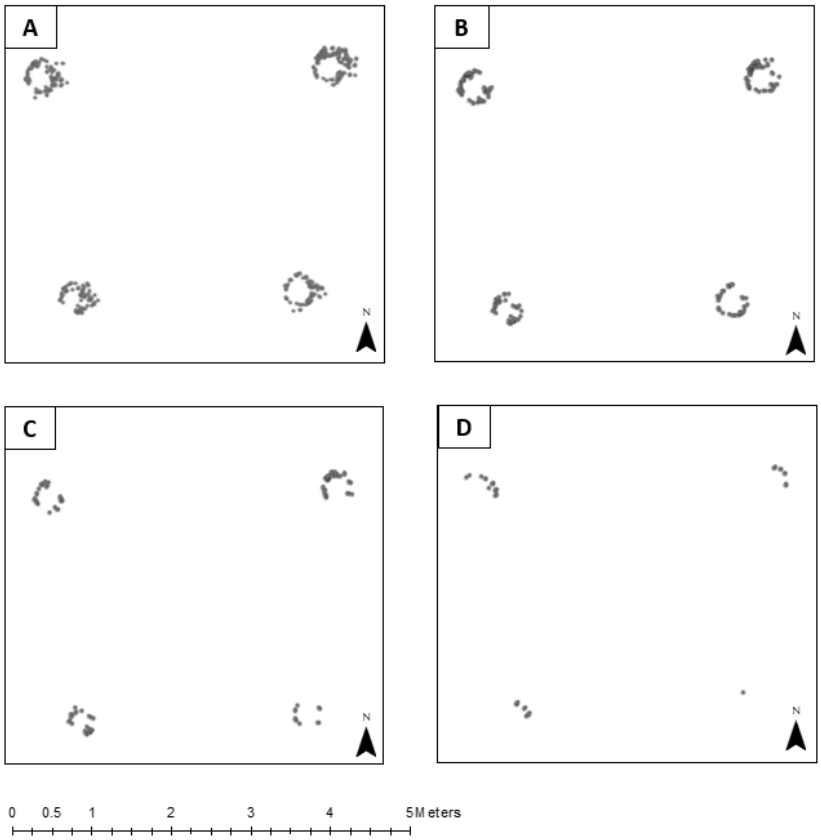

Figure 11 – Example of trunk detection with TreeLS (Plot 1 TreeId 7-10) by flight path configuration.

5. Discussion

5.1 Flight altitude

The first analysis carried out, investigated which point cloud from three different flight altitude produces the number of peaks, the total height (Ht) and the DBH closest to the field measurements. The number of peaks estimated with the automatic procedure was similar to the "field peaks" in most of the plots. However, even if the study was carried out in Pinus radiata stands with low tree density, the peaks visible from the top will hardly match the number of trees visible from the ground. As expected, the height analysis demonstrated that there is not a significant difference between the three surveys. The 30m AGL flight underestimated the maximum tree height of 0.40m compared with the field data, the 90m AGL underestimated the maximum tree height of 0.25m while the 60m AGL resulted the closest dataset to the field measurement with an underestimation of 0.20m.

The regression study of field Ht and peaks Ht by flight altitude have reached an average R^2 of 0.57 and an average RMSE of 1.25m. This result is in line with the study of Næsset (2004b) who found, even with a lower pulse density, that Ht max didn't differ significantly between the flying altitudes.

Indeed, Ht max is one of the most tested attributes of the forest and well related with the LiDAR metrics.

The analysis carried out with the last-only pulse of VUX-1LR data is one of the first attempt (Brede et al., 2017; Dalponte et al., 2018) to analyse a very large amount of ALS data for stem detection. Both the visual check and the automatic diameter detection performed with TreeLS proved that the highest correlation was achieved with the point cloud acquired at 60m AGL. Whit this point cloud all the stems were detected. Wallace et al. (2014) detected 98% of single trees with a point cloud density of 50 points/m^2.

The TreeLS analysis of half meter horizontal cross slices of the 60m AGL and the 30m AGL point clouds provided a good estimation of DBH. With the 60m AGL an average R^2 of 82% and an RMSE always less than 3.6cm was achieved. With the 30m AGL flight an average R^2 of 72% and an RMSE always less than 3.7cm was obtained. Compared with the 60m point cloud results, the 30m point cloud reached a lower R^2 in all plots. The number of points in the 30m AGL would be more than enough to detect the diameter with an automatic procedure like TreeLS, in fact a DBH estimation was obtained for all trunks. However, the 30m dataset presented an offset (due to the sensor calibration) that affected the diameter estimation. The 90m AGL flight didn't returns enough points to detect the diameter of the trees and therefore the R^2 and RMSE resulted insufficient.

These results achieved with the 60m AGL and 30m AGL point clouds are comparable with the ones reported by other authors: Dalponte et al. (2018) detected 60% of the trees with DBH greater than 10cm, with R^2=0.57 and RMSE=5.4cm; Brede et al. (2017) detected 32% of the stems with R^2=0.98 and RMSE=4.2cm.

5.2 Flight path

This part of the study focuses on the effect of different flight path configuration (direction, number of flight lines and flight lines spacing) for the detection of DBH.

With configuration A, all trunks were detected and successfully estimated, with a maximum R^2=90%, an average R^2=82% and an average RMSE=2cm.

With configuration B, 97% of stems were detected, with a maximum R^2 of 86%, an average R^2 of 78% and an average RMSE of 2.4cm. Results of configuration B indicate that a flight in only one direction with 15m of flight lines spacing is sufficient for stem detection, independently of the direction.

Dropping alternate flight lines to increase the flight line spacing distance (from 15m to 30m), configuration C, decreased the percentage of trunks detected from 97% to 62%. The relative average

R^2 of 65% cannot be taken into consideration since is not consistent. Therefore, if the distance between flight lines is improved, the accuracy of DBH estimation will decrease.

The Virtual Plots analysis gave an idea of the possible achievement with a narrower flight line spacing (10m). Where the flight lines were straight and close to each other about 10m the detection of the trunks was visually possible with all the configurations. The automatic diameter detection with configuration A_2 and B_2 provided sufficient results (R^2=65.5%). However, the next LiDAR survey should be planned with a platform able to follow precisely the theorical path with a flight line spacing of 10m to confirm these results.

The dense flight path and the low speed (5m/s) design for this study was a challenge. The helicopter flight resulted with a high range of distances between the lines. To achieve consistently good results a UAV with the LiDAR sensor should be used, since it is characterized by a predetermined flight path that the UAV would follow precisely. The forest industry is certain that the next generation of LiDAR survey should be done with an UAV equipment.

6. Conclusions

The study was conducted to find the optimal flight parameters of the VUX-1LR to obtain a high dense point cloud suitable for be measured in a Virtual Reality environment or with a software procedure. The dataset shows to be suitable to conduct full plot inventories in the 3D point cloud. Traditional forest inventory data would be necessary only for validation.

The following conclusions can be drawn from the study:

The optimal flight altitude for a LiDAR survey resulted 60m height for the computation of the parameters DBH and Height.

The number of flight lines is highly correlated with the quality of the data. Optimal results were achieved using 27 flight lines (two direction of survey) as well as 13 flight lines (one direction of survey).

The closest the flight line spacing is the better accurate the dataset will be. The optimal flight line spacing resulted 15m.

Regular and straight flight path leads to consistent dataset for DBH detection.

The next challenge will be to test a LiDAR survey with single direction of acquisition with 15 or 10m flight line spacing with an UAV platform at an AGL between 30m and 60m.

Acknowledgments

This work was possible thanks to Forest & Wood Products Australia (FWPA) and the Ministry for Business Industry and Employment (MBIE) Strategic Science Investment Fund (SSIF), who supported this project financially.

Assistance provided by Forestry Corporation of New South Wales and NSW Department of Primary Industries was greatly appreciated.

Special thanks to Interpine Group Ltd that hosted the main author for six months and provided useful knowledge about remote sensing.

References

Akay A., Oðuz H., Karas I., Aruga K. (2009) Using LiDAR technology in forestry activities. Environmental Monitoring and Assessment, 151: 117-124. doi: http://dx.doi.org/10.1007/s10661-008-0254-1.

Ayrey E., Fraver S., Kershaw J. A., Kenefic L. S., Haye D., Weiskittel A. R., Roth B. E. (2017) Layer stacking: A novel algorithm for individual forest tree segmentation from LiDAR point clouds. Canadian Journal of Remote Sensing 43(1) 16-27.

Beets P. N., Brandon A., Fraser B. V., Goulding C. J., Lane P. M., Stephens P. R. (2010) National forest inventories: New Zealand. In E. Tomppo, T. Gschwantner, M. Lawrence, & R. E. McRoberts (Eds.), National forest inventories — Pathways for common reporting (pp. 391–410) Springer.

Beucher S., Lantuéjoul C. (1979) Use of watersheds in contour detection http://cmm.ensmp.fr/~beucher/publi/watershed.pdf

Berman M., Diggle P. (1989) Estimating weighted integrals of the second-order intensity of a spatial point process. Journal of the Royal Statistical Society, series B 51, 81–92.

Bottalico F., Chirici G., Giannini R., Mele S., Mura M., Puxeddu M., McRoberts R.E., Valbuena R., Travaglini D. (2017) Modeling Mediterranean forest structure using airborne laser scanning data. International Journal of Applied Earth Observation and Geoinformation, 57: 145-153. doi: 10.1016/j.jag.2016.12.013.

Brede B., Lau A., Bartholomeus H., Kooistra L. (2017) Comparing RIEGL RiCOPTER UAV LiDAR Derived Canopy Height and DBH with Terrestrial LiDAR. Sensors, 17(10), p.2371.

Bryson M., Gordon J. (2018) Algorithms and 3D modelling techniques for tree detection and tree-level volume estimates. Optimising remotely acquired, dense point cloud data for plantation inventory. (PNC377-1516) Final Report for Forest & Wood Products Australia.

Chinthammit W., Seibel E., Furness III TA. (2005) Virtual image registration in augmented display field. US Patent 6,867,753

Corona P., Cartisano R., Salvati R., Chirici G., Floris A., Di Martino P., Marchetti M., Scrinzi G., Clementel F., Travaglini D., Torresan C. (2012) Airborne Laser Scanning to support forest resource management under alpine, temperate and Mediterranean environments in Italy. Eur J Remote Sens, 45: 27–37. doi: 10.5721/EuJRS20124503.

Dalponte M., Frizzera L., Ørka H.O., Gobakken T., Næsset E., Gianelle D. (2018) Predicting stem diameters and aboveground biomass of individual trees using remote sensing data. Ecological Indicators, 85: 367-376. doi: 10.1016/j.ecolind.2017.10.066 handle: http://hdl.handle.net/10449/44156

de Conto T., Olofsson k., Bastos Görgensc E., Estraviz Rodriguezd L. C., Almeidad G. (2017) Performance of stem denoising and stem modelling algorithms on single tree point clouds from terrestrial laser scanning. Computers and Electronics in Agriculture 143 165–176

Duncanson L. I., Cook B. D., Hurtt G. C., Dubayah R. O. (2014) “An efficient, multi-layered crown delineation algorithm for mapping individual tree structure across multiple ecosystems.” Remote Sensing of Environment, Vol. 154: pp. 378–386.

Gonzalez Aracil S., Herries D., Rawley B. (2015) Evaluation of an additional LiDAR metric in Forest Inventory. Silvilaser2015 Conference, La Grande Motte, France, September 2015

He Y., Song Z., Liu Z. (2017) Updating Highway Asset Inventory Using Airborne LiDAR. Measurement. 104. 132-141. 10.1016/j.measurement.2017.03.026.

Hyyppä J., Holopainen M., Olsson H. (2012) Laser scanning in forests. Remote Sens., 4, 2919–2922.

Jaakkola A., Hyyppä J., Kukko A., Yu X., Kaartinen H., Lehtomäki M., Lin Y. (2010) A low-cost multi-sensoral mobile mapping system and its feasibility for tree measurements. ISPRS J. Photogramm. Remote Sens.,65, 514–522.

Khosravipour A., Skidmore A.K., Isenburg M., Wang T. J. (2015) Development of an algorithm to generate pit-free Digital Surface Models from LiDAR, Proceedings of SilviLaser 2015, pp. 247-249, September 2015

Koch B., Kattenborn T., Straub C., Vauhkonen J. (2014) “Segmentation of forest to tree objects.” In Forestry Applications of Airborne Laser Scanning, Springer.

Lamprecht S., Stoffels J., Dotzler S., Hab E., Udelhoven. T. (2015) aTrunk - An ALS-Based Trunk Detection Algorithm. Remote Sensing, 7, 9975-9997; doi:10.3390/rs70809975.

Li W., Qinghua G., Marek J., Maggi K. (2012) A New Method for Segmenting Individual Trees from the Lidar Point Cloud. Photogrammetric Engineering and Remote Sensing. 78. 75-84. 10.14358/PERS.78.1.75.

Magnussen S., Nord-Larsen T., Riis-Nielsen T. (2018) Lidar supported estimators of wood volume and aboveground biomass from the Danish national forest inventory (2012–2016). Remote Sensing of Environment 211, pp. 146–153. DOI: 10.1016/j.rse.2018.04.015

McGaughey R. J. (2015) FUSION/LDV: Software for LiDAR Data Analysis and Visualization - US Department of Agriculture Forest Service, Pacific

McRoberts R., Tomppo E. (2007) Remote sensing support for national forest inventories. Remote Sensing of Environment 110 (2007) 412–419.

Næsset E. (1997) Determination of mean tree height of forest stands using airborne laser scanner data. ISPRS Journal of Photogrammetry and Remote Sensing 52:49-56.

Næsset E. (2002) Predicting forest stand characteristics with airborne scanning laser using a practical two-stage procedure and field data. Remote Sensing of Environment, 80: 88–99.

Næsset E., Økland T. (2002) Estimating tree height and tree crown properties using airborne scanning laser in a boreal nature reserve, Remote Sensing of Environment, 79 (1):105– 115.

Næsset E. (2004a) Practical large-scale forest stand inventory using a small-footprint airborne scanning laser. Scandinavian Journal of Forest Research, 19(2), 164-179, doi:Doi 10.1080/02827580310019257.

Næsset E. (2004b) Effects of different flying altitudes on biophysical stand properties estimated from canopy height and density measured with a small-footprint airborne scanning laser. 91:243–255. doi: 10.1016/j.rse.2004.03.009

PLOTSAFE Overlapping Feature Cruising Forest Inventory Procedures (2007)

Reitberger J., Schnörr C., Krzystek P., Stilla U. (2009) 3D segmentation of single trees exploiting full waveform LIDAR data. ISPRS Journal of Photogrammetry and Remote Sensing, Vol. 64(No. 6): pp. 561–574.

RIEGL (2017) RIEGL VUX-1LR Datasheet 2017-09-01 http://www.riegl.com/uploads/tx_pxpriegldownloads/RIEGL_VUX-1LR_Datasheet_2017-09-01.pdf

Solberg S., Naesset E., Bollandsas O.M. (2006) Single tree segmentation using airborne laser scanner data in a structurally heterogeneous spruce forest. Photogramm. Eng. Remote Sens. 72, 1369–1378.

Vastaranta M., Kankare V., Holopainen M., Yu X., Hyyppä J., Hyyppä H. (2012) - Combination of individual tree detection and area-based approach in imputation of forest variables using airborne laser data. ISPRS Journal of Photogrammetry and Remote Sensing, 67: 73-79. doi: http://dx.doi.org/10.1016/j.isprsjprs.2011.10.006.

Véga C., Durrieu S. (2011) Multi-level filtering segmentation to measure individual tree parameters based on lidar data: application to a mountainous forest with heterogeneous stands. Int. J. Appl. Earth Obs. Geoinf. 13, 646–656. http://dx.doi.org/10.1016/j.jag.2011.04.002.

Wallace L., Lucieer A., Watson C., Turner D. (2012) Development of a UAV-LiDAR system with application to forest inventory. Remote Sens. 2012, 4(6), 1519-1543; https://doi.org/10.3390/rs4061519

Wallace L., Lucieer A., Watson C.S. (2014) Evaluating Tree Detection and Segmentation Routines on Very High Resolution UAV LiDAR Data. IEEE Trans. on Geoscience and Remote Sensing, 52(12).

Watt M. S., Adams T., Aracil Gonzalez S., Marshall, H., Watt, P. (2013) The influence of LiDAR pulse density and plot size on the accuracy of New Zealand plantation stand volume equations. New Zealand Journal of Forestry Science, 43(1), 15.

Watt P., Watt M. S. (2013) Development of a national model of Pinus radiata stand volume from LiDAR metrics for New Zealand. International Journal of Remote Sensing

Widjojo E., Chinthammi W., Ulrich E. (2017) Virtual Reality-Based Human-Data Interaction. 1-6. 10.1109/BDVA.2017.8114627

Paper III

Below Canopy UAS Photogrammetry for Stem Measurement in a Radiata Pine Plantation

Sean Krisanski[a], Barbara Del Perugia[b], Mohammad Sadegh Taskhiri[a], Paul Turner[a]

[a]ARC Centre for Forest Value, Discipline of ICT – College of Science and Engineering, University of Tasmania, Hobart, TAS 7001, Australia

[b]geoLAB Laboratory of Forest Geomatics - Department of Agricultural, Food and Forestry Systems, University of Florence

Abstract

Unmanned Aerial Systems (UAS) are a cost-effective means of collecting forest data conventionally used above the forest canopy. Where forest canopies are dense, limited information about stem structures can be extracted directly due to obscuration by foliage. In these circumstances, complementary ground-based methods including manual measurement and terrestrial laser scanning are deployed, but these techniques are often limited in terms of the scope and scale of data collected by factors including time, field cost and site accessibility. This paper describes the application of a UAS flown below the forest canopy as an efficient and effective approach for stem measurement in areas where the canopy is difficult to penetrate, and as a potential solution to measuring trees in areas of dense undergrowth. The study plots were scanned with a helicopter-mounted VUX-1LR LiDAR sensor at three different altitudes (30m, 60m and 90m) and the resulting point clouds were used as a comparison dataset. The measurements extracted from these point-clouds were compared with ground-based measurements of diameter at breast height and relative positions. The below-canopy UAS and the VUX-1LR at 30m had the lowest root-mean-squared-error (RMSE) of 4.1cm, followed by the VUX-1LR at 90m with a RMSE of 4.4cm. The VUX-1LR 60m flight was the most consistent with the highest coefficient of determination, however due to a positive bias, there was an RMSE of 4.5cm. The photogrammetry-based, below-canopy UAS was found to be an efficient and accurate method of extracting DBH and relative position of stems in forests.

Keywords: Unmanned Aerial System, Photogrammetry, Below-canopy UAV, VUX-1LR LiDAR, Radiata pine plantation, Forest Inventory

1. Introduction

The use of robotics to gather remotely sensed data is becoming widespread in scientific pursuits as well as in industries such as agriculture and forestry. Such systems make it practical to collect measurements over larger areas and at a higher frequency than when manual data collection methods or manned aircraft are used. The ongoing improvements in Unmanned Aerial Systems (UAS) have made it possible for farmers to rapidly collect high-resolution topographic maps of their fields to deal with drainage and erosion issues (Pineux et al., 2017), as well as monitor crops throughout the season for growth and health issues. Such technology allows farmers to improve local conditions and maximise yield from their crops (Reinecke and Prinsloo, 2017). The forestry sector is also benefiting from the rise of the robots. There have been many studies showing the effectiveness of UAS imagery and laser scanning for forest health monitoring (Dash et al., 2017; Näsi et al., 2015), forest inventory (Wallace at al., 2012; Hyyppä et al., 2008) and automated forest fire monitoring (Merino et al., 2012). UAS are conventionally operated above the forest for these applications, allowing for efficient data collection over large areas. However, there are situations where above-canopy remote sensing techniques face difficulties.

One of the challenges faced by above-canopy remote sensing methods is that when the canopy is dense, LiDAR and photogrammetric methods can fail to penetrate sufficiently to the subcanopy (Abalharth et al., 2015). In such situations, the information obtained from the canopy can be used to predict properties of the forest based on information from reference plots in a process known as imputation.

Reference datasets in dense forests can be obtained by manual plot measurements, terrestrial laser scanning (moving or stationary) and close-range, ground-based photogrammetry. These techniques can be very accurate, however are often time-consuming and laborious, especially so in areas of dense undergrowth. Forest workers can be required to traverse rough and potentially hazardous terrain to take measurements or to set up terrestrial laser scanning equipment.

Trips and falls are among the leading causes of injury to forest workers (Marshall et al., 1994; Tsioras et al., 2014). The application of robotics to the problem of collecting reference measurements of

forests could allow workers to operate robots remotely from a safe location. While robotic technologies are being developed for many aspects of forest management, planting and harvesting, the scope of this paper will be limited to robots for the collection of reference datasets for forest inventories.

There have been a number of studies investigating the use of robots for forest inventory applications, however many of these have been ground based and limited to gentle terrain with minimal or no understorey (Morita et al., 2018; Pierzchała et al., 2018) Chisholm et al. (2013) made one of the few attempts at below-canopy UAS forest surveys, however there has been very limited research so far on the potential of below-canopy UAS for mapping forests. The problem of aerial navigation within complex environments is something that is actively being researched (Cui et al., 2016; Giusti et al., 2015), and such technology can already be bought off-the-shelf in the form of consumer-off-the-shelf drones, however, these technologies have seen very limited application so far in below-canopy UAS forest mapping. There is much potential for future research on this topic.

Chisholm et al. (2013) used a 2D LiDAR mounted in a horizontal position for their below-canopy UAS and assumed that the UAS attitude did not change as a result of the slow and gentle flight. Using this approach, they generated a 2D map of the stems and were able to achieve a root-mean-squared-error (RMSE) accuracy of 25.1% for their diameter at breast height (DBH) measurements. They were able to detect 73% of the trees greater than 200 mm DBH that were within 3m of the UAS's flight path. This study appears to have been the only below-canopy UAS mapping paper of its kind so far.

In this study, a close-range photogrammetry approach was taken, partially inspired by Demetrios et al. (2015) who investigated the use of small-UAS-based photogrammetry for tree dimensionality assessment. Demetrios et al. investigated various flight patterns for the most complete reconstructions of trees using close-range, off-nadir photogrammetry. Since they measured single trees or small clumps of trees, they were able to rely upon GPS positioning to avoid collisions with obstacles. Sub-canopy flight in dense forests does not typically allow for highly accurate GPS positioning due to the absent or degraded GPS signal. The flight path would need to be meticulously planned between obstacles and followed with sub-meter accuracy. A few meters of inaccuracy would almost guarantee collisions (without pilot intervention) in an obstacle rich environment such as a forest. To achieve systematic flying patterns for sub-canopy flight, a high level of obstacle avoidance and sophisticated path planning would be required. The planning of an optimal flight path for capturing photogrammetric models in such an environment was outside the scope of this article, however this is an interesting challenge for future research.

This study aims to investigate the accuracy of sub-canopy UAS photogrammetry relative to aerial laser scanning and manual stem measurement in terms of ability to extract the DBH and position measurements of the stems.

2. Methods

2.1 Study Site

The study was performed in Carabost State Forest, in southern New South Wales, Australia, managed by Forestry Corporation of NSW. Two stand areas of 200 x 200m were selected, targeting a similar range of Pinus radiata structures. Both stands were mature and were pruned in 2004 and thinned in 2017. From these two stands, two plots were created, from here on referred to as Plot A and B. In Figure 1, Plot A is shown with minor ground debris in the plot and blackberry infestation in the background. Both plots contained 15 trees, giving a stem density of approximately 283 stems/hectare. The chosen sites had an open canopy which allowed the helicopter-mounted LiDAR scanner to penetrate thoroughly, providing a high-resolution dataset for comparison with the sub-canopy UAS point cloud.

Figure 1: Left – Photo showing canopy density of Plot A (photo courtesy of Interpine). Right – Photo of Plot A showing tree spacing and ground debris. This terrain could be challenging to walk over yet can be easily flown over (photo courtesy of Arko Lucieer, TerraLuma).

2.2 Manual Plot Method

A forest inventory was carried out in the study area in the same week of the remotely sensed data acquisition. The two plots were established in Plot A and B with a radius of 13.82 m (0.06 ha). The

PLOTSAFE (2007) protocol for the inventory was used by Interpine. For each tree, the diameter was measured with a measuring tape at 1.3 m above the base. If swelling or branching interfered with the measurement at this height, the measurement position can be shifted up to 10cm up or down. Where it was necessary to move more than 10 cm away, 2 equidistant measurements were taken above and below 1.3 m and averaged. The distances and bearings to the trees, from the center of the plot, were measured using a Haglof VL5 Vertex laser measurement device and a Suunto Kb-14 compass. The laser was handheld at 1.3 m above the ground at the plot centre and distances/bearings to each tree were taken level with this position. As the laser strikes the side of the tree nearest to the plot centre, the measurement is not to the tree centre. To correct for this, the measured tree radius is added to the measured distance as per Figure 2.

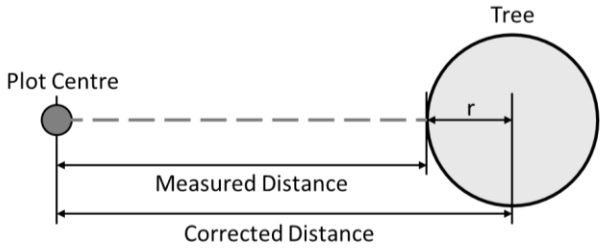

Figure 2 – Diagram showing distance correction applied to laser measurement of tree positions.

2.3 UAS Platform

The UAS platform was specifically designed for the task and consists of 3D-printed structural components and carbon-fiber tubing. The ~2kg aircraft was designed using Autodesk Inventor and can be seen in Figure 3. The upper section of the aircraft is a vibration-isolated payload housing containing a Pixhawk 2.1 flight-controller, Nvidia TX2 computer and telemetry systems. A modular attachment point on the payload housing allows for a rigid connection between the mapping sensor and the inertial measurement unit of the flight controller. The relatively high mass of the payload system minimises vibration transfer to the camera and flight controller; resulting in improvements to image quality and flight performance when compared to an airframe without vibration damping.

Figure 3: Left: A computer-generated model of the UAS. Right: The UAS in sub-canopy flight in a radiata pine forest, Carabost State Forest, NSW (photo courtesy of Arko Lucieer, TerraLuma).

2.4 Below Canopy UAS Photogrammetry Method

Aerial surveys are typically flown in a series of parallel lines, however due to the multitude of obstructions present in the forest, this approach would not work unless combined with advanced obstacle avoidance. In addition to this, the forward-facing camera should ideally face all sides of a tree for the most complete photogrammetric reconstruction. The trees were not in neat rows and the plot was circular. The best attempt was made to systematically cover all trees in the plot, however, due to the complexity of this environment and the need to point the camera at each tree in a variety of orientations, the coverage was not uniform, and the flight path was sub-optimal. Both of these challenges are well-suited to be dealt with through automation. Ground control targets were not used as this system is intended to operate in areas which are difficult for humans to traverse. If ground control points were required, humans would still need to place them throughout the plot, thus negating the benefits of this system.

Imagery was captured using a Stereolabs ZED stereo camera at 720p resolution and 60 frames per second. Images were extracted from the video to give approximately 1000 images per plot. Images were processed in the photogrammetry software MicMac (Rupnik et al., 2017).

The photogrammetric point clouds were each reconstructed in a single batch. Other photogrammetry packages such as Agisoft Photoscan and Colmap were tested, however only MicMac was able to reconstruct the full model without tree duplications or other problematic reconstruction errors (with the settings tested). Once the point cloud was generated, this was subjected to statistical outlier filtering in CloudCompare (Girardeau-Montaut , 2018), and was trimmed to a 15m radius. Any obvious noise was manually cleaned prior to post-processing. A photogrammetric reconstruction of Plot B can be seen in Figure 4.

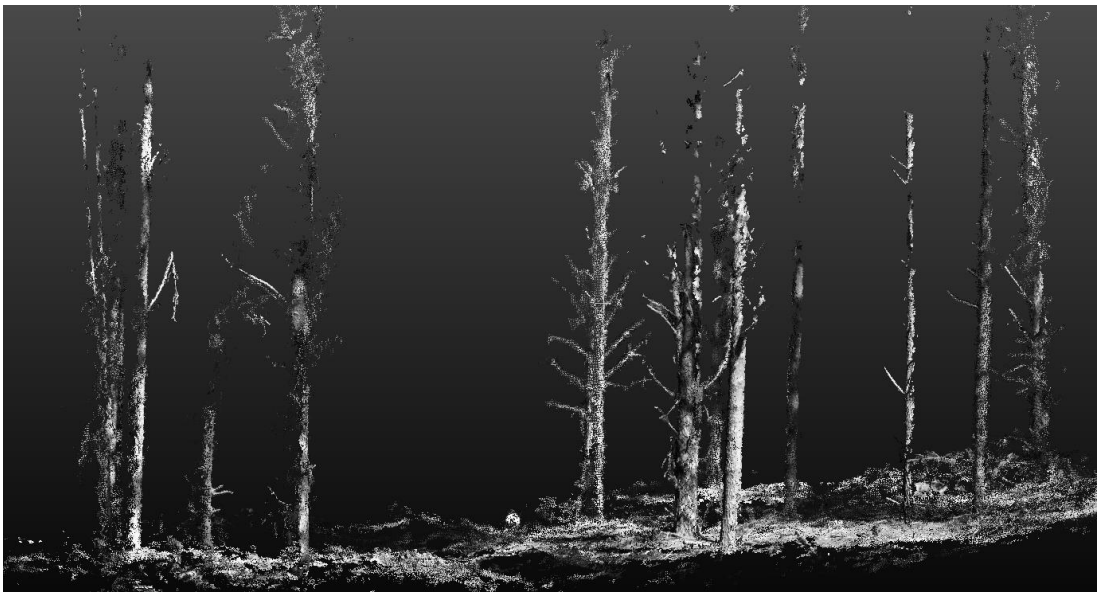

Figure 4: Photogrammetric reconstruction of Plot B from a sub-canopy UAS. The high-visibility marker ball representing the plot centre can be seen in the middle of the image on the ground.

2.5 Helicopter Platform

The LiDAR survey was carried out by Geomatics Technologies (Melbourne, Victoria) on the 22nd of February 2018 using a helicopter equipped with a Riegl VUX-1LR LiDAR sensor (specifications shown in Table 1, aircraft and LiDAR sensor shown in Figure 5). The survey consisted of three flights at altitudes of 30 m, 60 m and 90 m above ground level (AGL) over two plots. The tree canopy height was just under 30 m (AGL). Flight lines were set at 15m apart with 27 flight lines per flight altitude. The flight speed was set at 5 m/s. The frequency was set to 400Mhz and the maximum field of view of the sensor was 170°.

VUX-1LR Specifications	
Max. Range @ Target Reflectivity 60%	1,350 m
Max. Range @ Target Reflectivity 20%	820 m
Minimum Range	5 m
Accuracy/Precision	15 mm / 10 mm
Max. Effective Measurement Rate	750,000 meas./sec
Max. Scan Speed	200 scans/sec
Max. Field of View (FOV)	330°
Max. Operating Flight Altitude AGL	530 m / 1,740 ft
Inertial Measurement Unit (IMU)	Trimble Applanix AP20
Laser Beam Divergence	0.5 mrad
Laser Beam Footprint	15mm at 30m, 30mm at 60m, 45mm at 90m

Table 1: VUX-1LR LiDAR sensor specifications

Figure 5: Photos of the VUX-1LR LiDAR setup on the helicopter.

2.6 Helicopter-based VUX-1LR LiDAR Pre-processing

The raw LiDAR dataset was pre-processed with LAStools (Rapidlasso, 2017) and quality checked with LAStools and QTModeler (Applied Imagery, 2017) (Del Perugia et al., 2018) The dataset was clipped to a 15m radius around each plot centre.

The average point density for plot A was over 3,000 points/m2 with up to 7 returns per pulse. The average point density for plot B was over 4,000 points/m2 with up to 7 returns per pulse. An example of the point cloud generated using the VUX-1LR LiDAR can be seen in Figure 6.

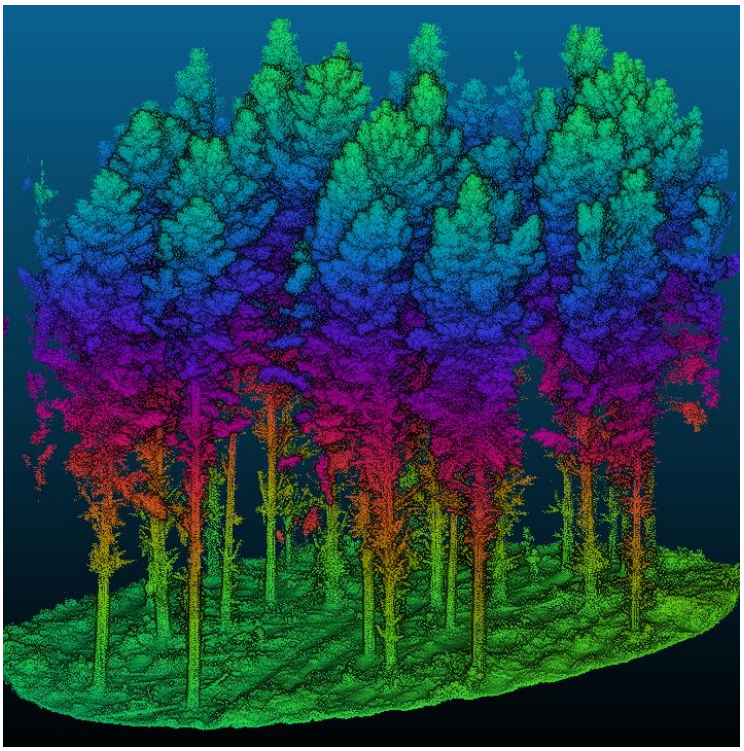

Figure 6: Point cloud from the helicopter mounted VUX-1LR LiDAR visualised in CloudCompare [20].

2.7 Measurement extraction from the Point Clouds (BCUAS and VUX-1LR-LiDAR)

The point clouds were exported from CloudCompare as LAS files so that they can be imported into DendroCloud (Koreň et al., 2017). A 1.5m resolution digital terrain model (DTM) is created using the lowest points and used to slice the point clouds between 1.15m and 1.45m above the DTM. This provides a slice of the tree at approximately breast height (1.3m). The slice height of 0.3m was chosen as smaller slices made circle fitting less accurate with the LiDAR datasets on some trees. This slice was exported/imported into CloudCompare for cleaning of the stem slices. As the slices revealed minor reconstruction errors and branching, the stem circles were not easily processed automatically. For this reason, the cleaning of the slices was performed manually. Branches were removed, and the clearest stem circle was kept from the point cloud in the event of two stem circles being present for a single tree. Figure 7 shows an example of branch points being removed using CloudCompare. Wherever there was doubt about whether or not a point represents the stem, the full point cloud was consulted to see if the point is likely to be part of the main stem or a branch. If it was still unclear, the point was not removed.

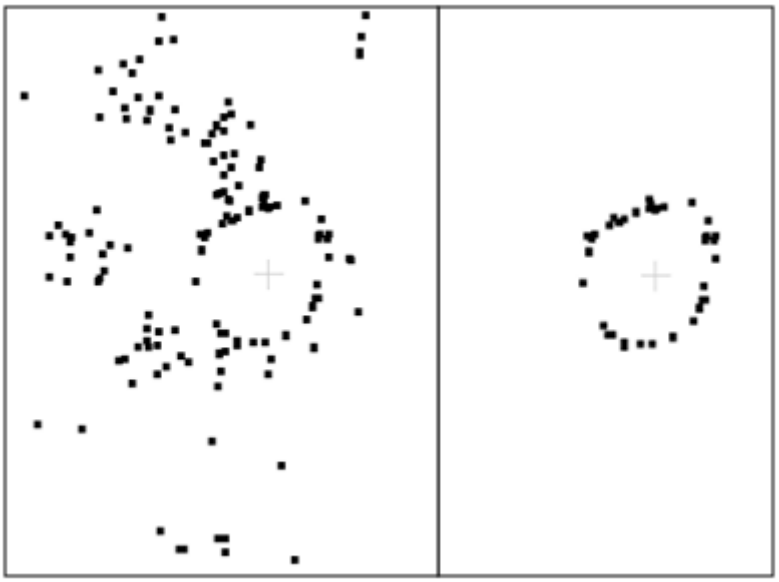

Figure 7: Stem slices were cleaned manually to remove branching. Left, stem circle before manual cleaning. Right, stem circle after manual cleaning. If there was any doubt about whether or not a point belonged to a stem, the point was not removed.

The cleaned stem slices were exported/imported back into DendroCloud, where the clustering and circle fitting tools were applied. The clustering groups the points into individual tree groups so that the circles can be fitted to points belonging to the same stem. The “Optimal Circle Method” with the Monte Carlo option, described by Koreň et. al. (2016), was used to fit circles to the cleaned stem circles. This data was exported to a CSV file for further analysis.

2.8 Comparison of the Measurements

Once measurements have been extracted, these measurements needed to be compared with the other measurements of the same tree. In order to automate this process and avoid human errors when matching the data, a Python script was written to match the data on a tree by tree basis. If a datapoint was within a given radius of a reference tree position (manually measured position), measurements were considered to be from the same tree. The script matches the data and allows the user to visually inspect these results to minimize the risk of comparing measurements of two different trees by mistake. An example of this visualization can be seen in Figure 9 in the results section. The aligned datasets were then compared using the SciPy – Statistics [27] package to fit a linear regression to the data.

3. Results

3.1 Diameter at Breast Height Comparison

Figure 8 shows the linear regression models fitted to the data. The manual measurement of DBH for each individual tree provides the x axis and the DBH measured from the same tree measured with a remotely sensed technique provides the y axis. A perfect agreement between the manual and remotely sensed measurements would result in the equation of $y = Ax + B$ where $A = 1$ and $B = 0$, a coefficient of determination equal to 1 and a root-mean-squared-error (RMSE) of 0. The below-canopy UAS and the VUX-1LR LiDAR at 30 m had the lowest RMSE of 4.1 cm, with the 60 m and 90 m altitude VUX-1LR flights achieving a RMSE of 4.5 cm and 4.4 cm respectively. All fitted models were statistically significant ($p < 0.001$) for the sample size of 30 trees. The 60 m altitude VUX-1LR measurements had the highest coefficient of determination (R2) indicating the most consistent measurement method, however this data overestimated the diameters by 3.5 cm on average, which penalized this data in the RMSE comparison.

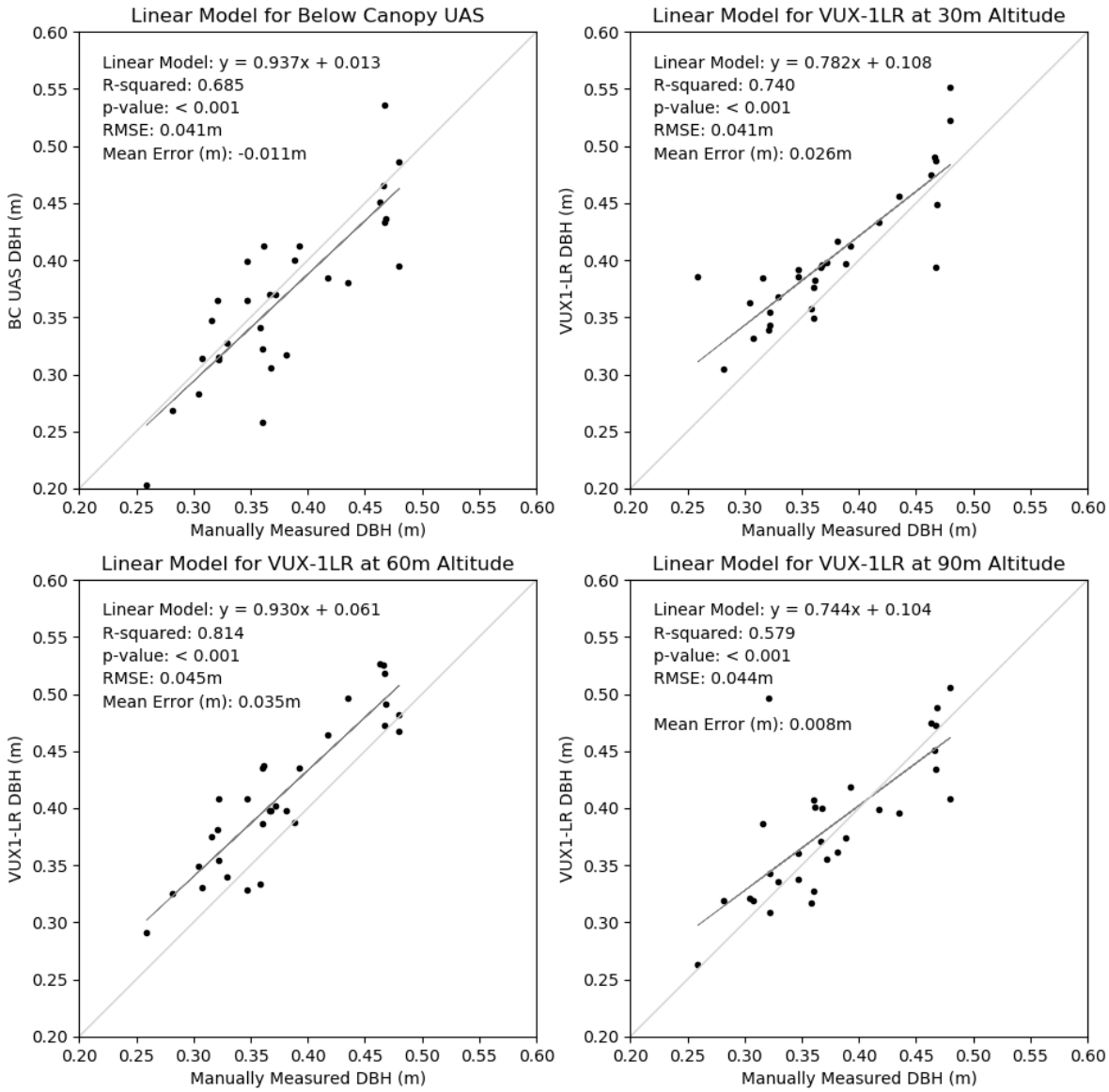

Figure 8: Linear regression of the individual tree measurements of diameter at breast height (DBH), showing the measurements of the remote sensing systems in comparison to the manually taken measurements on a tree-by-tree basis.

With the exception of some outliers, all methods gave reasonably accurate predictions of the DBH at an individual tree level relative to the manually measured DBH. No trees within the 13.82 m radius plot were missed by any of the methods.

3.2 Relative Position Comparison

In the VUX-1LR LiDAR point clouds, the plot centre marker was not easily recognizable, so a clear plot centre was not able to be used for comparison of tree locations. For this reason, the datapoints had to be aligned using the tree centre locations. All tree centre positions were found to reside within 0.6

m of all other matching tree positions for both plots. A map of the stems at Plot A can be seen in Figure 9.

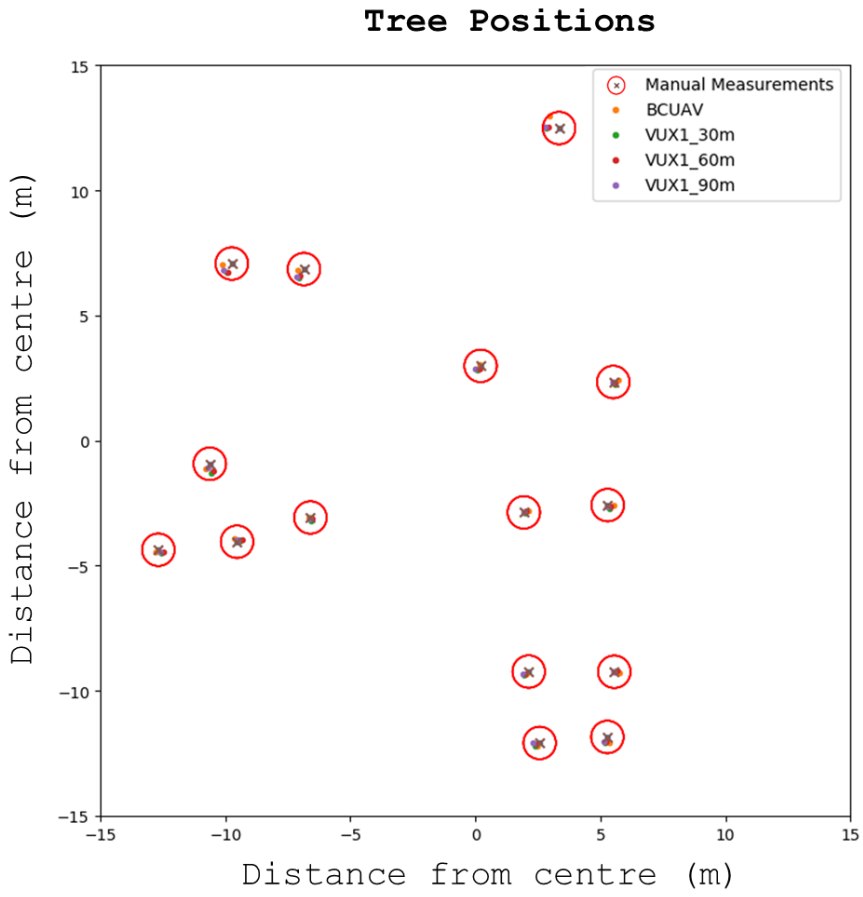

Figure 9: Tree positions from Plot A, showing position estimates from a manual plot, airborne laser scanning from a VUX-1LR LiDAR and a below-canopy, photogrammetry based UAS mapping system. Red circles indicate a 0.6 m radius from the manually measured position.

3.3 Limitations

There were limitations to this study which should be noted. The manual removal of branches and noise from the point cloud slices is subject to human error and bias and would have affected the results slightly, however all possible care was taken to be consistent and impartial in this process. The manually measured reference positions were taken from a handheld position rather than from a tripod, so the accuracy of the bearing and distance measurements would have been influenced by the steadiness and skill of the operator.

4. Discussion

The below-canopy UAS photogrammetry technique demonstrated shows promising results when compared to those obtained with a high-end VUX-1LR LiDAR scanner. This approach has been shown to be both a cost and time-efficient method of collecting reference data from beneath the canopy with less field time required than for manual measurements. With greater autonomy, it is foreseeable that such a system has the potential to change the way reference plots are measured where highly accurate data is required for imputation purposes. This technology is not intended to replace above-canopy remote sensing techniques, instead it should be considered to be a complementary technology; one which can capture data in places where above-canopy techniques face limitations.
The next stage of this research will see the system tested in denser forests where above-canopy techniques would be unable to capture information from the stems directly. Further research will seek to automate the navigation beneath the canopy, as well as explore different flying patterns and sensor choice on the completeness and accuracy of the model reconstruction.

5. Conclusion

Two plots of radiata pine forest were measured using a photogrammetry-based below-canopy UAS, a helicopter mounted, VUX-1LR LiDAR at heights of 30 m, 60 m, and 90 m above ground level, and manually using measuring tapes. The aim of this study was to test whether below-canopy UAS photogrammetry was able to obtain comparable accuracy to manual measurements of DBH, and to compare these results with those obtained using a high-quality aerial laser scanner. To compare the results, a linear model was fitted to each dataset relative to the manual measurements of DBH. The below-canopy UAS and the VUX-1LR at 30 m had the lowest RMSE of 4.1 cm, followed by the VUX-1LR at 90 m with an RMSE of 4.4 cm. The VUX-1LR 60 m flight was the most consistent with the highest coefficient of determination, however due to an average overestimation of 3.5 cm, there was an RMSE of 4.5 cm. The photogrammetry-based below-canopy UAS was found to be an efficient and accurate method of extracting DBH and relative position of stems in forests. This study is believed to be the first of its kind to investigate the use of below-canopy UAS photogrammetry for forest inventory applications. Further research will investigate the automation of this process and explore

the effect of flying patterns on the accuracy and completeness of the data captured in denser forests, where above canopy techniques cannot capture sufficient sub-canopy information.

Acknowledgements

Interpine Group Ltd for providing field measurements, LiDAR data and to Susana Gonzalez for designing the flight path for the LiDAR acquisition.

Maciej Matuszak (University of Tasmania) for his incredibly valuable help with setting up the Nvidia TX2 in a very short time-frame.

The TerraLuma (University of Tasmania) team for their assistance in transporting equipment interstate and for use of their plot photos.

Future Forest Research for allowing us to participate in this remote sensing campaign.

Australian Research Council - Centre for Forest Value for providing my PhD scholarship.

References

Abalharth M., Hassan M. A., Klinkenberg B., Leung V., McCleary R. (2015) Using LiDAR to characterize logjams in lowland rivers. Geomorphology, 246, 531-541

Dash J. P., Watt M. S., Pearse G. D., Heaphya M., Dungeya H. S. (2017) Assessing very high resolution UAV imagery for monitoring forest health during a simulated disease outbreak. ISPRS Journal of Photogrammetry and Remote Sensing, 131, 1-14 https://doi.org/10.1016/j.isprsjprs.2017.07.007

Chisholm R. A., Cui J., Lum S. K. Y., Che B. M. (2013) UAV LiDAR for below-canopy forest surveys. Journal of Unmanned Vehicle Systems, 01(01), 61-68

Cui J. Q., Lai S., Dong X. (2015) Autonomous Navigation of UAV in Foliage Environment. Journal of intelligent & robotic systems. 84(1-4), pp 259-276.

Del Perugia B., Travaglini D., Chirici G., Aracil Gonzalez S. Optimal acquisition specifications for the Riegl VUX-1LR over a Pinus radiata plantation. ((Due for publication 2019)).

Gatziolis D., Lienard J. F., Vogs A. Nikolay, Strigul S. (2015) 3D Tree Dimensionality Assessment Using Photogrammetry and Small Unmanned Aerial Vehicles. PLOS ONE, 10(9), e0137765.

Giusti A., Guzzi J., Ciresan D. C., He F., Rodríguez J. P., Fontana F., Faessler M., Forster C., Schmidhuber J., Di Caro G., Scaramuzza D., Gambardella L. M. (2016) A Machine Learning Approach to Visual Perception of Forest Trails for Mobile Robots. IEEE Robotics and Automation Letters, 1(2), 661-667

Koreň M., Mokroš M., Bucha T. (2017) Accuracy of tree diameter estimation from terrestrial laser scanning by circle-fitting methods," International Journal of Applied Earth Observation and Geoinformation, 63, 122-128.

Hyyppä J., Hyyppä H., Leckie D., Gougeon F., Yu X., Maltamo M. (2008) Review of methods of small-footprint airborne laser scanning for extracting forest inventory data in boreal forests, International Journal of Remote Sensing, v.29 n.5, p.1339-1366. Doi: 10.1080/01431160701736489

Jones E., Oliphant T., Peterson P. (2001) SciPy: Open Source Scientific Tools for Python.

Marshall S. W., Kawachi I., Cryer P. C., Wright D., Slappendel C., Laird I. (1994) The epidemiology of forestry work-related injuries in New Zealand, 1975-88: fatalities and hospitalisations. The New Zealand Medical Journal, 107(988):434-437.

Merino L., Caballero F., Martínez-de-Dios J. R J., Maza I., Ollero A. (2012) An Unmanned Aircraft System for Automatic Forest Fire Monitoring and Measurement. Journal of Intelligent & Robotic Systems, 65(1), 533-548.

Morita M., Nishida T., Arita Y. (2018) Development of robot for 3D measurement of forest environment. Journal of Robotics and Mechatronics, 30(1), 145-154.

Näsi R., Honkavaara E., Lyytikäinen-Saarenmaa P., Blomqvist M., Litkey P., Hakala T., Viljanen N., Kantola T., Tanhuanpää T., Holopainen M. (2015) Using UAV-Based Photogrammetry and Hyperspectral Imaging for Mapping Bark Beetle Damage at Tree-Level. Remote Sensing, 7(11), 15467.

Pierzchała M., Giguère P., Astrup R. (2018) Mapping forests using an unmanned ground vehicle with 3D LiDAR and graph-SLAM. Computers and Electronics in Agriculture, 145, 217-225.

Pineux N., Lisein J., Swerts G., Bielders C. L., Lejeune P., Colinet G., Degré A. (2017) Can DEM time series produced by UAV be used to quantify diffuse erosion in an agricultural watershed?. Geomorphology, 280, 122-136.

PLOTSAFE Overlapping Feature Cruising Forest Inventory Procedures, (2007).

Reinecke M., Prinsloo T. (2017) The influence of drone monitoring on crop health and harvest size. IEEE 1st International Conference in Next Generation Computing Applications (NextComp), pp. 5-10.

Rupnik E., Daakir M., Pierrot Deseilligny M. (2017) MicMac – a free, open-source solution for photogrammetry. Open Geospatial Data, Software and Standards, 2(1), 14.

RIEGL Laser Measurement Systems (2015) Technical Data RIEGL VUX-1LR.

Tsioras P. A., Rottensteiner C., StampferK. (2014) Wood harvesting accidents in the Austrian State Forest Enterprise 2000–2009. Safety Science, 62, 400-408.

Wallace L., Lucieer A., Turner D., Watson C. (2011) Error assessment and mitigation for hyper-temporal UAV-borne LiDAR surveys of forest inventory," Proceedings of Silvilaser, 1-13.

Wallace L., Lucieer A., Watson C., Turren D. (2012) Development of a UAV-LiDAR System with Application to Forest Inventory. Remote Sensing, 4(6), 1519.

Paper IV

Automatic detection of diameter in an ultra-dense point cloud.

Barbara Del Perugia[1], Davide Travaglini[1], Gherardo Chirici[1], Susana Gonzalez Aracil[2]

[1] geoLAB Laboratory of Forest Geomatics - Department of Agricultural, Food and Forestry Systems, University of Florence; barbara.delperugia@unifi.it

[2] Interpine Group Ltd, 99 Sala Street, Rotorua, New Zealand; susana.gonzalez@interpine.nz

*Corresponding Author: barbara.delperugia@unifi.it

Abstract

The diameter at breast height (DBH) is one of the most important parameters required for forest inventory. Several studies have tested methods for DBH detection and estimation with laser scanning techniques, such as Terrestrial Laser Scanner (TLS) and the derived point clouds. However, only few studies have tested the performance of Airborne Laser Scanner (ALS) point clouds for such purposes. The new generation of LiDAR sensors for ALS survey can acquire ultra-dense point clouds that could be used for diameter estimation. In this study we assessed the performance of three different methods for automatic diameter detection and estimation from a ultra-dense ALS point cloud. Two open source software were used: DendroCloud software and TreeLS R package. DendroCloud is based on two refining (Monte Carlo and Optimal circle) circle-fitting methods for DBH estimation, while TreeLS is based on Hough Transformation with RANSAC technique. The accuracy of diameter estimation was evaluated using field measurements as reference data. Our results show that 98% of the stems were detected. The accuracy of circle-fitting methods was significantly different from the accuracy of Hough Transformation method with RANSAC technique. The Hough Transformation algorithm implemented in the TreeLS package proved to be the most accurate method for diameter estimation, achieving an average R^2 of 0.85 and an average RMSE of 1.96cm.

Keywords: ALS, VUX-1LR LiDAR, Radiata pine plantation, Forest Inventory, DBH, automatic detection

1. Introduction

Airborne Laser Scanning (ALS) application to forest measurements has been shown to be effective for estimating forest inventory variables. The combined use of ALS and forest inventory data has effectively increased the estimation of forest stand characteristics such as growing stock volume and biomass (Næsset, 2002, Næsset, 2007; McRoberts et al., 2013).

Remotely sensed data have been tested for single-tree attribute estimation. Terrestrial Laser Scanner (TLS) has been proven to provide accurate and high resolution data at tree level (Liang et al., 2016), and several studies have tested methods for single-tree modelling from TLS data (Bienert et al., 2007; Maas et al., 2008; Liang et al., 2012).

Diameter at Breast Height (DBH) is one of the most important parameters required in forest inventory, which is usually measured with callipers or DBH tapes at 1.30m height. Several studies have been carried out with a focus on DBH detection from TLS point cloud (Liang and Hyyppä, 2013; Kankare et al., 2015; Cabo et al., 2018). In these studies, DBH is calculated using different methods such as cylindrical or circular least squares fitting methods (Hopkinson et al., 2004; Henning and Radtke, 2006; Koreň et al., 2017;) and Hough transform for circle fitting (Hough, 1962; de Conto et al., 2017). An overview of studies focused on DBH estimation from TLS point clouds was conducted by Pueschel et al. (2013). DBH bias reported by authors varied from underestimation of −1.5cm to overestimation greater than 4cm.

Circle fitting is a mathematical problem subject of many works (Čerňava et al., 2017; Koreň et al., 2017). The position and diameter of the circle can be estimated by circle-fitting algorithms from a spatial cluster of points like the LiDAR point cloud. Circle-fitting methods are based on horizontal cross-sectional slices of point clouds (Koreň et al., 2017). Using these methods for DBH estimation from TLS data, Koreň et al. (2017) obtained an absolute value of bias smaller than 1cm.

Hough Transform (Hough, 1962; Aschoff and Spiecker, 2004; de Conto et al., 2017) is a feature extraction technique used in image analysis. Hough Transform is a method for detecting lines, circle and other parameterized shapes in raster images. It has been successfully used in several field of computer vision, and digital image processing (Hulk et al., 2014; Yao and Yi, 2016; Mukhopadhyay and Chaudhuri, 2015). de Conto et al. (2017), using the Hough transformation method for DBH detection from TLS point cloud obtained a RMSE of 2.15cm and a bias of 1.09cm.

However, few studies have tested the potential of ALS point clouds for DBH detection (Brede et al., 2017; Dalponte et al., 2018; Krisanski et al., 2018) because ALS acquisition density is lower than TLS, usually in the order of 1 to 10 points/m^2 against millions of points per scan position provided by TLS acquisition (Brede et al., 2017). The current LiDAR technology can acquire very accurate, ultra-dense point cloud suitable for testing algorithms originally developed for TLS point clouds. For instance, Brede et al. (2017) using the Riegl VUX-1UAV sensor obtained a point density of 140 points/m^2 for a single flight line and an average plot density of ~3000 points/m^2, which was successfully used to detect single-tree attributes. Wallace et al. (2012) using the Ibeo LUX laser scanner produced point clouds with up to 50 points/m^2, and Jaakkola et al. (2010) obtained point clouds with 100 to 1500 points/m^2 integrating an Ibeo Lux with a Sick LMS151 profile scanner.

In this study we tested the VUX-1LR LiDAR sensor for DBH estimation from ultra-dense ALS point clouds using three different methods. We compared the use of DendroCloud software with two circle-fitting methods, and the R package TreeLS based on Hugh Transformation method. The accuracy of diameter estimation was evaluated using field measurements as reference data.

2. Material and methods

2.1 Study Area

The study was carried out in the Carabost State Forest, near Tumut, in southern New South Wales (NSW), Australia, managed by Forestry Corporation of NSW. Four sites of 4ha each (200x200m) were selected targeting a different range of Pinus radiata plantation (Figure 1). Two sites (1 and 4) were planted in 1995 and two sites (2 and 3) were planted in 1987. The stands were regularly pruned and thinned, except for site 2 whose first thinning was delayed and the second not performed yet. The average tree density in the four sites was 272 trees/ha, with a maximum of 500 trees/ha and a minimum of 133 trees/ha.

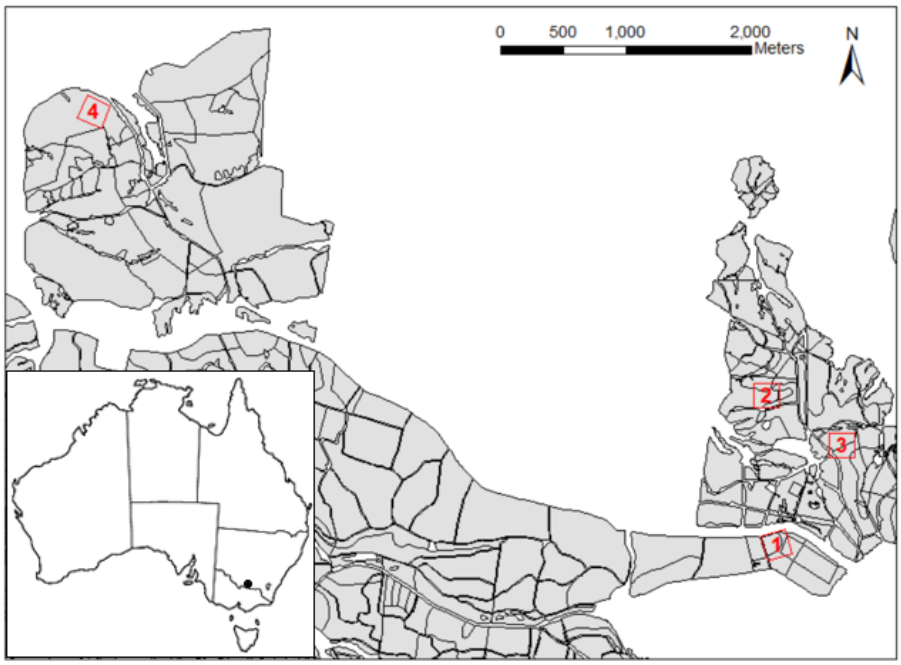

Figure 1. Map presenting the location of Tumut, NSW, Australia (on the bottom left), and the location of the study sites (red boxes). Scale 1:22,000.

2.2 Airborne laser scanning data

In February 2018, a flight was carried out by Geomatics Technologies (Melbourne, Victoria) using a helicopter equipped with a Riegl VUX-1 Long Range LiDAR sensor.

This sensor is a very light-weight (3.5kg) and compact (227x180x125 mm) laser instrument. The light-weight, survey-grade laser scanner was set with a Field Of View (FOV) of 170° and a pulse repetition frequency of 400Mhz. The flight speed was set at 5m/s or 10knots. Flight lines were set at 15m apart each other, with a total of 27 flight lines for each study site. The flight altitude was 60m Above Ground Level (AGL). The LiDAR point cloud resulted ultra-dense, with an average point density of 121 points/m^2 for a single flight line and an average plot density of 6,435 returns/m^2 (Figure 2).

The Riegl VUX-1LR dataset used in this study was acquired as part of a FWPA Trans-Tasman project (PNC377-1516) that links forest inventory and data processing to optimize remotely acquired, dense point cloud data for plantation inventory.

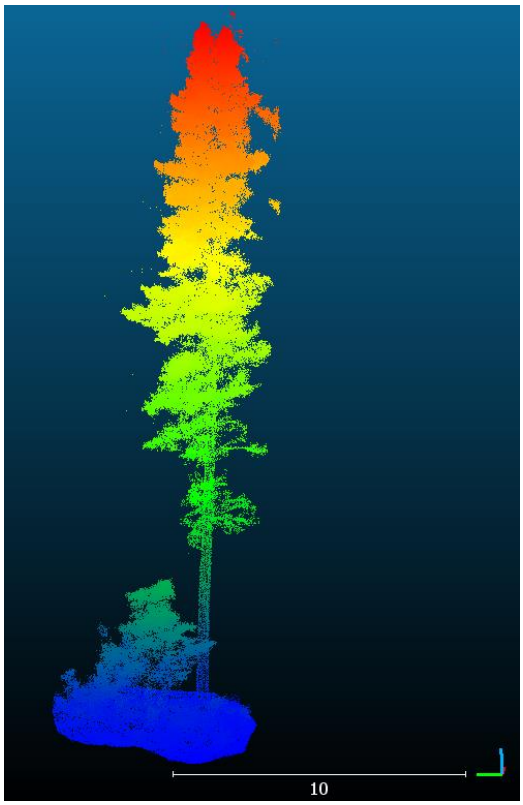

Figure 2. Example of the point cloud of a single tree (Plot 1 - Site 2).

2.3 Field data

Field work was carried out in the study sites during the same week of the LiDAR acquisition. Nine circular plots were established with a radius of 13.82m (=0.06ha). Three plots were located in site 2 and two plots were positioned in sites 1, 3 and 4. Field data were collected with Juniper Allegro 2 field computer using the software PLOTSAFE (2007) developed by Silmetra Ltd, Tokoroa, New Zealand. For each tree the position was noted and the DBH was measured. According to the PLOTSAFE protocol, the x,y coordinates of the plot centre were collected using a Trimble® Geo 7X receiver connected to an external high quality GNSS antenna, with a positional error of 5-50cm in post processing. Each tree was marked with a unique identifier (TreeId). For each tree the position was recorded by measuring the distance from the plot centre and the azimuth. The distance was measured using a Vertex Haglof VL5 and the azimuth with a Suunto Kb-14 compass. The DBH was measured at 1.30m from the ground with a DBH tape. The PLOTSAFE protocol established that the collecting point for the DBH may be shifted up or down a maximum of 10cm to remove the effect of the swelling; if a shift higher than 10cm is required, the diameter should be taken equidistant above and below the breast height and then averaged. The tolerance for the diameter measurement is

0.5cm up to a diameter of 50cm and 1cm for diameter over 50cm. The collected field data was processed and used as a reference for the validation of the VUX-1LR datasets.

A summary statistics of field data for the plots is reported in Table 1.

Site	Plot	Num. of measured trees	DBH minimum	DBH maximum	DBH mean	DBH standard deviation
1	1	30	23.5	42.5	31.6	4.7
	2	25	13.7	48.3	30.0	7.5
2	3	15	28.2	46.8	36.1	4.7
	4	15	25.1	49.1	37.5	5.4
	5	12	27.7	48.0	37.5	6.1
3	6	15	25.9	48.0	39.3	7.6
	7	17	31.1	46.1	38.2	4.3
4	8	8	31.0	51.9	41.5	6.4
	9	10	22.5	52.0	36.7	10.0

Table 1. Summary statistics of field data for all plots; DBH are reported in centimetres.

2.4 Data processing for DBH estimation

The LiDAR point cloud was divided by site and classified with LAStools (version 14 September 2017-rapidlasso GmbH) as ground and non-ground points. The quality of the VUX-1LR dataset was checked using LAStools and QTModeler (8.0.7 - Quick Terrain Modeler, Applied Imagery) software. The overlap of flights lines and the ground coverage were checked to evaluate an adequate coverage of the study sites by the LiDAR survey. LAStools was used to normalize the heights of non-ground points into relative heights above ground.

For a consistent comparison with the reference DBH measured in the field, the normalized point cloud was sliced into horizontal cross-sections between 1m and 2m above ground. Given the high density of the dataset only the “last only” points were kept in the slices.

To estimate the diameters in the point cloud a clustering procedure based on spatial density aggregation was developed in this study and applied to the horizontal cross-sections. The distribution of the points in the horizontal cross-sections was transformed in a raster of density, number of points per unit area. The density was calculated by applying kernel smoothing algorithm based on Berman

and Diggle (1989) method with a function of R package *spatstat.* The density information was transformed into contours of equal value, like those used to represent elevations. The contours levels were converted into polygons, the clusters. A buffer of 0.08m (value established based on the visual inspection of the point clouds) was generated around each cluster to ensure the inclusion of all the points of the stems. Clusters with areas greater than $3m^2$ (value established based on field observations and visual inspection of the point clouds) were excluded to remove most of the noise present in the plots due to low branches or shrubs. The horizontal cross-section of the point cloud was clipped with the cluster polygons.

Circle-fitting and Hough transformation methods were used to estimates the diameters of the stems. DendroCloud software was used to test circle-fitting methods. In this software, five circle-fitting algorithms are available to estimate the diameters and the centres of the stems. The algorithms are divided into two categories, "initial methods" and "refining methods". The initial methods derive the position and the diameter of a stem based on basic measurements of geometrical properties of the spatial cluster of points. The refining methods use optimization algorithms to minimize the distance between the derived circle and the set of points in the spatial cluster representing the horizontal cross-section of a stem; the distance is measured using root mean square error (Koreň et al., 2017):

$$RMSE_D = \sqrt{\frac{\sum_{i=1}^{n}(r_i - r)^2}{n}}$$

where r is the radius of the derived circle, r_i is the Euclidean distance between the point $P_i = (x_i, y_i)$ and the centre $P = (x, y)$ of the derived circle, and n is the number of points in the spatial cluster.

The two refining methods available in DendroCloud were tested: Monte Carlo and Optimal Circle. The Monte Carlo (MC) method improves the initial estimation of a circle's position and diameter by generating many small shifts in diameter and position of the circle until the maximum allowed number of repetitions is reached or until the required accuracy of the stem approximation is met. The Optimal Circle (OC) method uses multidimensional mathematical optimization algorithm to find the circle with minimum value of $RMSE_D$ (Koreň et al., 2017). Points in the cross-section grouped with the spatial clustering procedure developed in this study were processed with DendroCloud software using the following criteria: a point was assigned to a cluster group if the distance of the point from other points in the group was less than or equal to a threshold of 1 cm; clusters with less than 50 points were not considered for tree identification and DBH estimation, as groups with a small number of points usually corresponded to low branches or shrubs. The spatial clusters were used to estimate the diameters with circle-fitting methods (MC and OC). To match the automatic diameter detection

with the reference data, the Euclidean distance between the centre of the clustered stems and the field tree location was computed, then the attributes TreeId and DBH of the field dataset were assigned to the clusters.

The R package TreeLS (de Conto et al., 2017) was used to test the Hough transformation method for DBH estimation. The clusters obtained with the spatial clustering procedure developed in this study were used as data input. TreeLS package was designed for terrestrial laser scanning data, which are usually denser than ALS data. The functions process individual tree points clouds from the dataset, focusing on stem isolation algorithms. The diameter detection is based on Hough transformation with Random Sample Consensus (RANSAC) techniques. The Hough transformation algorithm searches for primitive shapes on raster datasets through a voting technique, that for each pixel determine all the possible shapes (in our case circular shapes) that are compatible with the pixel and cast a "vote" for its parameter sets (coordinate centre and radius in case of a circular shape). The sets of parameters with most votes are then found (Mukhopadhyay and Chaudhuri, 2015). The Hough transformation algorithm implemented in TreeLS package (de Conto et al., 2017) is adapted to find circular shapes on two dimensional horizontal layers of the point clouds. TreeLS sub-divided the point cloud in smaller intervals providing as result three potential diameters. The diameter more similar to the reference diameter was selected. The Euclidean distance between the centre of the detected stems and the field trees location was computed to match the estimated diameters to the reference data.

The performances of circle-fitting and Hough transformation methods were assessed by comparing estimated diameters with field measurements. Coefficient of determination (R^2) and root mean square error (RMSE) were computed:

$$RMSE = \sqrt{\frac{\sum_{i=1}^{n}\left(\hat{d}_i - d_i\right)^2}{n}}$$

where $\hat{d}_i$ is the estimated diameter at the ith observation, d_i is the observed diameter at the ith observation and n is the number of observations.

A statistical analysis based on absolute error between observed and estimated values was carried out to investigate statistically significant differences between the methods. The normality of the variable was tested by means of the Kolmogorov-Smirnov Tests after a logarithmic transformation. ANOVA and post-hoc test (Duncan test) were used.

4.Results

On a total of 147 trees, only two trees were not detected in the ultra-dense point cloud cross-sections (98% of success). 12 spatial clusters (8% of the cases) were affected by noise due to low branches or shrubs, which were highly present in some plots.

The accuracy of DBH estimation obtained with circle-fitting methods using DendroCloud software is reported in Table 2. Using Monte Carlo (MC) algorithm R^2 varied between 0.239 and 0.943, with an average value of 0.677, and RMSE varied between 1.25cm and 5.85cm, with an average value of 3.18cm. Using the Optimal Circle (OC) algorithm R^2 varied between 0.238 and 0.908, with an average value of 0.650, and RMSE varied between 1.26cm and 6.84cm, with an average value of 3.63cm. Figure 3 shows an example of diameter detection with circle-fitting methods.

The results of the accuracy of DBH estimation achieved with Hough transformation method with RANSAC technique implemented in TreeLS software are reported in Table 2. The Hough transformation algorithm had a higher performance compared to circle-fitting algorithms for diameter estimation. Using Hough transformation method R^2 varied between 0.607 and 0.975, with an average value of 0.853, and RMSE varied between 1.10cm and 3.6cm, with an average value of 1.96cm. An example of diameter detection with Hough transformation algorithm is reported in Figure 4. The reference data DBH values regressed against estimated DBH values by TreeLS with Hough transformation method are plotted in Figure 5.

Site	Plot	MC		OC		TreeLS	
		R^2	RMSE	R^2	RMSE	R^2	RMSE
1	1	0.543	2.36	0.453	2.45	0.607	2.50
	2	0.239	4.21	0.238	4.49	0.868	2.10
2	3	0.740	2.78	0.715	2.98	0.945	1.60
	4	0.916	1.25	0.877	1.26	0.928	1.10
	5	0.943	1.77	0.908	2.24	0.893	1.70
3	6	0.801	5.20	0.803	6.03	0.831	3.60
	7	0.609	3.23	0.571	4.06	0.683	2.70
4	8	0.896	1.96	0.885	2.29	0.945	1.20
	9	0.402	5.85	0.399	6.84	0.975	1.10

Table 2. Accuracy of DBH estimation with circle-fitting methods (MC = Monte Carlo, OC = Optimal Circle) and Hough transformation with RANSAC (TreeLS) technique. RMSE is in cm.

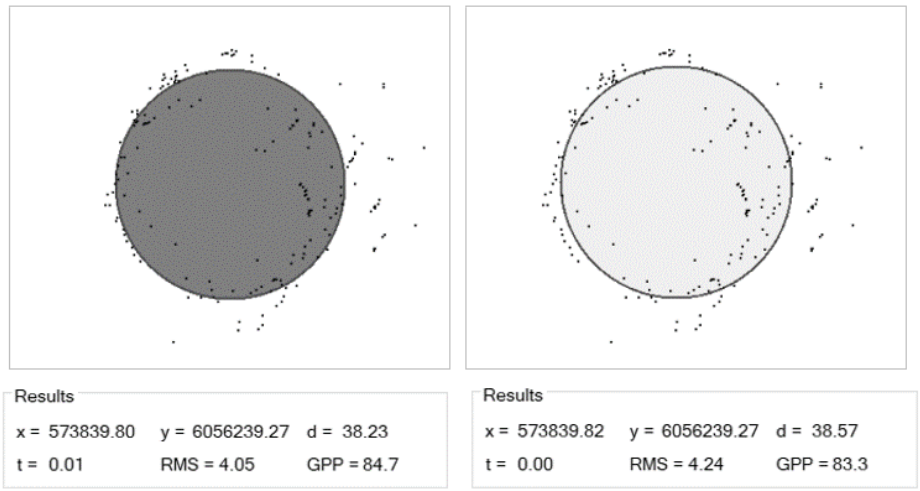

Figure 3. Example of circle detection with DendroCloud software using Monte Carlo algorithm (on the left side) and Optimal Circle algorithm (on the right side). Horizontal cross-section of cluster number 2, plot 4. In the box, the following information are reported: coordinates of the cross-section's centre (x, y), computation time (t, in milliseconds), estimation of the diameter (d), root mean square error ($RMSE_D$) and estimation of the girth coverage by points (GPP, %).

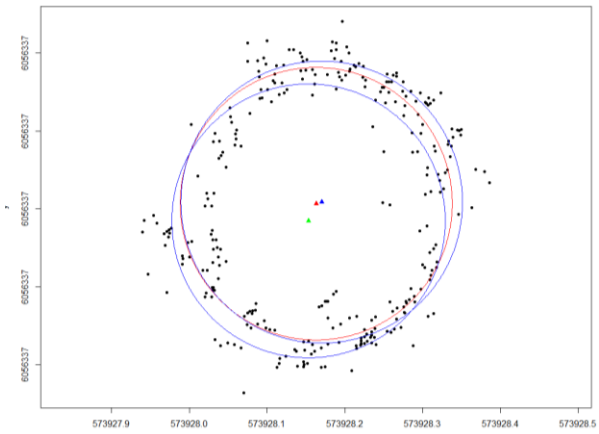

Figure 4. Example of circle detection with TreeLS software using Hough transformation with RANSAC algorithm. Horizontal cross-section of tree number 1, plot 4. The three diameters estimated by TreeLS are marked in different colour. The diameter more similar to the reference diameter was selected for accuracy assessment.

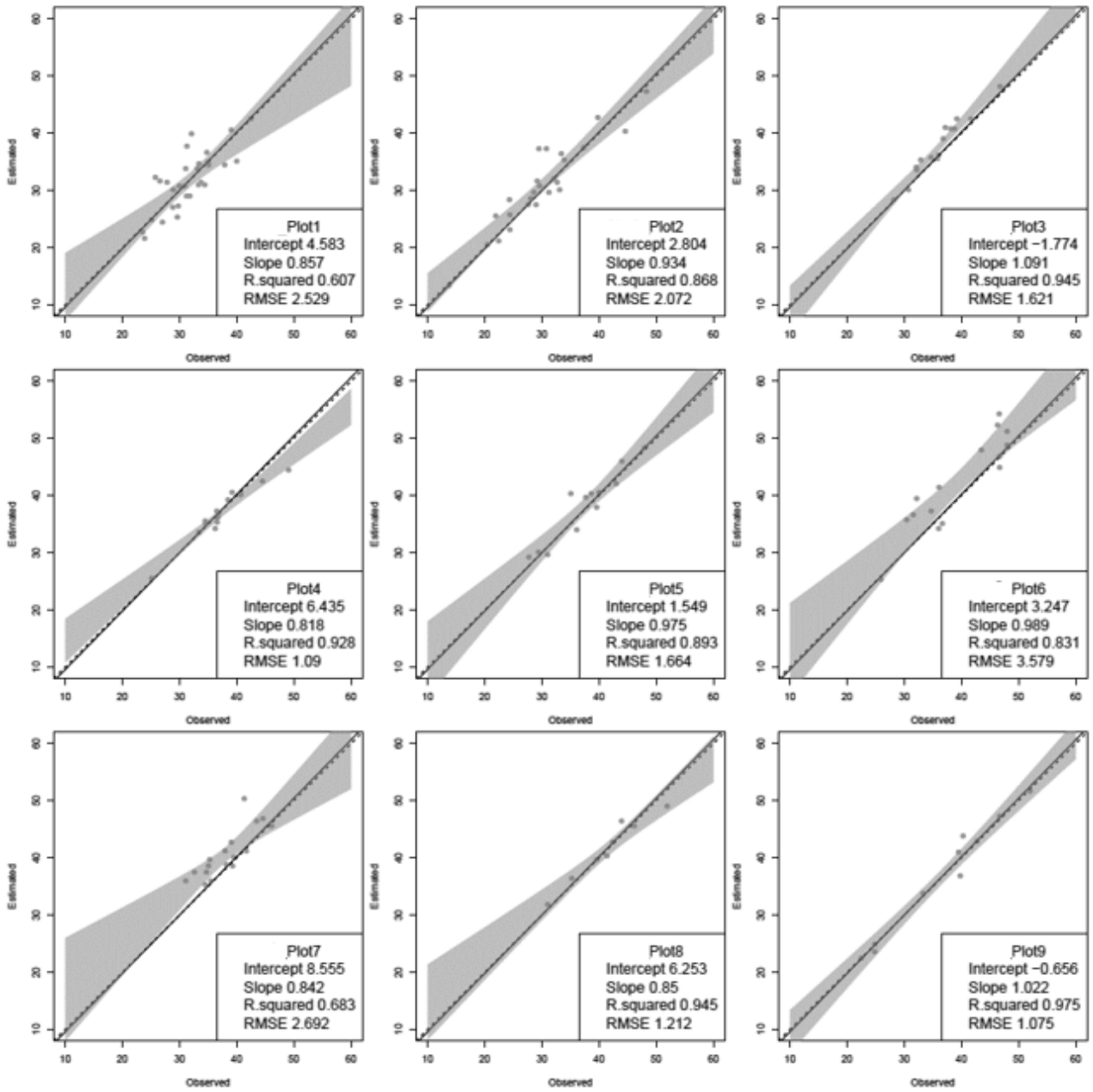

Figure 5. Performance of diameter estimation with the TreeLS software using Hough transformation method with RANSAC technique. Values in centimetres. The dashed line is the 1:1 line, the continuous line is the fitted line. The confident interval is reported in grey.

The statistical analysis (ANOVA) performed on absolute error between observed and estimated values indicated that error values from different diameter detection methods were significantly different (p<0.05). The Duncan test showed that no significant differences were detected in error values between the Monte Carlo and Optimal Circle algorithms, which had an average error value of 3.2cm and 3.6cm, respectively, whereas significant differences were found in error values between

circle-fitting (Monte Carlo and Optimal Circle) and Hough transformation (TreeLS) methods, the latter with an average error value of 1.2cm (Figure 6).

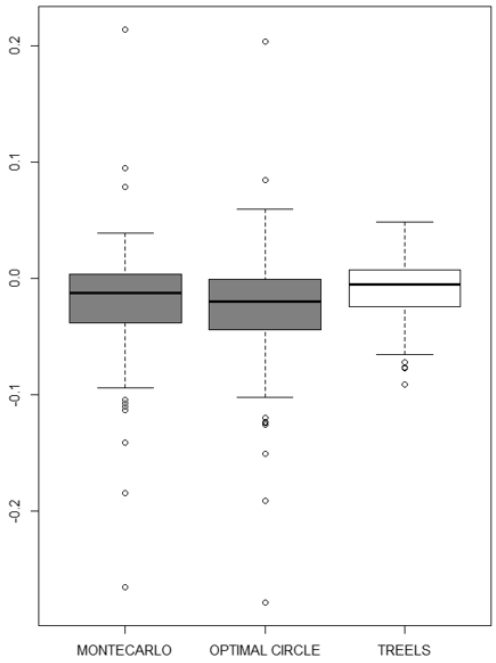

Figure 6. Results of the Duncan test. Different colours indicate significant statistical differences (p<0.05).

5.Discussion

One of the current challenges in forest inventory is to fully automate the process for extracting single-tree attributes from 3D point clouds. TLS point clouds have been proved to reach millimetric precision in DBH estimation (Liang et al., 2016). The new generation of LiDAR sensor for airborne survey can acquire ultra-dense point clouds that could be used for diameter estimation. ALS is a cost-efficient system compared to TLS, since it can cover large forest areas in less time.

However, only few studies were conducted on automatic detection of diameters from ALS point clouds. For instance, Dalponte et al. (2018) using ALS data in combination with hyperspectral information in a predictive model detected 60% of the trees with DBH greater than 10 cm. The best R^2 achieved by these authors was 0.57 with a maximum RMSE=5.4 cm. Brede et al. (2017), who tested the RIGEL RiCOPTER VUX-1 ALS system and compared it with a TLS system for diameter estimation detected 32% of the stems, and found a good agreement between ALS DBH and TLS DBH with R^2=0.98 and RMSE=4.2 cm.

Our study was conducted in a *Pinus radiata* plantation. The relatively low number of trees per plot and the new generation LiDAR sensor VUX1-LR allowed to obtain ALS point clouds with stems clearly visible (Figure 2), which is a condition necessary to automate the process for stem detection from laser scanning data (de Conto, 2017).

Using the spatial clustering procedure developed in study 98% of the stems were detected (only two stems over 147 were undetected). The spatial clustering procedure was also able to automatically reduce the noise present in the plots.

The circle-fitting methods available in DendroCloud software provided similar results for DBH estimation. The average R^2 was 0.68 and 0.65 for Monte Carlo method and Optimal Circle method, respectively. The average RMSE was 3.2 cm and 3.6 cm for Monte Carlo algorithm and Optimal Circle algorithm, respectively. The circle-fitting methods were evaluated by Koreň et al. (2017) for deriving DBH from TLS point clouds acquired in multi-scan mode and single-scan mode. The best results achieved by these authors were obtained using the Optimal Circle method (RMSE=0.77cm for the multi-scan mode and RMSE=1.71cm for the single-scan mode). Contrary to what found by Koreň et al. (2017), in our study the Monte Carlo method (max RMSE=5.8cm) performed slightly better than the Optimal Circle method (max RMSE=6.8cm). However, no significant differences were found in our study between the accuracy of the Monte Carlo method and the accuracy of the Optimal Circle method. The DendroCloud software was also tested by Krisanski et al. (2018). Krisanski's study compared the estimation of DBH from VUX1-LR ALS point clouds collected at three different altitudes (30m, 60m and 90m above ground level) and from below-canopy UAS point cloud. The below-canopy UAS point cloud and the VUX1-LR ALS point cloud collected at 30m altitude provided the best accuracy for DBH estimation (RMSE = 4.1cm).

The accuracy of circle-fitting methods was significantly different from the accuracy of Hough Transformation method with RANSAC technique. The Hough Transformation algorithm with RANSAC implemented in the TreeLS package proved to be the most accurate method for diameter estimation from ALS point clouds. The average R^2 was 0.85 and the average RMSE was 1.95cm. The TreeLS package for DHB estimation with Hough Transformation and RANSAC technique was previously tested by de Conto et al. (2017) on TLS point clouds, achieving an average RMSE of 1.84 cm on pine trees. Olofsson et al. (2014) using Hough Transformation and RANSAC algorithm for DBH estimation from TLS point clouds on boreal tree species found diameter RMSE values in the range of 2.4-7.5cm. Although an objective comparison of results is not possible, due to different scanning methods and parameters, tree species, and point cloud processing procedure, the diameter RMSE values obtained

in this study from ultra-dense ALS point clouds are comparable with the results obtained in other studies based on ALS and TLS point clouds.

6. Conclusions

This study provides insight into the performance of ultra-dense ALS point clouds for diameter estimation. The study was carried out in a *Pinus radiata* plantation. The relatively low number of trees per plot and the new generation LiDAR sensor VUX1-LR allowed to obtain ALS point clouds with stems clearly visible, which made possible to test three different methods for DBH estimation. The Hough transformation method with RANSAC technique was significantly more accurate than circle-fitting methods (Monte Carlo and Optimal circle). Ultra-dense ALS point clouds can be useful for inventory purposes in productive forests like those investigated in this study. However, further studies are necessary to test the performance of ultra-dense ALS point clouds in other forest types characterized by different species composition and more complex forest structures.

Acknowledgments

This work was possible thanks to Forest & Wood Products Australia (FWPA) and the Ministry for Business Industry and Employment (MBIE) Strategic Science Investment Fund (SSIF), who supported this project financially. Assistance provided by Forestry Corporation of New South Wales and NSW Department of Primary Industries was greatly appreciated.

Special thanks to Interpine Group Ltd that hosted the main author for six months and provided useful knowledge about remote sensing and LiDAR analysis.

References

Aschoff T., Spiecker H. (2004) Algorithms for the Automatic Detection of Trees in Laser Scanner Data. The International Archives of the Photogrammetry, Remote Sensing and Spatial Information Sciences Volume XXXVI – 8/W2

Bienert A., Scheller S., Keane E., Mohan F., Nugent C. (2007) Tree Detection and Diameter Estimations by Analysis of Forest Terrestrial Laserscanner Point Clouds. ISPRS Workshop on Laser Scanning and SilviLaser, Espoo, Finland.

Brede B., Lau A., Bartholomeus H., Kooistra L. (2017) Comparing RIEGL RiCOPTER UAV LiDAR Derived Canopy Height and DBH with Terrestrial LiDAR. Sensors, 17(10), p.2371.

Cabo C., Ordóñez C., López-Sánchez C., Armesto J. (2018) Automatic dendrometry: Tree detection, tree height and diameter estimation using terrestrial laser scanning. Int J Appl Earth Obs Geoinformation 69 (2018) 164–174

Čerňava J., Tuček J., Koreň M., Mokroš M. (2017) Estimation of diameter at breast height from mobile laser scanning data collected under a heavy forest canopy Journal of Forest Science, 63, 2017 (9): 433–441 doi: 10.17221/28/2017-JFS

Côté J.F., Fournier R.A., Egli R. (2011). An architectural model of trees to estimate forest structural attributes using terrestrial LiDAR. Environ. Model. Soft. 26 (6), 761–777.

Dalponte M., Frizzera L., Ørka H. O., Gobakken T., Næsset E., Gianelle D. (2018) Predicting stem diameters and aboveground biomass of individual trees using remote sensing data. Ecological Indicators, 85: 367-376. doi: 10.1016/j.ecolind.2017.10.066

de Conto T., Olofsson k., Bastos Görgens E., Estraviz Rodriguez L. C., Almeida G. (2017) Performance of stem denoising and stem modelling algorithms on single tree point clouds from terrestrial laser scanning. Computers and Electronics in Agriculture 143 165–176

Henning J.G., Radtke P. (2006) Detailed stem measurements of standing trees from ground-based scanning LIDAR. Forest Science. 52. 67-80.

Hopkinson, C., Chasmer, L., Young-Pow, C., Treitz, P. (2004) Assessing forest metrics with a ground-based scanning lidar. Can. J. For. Res. 34 (3), 573–583.

Hough P.V.C. (1962) Method and means for recognizing complex patterns, U.S. Patent 3,069,654.

Hulk R., Spanel M., Smrz P., Materna Z. (2014) Continuous plane detection in point-cloud data based on 3D Hough Transform. Journal of Visual Communication and Image Representation Volume 25, Pages 86-97

Jaakkola A., Hyyppä J., Kukko A., Yu X., Kaartinen H., Lehtomäki M., Lin Y. (2010) A low-cost multi-sensoral mobile mapping system and its feasibility for tree measurements. ISPRS J. Photogramm. Remote Sens.,65, 514–522.

Kankare V., Liang X., Vastarant M., Yu X., Holopainen M., Hyyppä J. (2015) Diameter distribution estimation with laser scanning based multisource single tree inventory. ISPRS Journal of Photogrammetry and Remote Sensing Volume 108, October 2015, Pages 161-171

Koreň M., Mokroš M., Bucha T. (2017) Accuracy of tree diameter estimation from terrestrial laser scanning by circle-fitting methods. Int. J. Appl. Earth Obs. Geoinf. 63, 122–128.

Krisanski S., Del Perugia B., Sadegh Taskhiria M., Turnera P. (2018) Below-canopy UAS photogrammetry for stem measurement in radiata pine plantation. Proc. SPIE 10783, Remote Sensing for Agriculture, Ecosystems, and Hydrology XX, 1078309 (10 October 2018); doi: 10.1117/12.2325480

Liang X., Hyyppä J. (2013) Automatic stem mapping by merging several terrestrial laser scans at the feature and decision levels. Sensors 13 (2), 1614–1634.

Liang X., Hyyppä J., Kaartinen H., Holopainen M., Melkas T. (2012) Detecting changes in forest structure over time with bi-temporal terrestrial laser scanning data. ISPRS Int. J. Geo-Inf. 1 (3), 242–255.

Liang X., Kankare V., Hyyppä J., Wang Y., Kukko A., Haggrén H., Yu X., Kaartinen H., Jaakkola A., Guan F., Holopainen M., Vastaranta M. (2016) Terrestrial laser scanning in forest inventories. ISPRS Journal of Photogrammetry and Remote Sensing. 115. 10.1016/j.isprsjprs.2016.01.006.

Maas H. G., Bienert A., Scheller S., Keane E. (2008) Automatic forest inventory parameter determination from terrestrial laser scanner data. Int. J. Remote Sens. 29 (5), 1579–1593.

Mukhopadhyay P., Chaudhuri B. (2015) A survey of Hough Transform. Pattern Recognition 48 993–1010.

Næsset E. (2002) Predicting forest stand characteristics with airborne scanning laser using a practical two-stage procedure and field data. Remote Sens. Environ. 80 (1), 88–99.

Næsset E. (2007) Airborne laser scanning as a method in operational forest inventory: status of accuracy assessments accomplished in Scandinavia. Scand. J. For. Res. 22 (5), 433–442.

Olofsson K., Holmgren J., Olsson H. (2014) Tree stem and height measurements using terrestrial laser scanning and the RANSAC algorithm. Remote Sensing, 6: 4323–4344.

PLOTSAFE Overlapping Feature Cruising Forest Inventory Procedures (2007)

Pueschel P., Newnham G., Rock G., Udelhoven T., Werner W., Hill J. (2013) The influence of scan mode and circle fitting on tree stem detection, stem diameter and volume extraction from terrestrial laser scans. ISPRS Journal of Photogrammetry and Remote Sensing, Volume 77, March 2013, Pages 44-56

Wallace L., Lucieer A., Watson C., Turner D. (2012) Development of a UAV-LiDAR system with application to forest inventory. Remote Sens. 2012, 4(6), 1519-1543; https://doi.org/10.3390/rs4061519

Yao Z., Yi W. (2016) Curvature aided Hough transform for circle detection. Expert Systems With Applications 51 26–33

Paper V

Influence of scan density on single-tree attributes estimation by hand-held mobile laser scanning

Del Perugia B.[1]*, Travaglini D.[1], Giannetti F.[1], Chirici G.[1]

[1] Dipartimento di Gestione dei Sistemi Agrari, Alimentari e Forestali, Università degli Studi di Firenze, via San Bonaventura, 13 – 50145 Firenze, Italy, e-mail: barbara.delperugia@unifi.it, davide.travaglini@unifi.it, francesca.giannetti@unifi.it, gherardo.chirici@unifi.it

Abstract

Nowadays, forest inventories are carried out using a combination of field measurement and remote sensing data, often acquired with LiDAR sensors. Several studies have investigated how laser scanner sensors, from different platforms, can aid at replacing traditional field instrument to detect single tree structures.

The present study, conducted in southern Tuscany, tested the ZEB1 instrument, a type of Hand-held Mobile Laser Scanner, in pure *Castanea sativa Mill* stands cultivated for fruit production. The influence of walking scan path density on single-tree attributes (number of trees, tree position, diameter at breast height, tree height and crown base height) was estimated. The point clouds were acquired walking along straight lines drawn with two different scan line densities (10m and 15m apart). A single-tree scan (walking around each tree) was used as reference data. The influence of the walking scan path was discussed in relation to the accuracy of single-tree attributes, as well as the time and cost of the field survey, to value the survey efficiency. The 10m apart scan provided the best results, with an omission difference of 6% of trees; the assessment of single-tree attributes was successful with values of R^2 and RMSE similar to the ones reported in other studies. This path has also proved to decrease the costs by about €14 for the pre-processing phase and a saving time (acquisition and derived single tree data) of about 37 minutes compared to the reference data.

Keywords: HMLS, ZEB1, Forest Inventory

1. Introduction

Collecting and updating different types of information on forest resources is becoming an important task to monitor and manage forest ecosystems at different spatial scales (i.e. from global, to national/regions, to plot and single tree levels). Usually, information on forest resources is acquired in the context of national and local forest inventories that allows the acquisition of precise information on different forest variables (i.e. growing stock volume, increment, forest area) (Corona et al., 2011; Kangas et al., 2018; Næsset et al., 2004; Tomppo et al., 2008). In the last few decades, the use of Remote Sensing technologies has played an important role in the optimization of forest measurements and estimation thanks to its advantage in collecting and updating information on forest resources. Today, a very large number of operational forest inventories are carried out using a combination of field measurement and remote sensing data (Corona et al., 2011; Kangas et al., 2018; Næsset et al., 2004; Tomppo et al., 2008; Liang et al., 2016). The most used forest inventory methods are (*i*) Area Based Approach (ABA) which uses relationship between field measurements in simple plots (i.e. 200–530m^2) and remotely sensed data to model forest variables (i.e. basal area, growing stock volume, dominant height) expressed in area units equal to those of forest inventory plots (Næsset et al., 2004; Tomppo et al., 2008); and (*ii*) single tree approach which allows the derivation of information on single trees (i.e. diameter at breast height (DBH), volume, height) from remote sensing data (Brosofske et al., 2014).

Of the variety of remote sensing technologies, Laser Scanner technologies plays an important role in forest inventories, as it allows accurate three-dimensional information of the environment, capturing data from a local to a global scale in a fast and accurate way (Kangas et al., 2018; Liang et al., 2016; Miller et al., 2015; Rahlf et al., 2014). In the last two decades, Airborne Laser Scanning (ALS) has played an important role in forest inventory tasks with its capacity of obtaining the spatial distribution of horizontal and vertical surface characteristics with dense point clouds (Kangas et al., 2018; Liang et al., 2016; Solberg et al., 2006; Wulder et al., 2008). Its advantage in mapping forest variables using ABA is well documented in literature over different forest types such as boreal (Hyyppä et al., 2001; Næsset et al., 2004; Yang et al., 2016), Mediterranean (Bottalico et al., 2014; Bottalico et al., 2017) and mixed temperate forests (Mura et al., 2015; Mura et al., 2016). Moreover, several studies highlight how ALS data with a dense point cloud (>20 point m^2) can also be used to derive single tree variables (Kankare et al., 2015; Solberg et al., 2006). When the ABA is used, ALS data are used in

combination with field data that are usually acquired through traditional survey techniques (i.e. registering tree position, DBH and height using calipers, hypsometers, compasses and other measuring methods).

Thanks to the implementation of LiDAR technology in a wide variety of platforms (e.g., ground platforms, mobile terrestrial platforms, personal and hand-held platforms) which allows the capture of spatial information for different purposes (i.e. mapping, resource inventory, ecological monitoring) at different spatial scales (Liang et al., 2016; Talbot et al., 2016), many studies has investigated the potential of LiDAR terrestrial sensors in replacing traditional instruments to measures trees in field plots or stands. In fact, the Terrestrial Laser Scanner (TLS) (a scanning system mounted on a tripod located on the ground) can capture a dense point cloud around the instruments which detects single tree structures under crown cover. TLS has been widely investigated in many fields, e.g. architecture, civil engineering, archaeology, cultural heritage, plant design and automation systems (robotics) (Zlot, 2014; Holopainen et al., 2013). These systems applied in forestry facilitate the accurate procurement of information on tree position and DBH (-1.5 cm < RMSE < 3.3 cm) (Hopkinson et al., 2004; Maas et al., 2008; Overland et al., 2018; Thies, et al. 2004). However, both Liang et al. (2016) and Dassot et al. (2011) in their review have underlined that several challenges still must be overcome to efficiently use TLS to replace manual field acquisition. The principal problem of TLS is the occluded areas which occur using the single-scan approach, that can be reduced with a multi-scan but not eliminated (Liang et al., 2016). Furthermore, the multi-scan approach requires more time for field data acquisition and more effort in data processing (Liang et al., 2016).

More recently, laser scanning has been put on moving platforms (e.g., vehicles) to build a Mobile Laser Scanning (MLS) system. MLS is a modification of ALS; it has a laser scanner, a GNSS receiver, an IMU and preferably cameras, allowing the investigation of larger areas compared to TLS techniques (Liang et al., 2014; Ryding et al., 2015). One of the biggest advantages of MLS is the reduction of occluded areas compared with the TLS system (Oveland et al., 2018). The use of a moving platform is an improvement in many fields (i.e. architecture, civil engineering) but has limitations in forest ecosystems, since it may not provide spatially continuous mapping and does not match with the non-destructive nature of LiDAR data acquisition (Bauwens et al., 2016). Moreover, the accuracy of MLS point clouds is usually lower than multi-scan TLS data, due to the low GNSS signal detection under forest cover (Forsman et al., 2016; Bauwens et al., 2016).

New to the MLS family is the Hand-held Mobile Laser Scanning (HMLS), a system introduced by Bosse et al. (2012) using the movement of the operator as a platform. HMLS systems minimize occlusion

effects since the movement through the plot results in a theoretically unlimited number of scan-positions. Unlike with MLS, forest cover is no longer a limitation, as HMLS does not need satellite positioning (GNSS) (Bauwens et al., 2016).

ZEB1 is a type of HMLS that has been tested for forest inventory applications in different forest types (Giannetti et al., 2018; Oveland et al., 2018; Ryding et al., 2015). Ryding et al. (2015) tested the potential of the instruments to extract the DBH and stem position from the point cloud in an ash dominated woodland. The results were promising, being a faster approach on complex topography and returning a more detailed point cloud compared with TLS survey. Oveland et al. (2018), in boreal forest, compared three different types of TLS and found comparable results between traditional static TLS (i.e. FARO FOCUS 3Dx130), HMLS (i.e. ZEB1) and the Backpack Laser Scanner (i.e.Velodyne VLP 16) in the measures of DBH and tree position. On the other hand, Bauwens et al. (2016) conducted a study to assess and compare HMLS (i.e. ZEB1) with TLS for the estimation of forest parameters in a wide range of forest types. Bauwens et al. (2016) confirm the advantages of HMLS over TLS for detection of several forest parameters but also point out the limitations of the instrument for the assessment of forest height; this was confirmed by the study of Giannetti et al. (2018) in Mediterranean forest types.

The main limitations reported in these studies are associated with the autonomy of the instrument and the resolution of the point cloud to allow acceptable feature extraction (Oveland et al., 2018). The laser range of the instruments is an important variable that must be taken into account when planning the walking scan path for HMLS survey, as the walking scan path influences the scan density and therefore the resolution of the point cloud. In Ryding et al. (2015), a free walking method was used to cover 10x10m subplots and where possible the user walked in straight lines up and down. In Bauwens et al. (2016), Oveland et al. (2018), and Giannetti et al. (2018), a fixed path was used in circular plots with a radius of 13-15m; that is, the user walked along four main directions (e.g., NS, SW-NE, EW, NE-SW) and the plot border was scanned at least once.

However, to our knowledge, no studies have been carried out to examine the relationships between walking scan paths and accuracy of forest variables estimations when an HMLS was used.

Moreover, the walking scan path influences the time for acquisition and therefore the cost of the field survey.

In this study, our objective was to investigate the influence of walking scan path density on single-tree attribute estimation by HMLS. The following tree-level attributes were considered: number of trees, tree position (TP), diameter at breast height (DBH), tree height (TH) and crown base height

(CBH). Using a single-tree scan approach as the reference data set, the estimates of single-tree attributes obtained by point clouds acquired walking along straight lines drawn with two different scan line densities were compared. Additionally, the influence of walking scan path was discussed in relation to time and cost of field survey in order to estimate survey efficiency.

2. Material and methods

2.1 Study area

The study was carried out in Mount Amiata, in the southern Tuscany region (Central Italy). Three pure sweet chestnut (Castanea sativa Mill.) stands cultivated for fruit production were identified in the area, hereinafter referred to as Area 1, Area 2 and Area 3 (Figure 1). In the region, the climate is Mediterranean, with rainfall of 919mm yr^{-1} at Castel del Piano meteorological station (data 1961-1990), with a minimum in July and a maximum in November. The mean daily temperature over the year is 12.7°C. Elevation ranges between 820m a.s.l. in Area 1 and 680m a.s.l. in Area 3. Area 1 is almost flat, while Area 2 and Area 3 are characterized by a slight slope. The average tree density in the three areas (with a DBH > 5 cm) is 110 trees ha^{-1}.

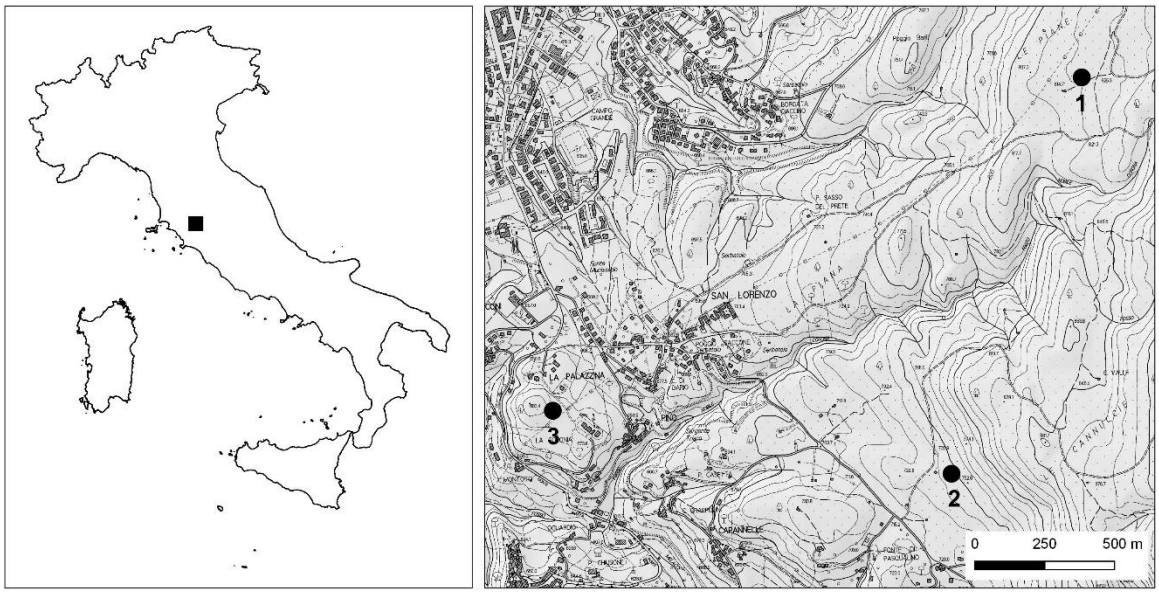

Figure 1. Location of the three study areas.

2.2. Hand-held Mobile Laser Scanning

We used the ZEB1 instrument as HMLS. The ZEB1 consists of a 3D laser scanner and an inertial measurement unit (IMU), both mounted on top of a spring, which is itself located on a hand grip (Bosse et al., 2012). While the user walks through the forest, the scanner on the head of ZEB1 swings back and forth creating a 3D scanning field with data being captured at the speed of movement. Instead of using GNSS, it utilises technology taken from the robotics community, Simultaneous Localization and Mapping (SLAM), which is an algorithm that locates the scanner in an unknown environment and allows it to register the whole 3D point cloud, relying on both the IMU data and feature detection algorithms (Bauwens et al., 2016). The reported operative laser range outdoors is 15-20m around the instrument, with a scan ranging noise of ± 30mm (GEOSLAM, 2017). The main technical specifications of the instrument are reported in Table 1. A complete description of the instrument can be found in Giannetti et al. (2018, 2017).

Feature	Description
Laser scanner sensor	905nm wavelength and a beam divergence of approximately 7 mrad
Weight	Hand-held sensor, 0.7 kg Data logger in backpack, 3.6 kg
Frequency of scanning	43,200 points/s (40 lines/s with a laser pulse interval of 0.25°)
Field of view	Horizontally 270° Vertically 120°
Measurement error	±30 mm at a range of 0.1 m to 10 m

Table 1. Technical specifications of HMLS (ZEB1).

2.3. Hand-held Mobile Laser Scanning data collection and pre-processing

Data acquisition was carried out on November 2016. In each area, the laser scanning data was collected within one circular plot with a radius of 30m (0.28ha).

Three spherical targets with a diameter of 14 cm were mounted on top of poles 1.5m long and fixed on the ground around the plots to georeference the point cloud in post-processing. The coordinates of the spherical targets were acquired using the GNSS receiver Trimble Geo 7X. The post-processed coordinates revealed standard deviations for x, y and z lower than 1cm and 2cm, respectively.

To assess the influence of scan density on accuracy estimation, three different survey paths were considered (Figure 2). The first scan (D0) was performed by a person walking with ZEB1 HMLS around

each tree to avoid the effects of shadow zones and obtain the highest scan density. The second and third scans were acquired by the same user walking up and down along straight lines (obstacles were avoided) drawn at a distance of 10m (D10) and 15m (D15) from each other, respectively. For scans D10 and D15, the alignments were traced on the ground using poles and a surveyor's cross. All the scans started and ended at a point fixed outside the plot to ensure a closed loop as required when the SLAM algorithm is used. The time needed to perform each scan was also recorded.

The raw ZEB1 HMLS data were pre-processed on-line to obtain point clouds using the GeoSLAM procedure, which uses the SLAM algorithm. The pre-processing on-line procedure is subject to charges (Giannetti et al., 2018; GEOSLAM, 2017). The charges costs depend from the length of scan walking path and the density of scan point and can range between 0,05 and 0,15 €/m (Giannetti et al., 2017; GEOSLAM, 2017). The costs of pre-processing on-line procedure are reported in Table 2. This procedure takes into account that the same objects are viewed from multiple directions as the system moves through the environment and measurements to these objects are then used to calculate position (Ryding et al. 2015). The SLAM algorithm processes IMU and laser data from the ZEB1 HMLS to locate the scanner in an unknown environment and to register the whole 3D point cloud without the need for GNSS (Bosse et al., 2012; Bauwens et al., 2016). More details on the SLAM algorithm can be found on-line at https://geoslam.com/slam/.

Once the 3D point cloud was obtained, we used the spherical targets to rotate and translate the cloud from the local coordinate system to a geographic coordinate system (i.e., WGS84 UTM32N). CloudCompare software (CloudCompare version 2.9, 2017) was used to automatically detect the spherical targets in the cloud and to assign the reference coordinate systems. The RMSE of roto-translation was approximately 4cm.

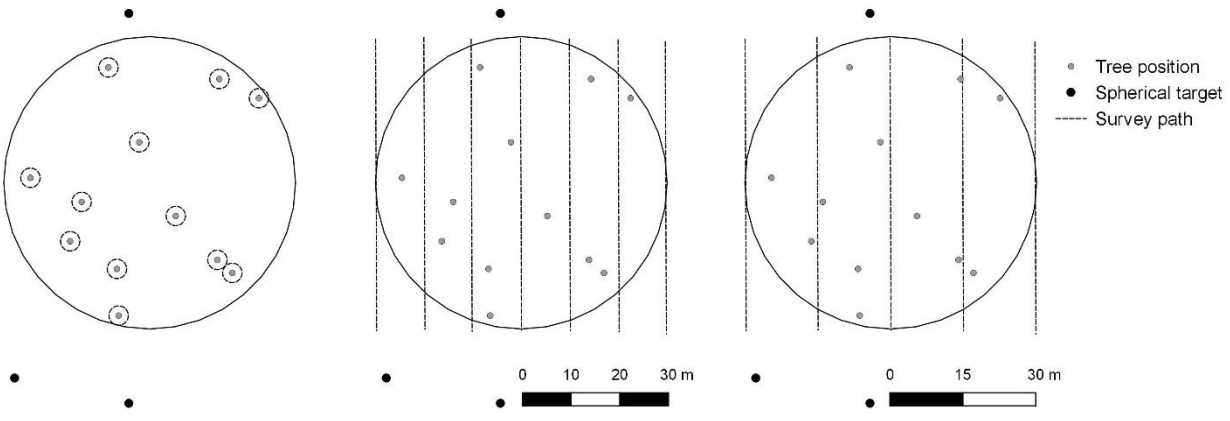

Figure 2. Survey paths used for the scans with HMLS (ZEB1): D0 scan (left), D10 scan (center) and D15 scan (right).

2.4. Extraction of single-tree attributes from the point clouds

The extraction of the single-tree attributes from the point clouds was done automatically with Computree software (http://computree.onf.fr), which is an open source processing platform. Computree generates a digital terrain model at plot level and provides tools for automatic stem detection, DBH and height estimation of each detected tree (Hackenberg et al., 2015; Bauwens et al., 2016). We used Computree to segment the point clouds into single-tree point clouds and to extract the single-tree attributes related to height (TH and CBH), DBH and TP. The procedure to extract single-tree attributes is the same as that adopted by Giannetti et al. (2018).

2.5 Reference data

The single-tree attributes extracted from the D0 scan (i.e., the scan performed walking around each tree) were assumed as error free here and used as reference data to evaluate the estimates produced on the bases of D10 and D15 scans.

The number of trees detected with the D0 scan in Area 1, Area 2 and Area 3 was 37, 25 and 36 trees, respectively. Figure 3 shows the box-plot of the single-tree attributes related to DBH, TH and CBH. The mean DBH was 44, 63 and 48 cm in Area 1, Area 2 and Area 3, respectively. Area 3 had a standard deviation of diameters higher than Area 1 and Area 2. The mean value of TH was 12m in Area 1, 10m in Area 2 and 8m in Area 3. CBH varied between 2 and 3m in all areas.

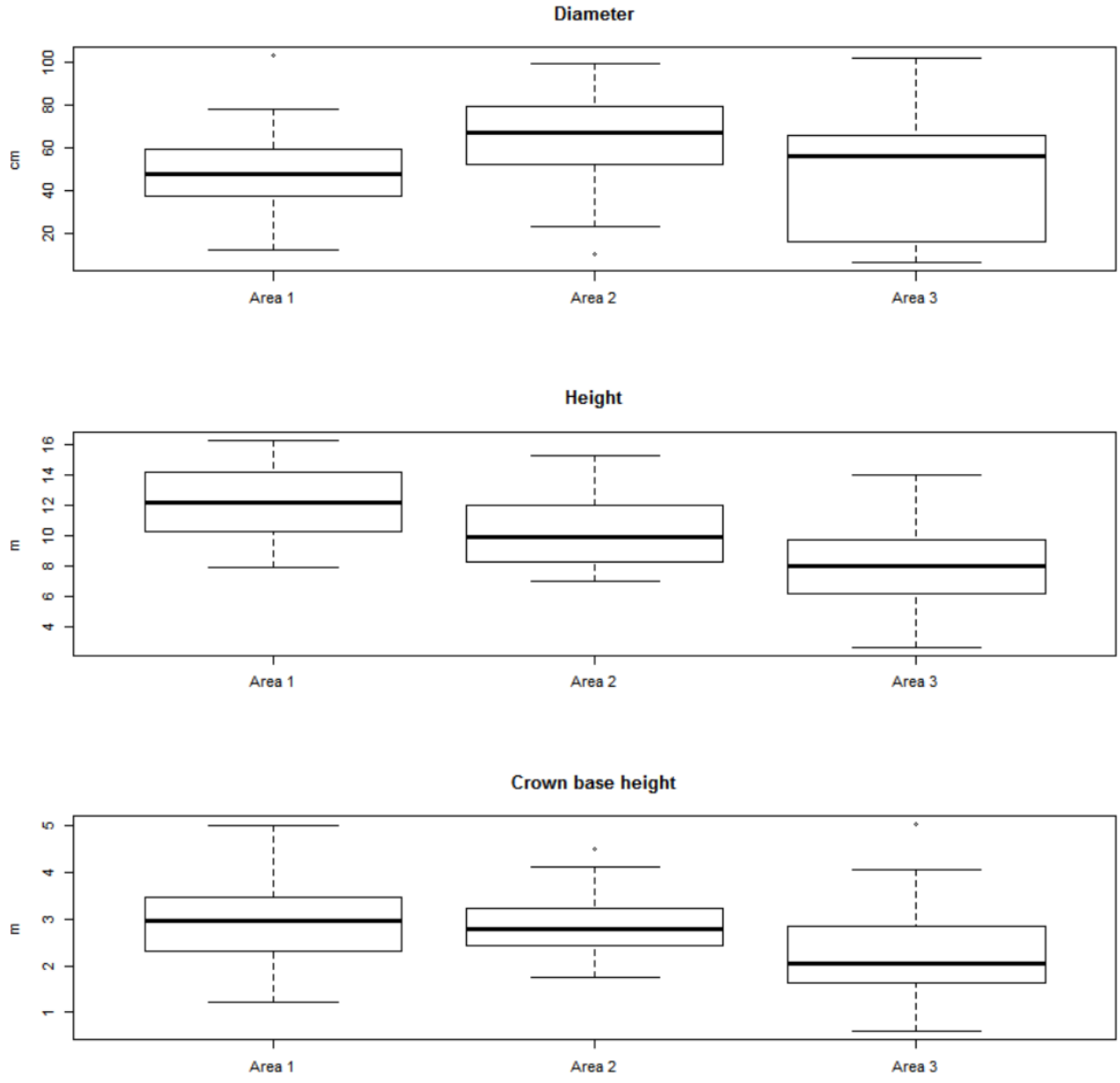

Figure 3. Boxplot with resulting values for DBH, TH and CBH of the reference data (D0 scan).

2.6. Accuracy assessment

The single-trees attributes estimated by the D10 and D15 scans were compared with single-tree attributes obtained by the D0 scan.

To assess the accuracy of TP, DBH, TH and CBH, we calculated the coefficient of determination (R^2), the root mean square error (RMSE), the relative root mean square error (RMSE%) and bias as follows:

$$RMSE = \sqrt{\frac{\sum_{i=1}^{n}(X_{oi} - X_{Si})^2}{n}}$$

$$RMSE\ \% = \frac{\text{RMSE}}{\bar{x}}$$

$$bias = \frac{\sum_{i=1}^{n}(X_{oi} - X_{Si})}{n}$$

where n is the number of trees resulting from the D0 scan, X_o is the value of the tree attribute computed in the D0 scan, X_s is the estimated value of the attribute for each *i-th* tree, and $\bar{x}$ is the mean value of the tree attribute computed in the D0 scan.

The number of trees estimated by the D10 and D15 scans was compared with the number of trees detected by the D0 scan; omission (i.e., stems that were detected in the D0 scan, but not in the D10 and D15 scans) and commission (i.e., stems that were not detected in the D0 scan, but were in the D10 and D15 scans) differences were computed. For omission errors, the size of the DBH of not detected trees was evaluated.

3. Results

The time spent to collect and elaborate the ZEB1 data and the cost related to the on-line pre-elaboration of point cloud by areas and by path scans (i.e. D0, D10 and D15) are reported in Table 2. The cost of pre-elaboration ranged between 0.10E/m and 0.06 E/m. In detail at plot level, it was found that between the D0 and the other two path scans, there were differences in time and in cost of pre-processing the data. Between D10 and D0 an average saving of a total time of 10 minutes was observed, while between D15 and D0 there was a saving of 26 minutes (Table 2). Moreover, for the pre-processing phase an average saving of €14 was observed between D10 and D0 and €39 between D15 and D0 (Table 2).

	Length of walking path (m)			Scan time (min)			Extraction of single tree data (min)			Pre-processing cost (€)			Average time/ha (min/ha)
Area	1	2	3	1	2	3	1	2	3	1	2	3	
D0	956	842	828	17	15	13	58	56	53	93	89	76	250
D10	722	721	704	15	14	12	49	45	46	72	75	69	213
D15	621	602	592	12	11	8	38	31	33	52	48	41	157

Table 2. Time and cost needed for HMLS (ZEB1) data acquisition and processing. Average time/ha column refers to the sum of Scan time and Extraction of single tree data columns. Time is reported in minutes, length in meters and costs in Euro.

Using the D0 scan as reference data, 98 trees were detected across all areas, with min/max DBH being 6cm and 103cm, respectively. Using the D10 scan data, 92 trees were estimated in the three areas, with DBH estimates in the range between 8cm and 109cm. Using the D15 scan data, the number of trees estimated in the three areas was 56 trees, with min/max DHB estimates between 8cm and 107cm, respectively. The omission difference across all areas compared to the reference data was 6% and 43% respectively for the D10 scan and the D15 scan (Table 3). Commission error was not found. The distribution of the DBH of not detected trees is reported in Figure 4. The map of the single-tree position is shown in Figure 5.

Area	Number of trees			Omission difference (%)	
	D0	D10	D15	D10	D15
1	37	37	24	0	35
2	25	25	12	0	52
3	36	30	20	17	44
All	98	92	56	6	43

Table 3. Number of trees estimated with D10 and D15 scans vs the reference data (D0 scan).

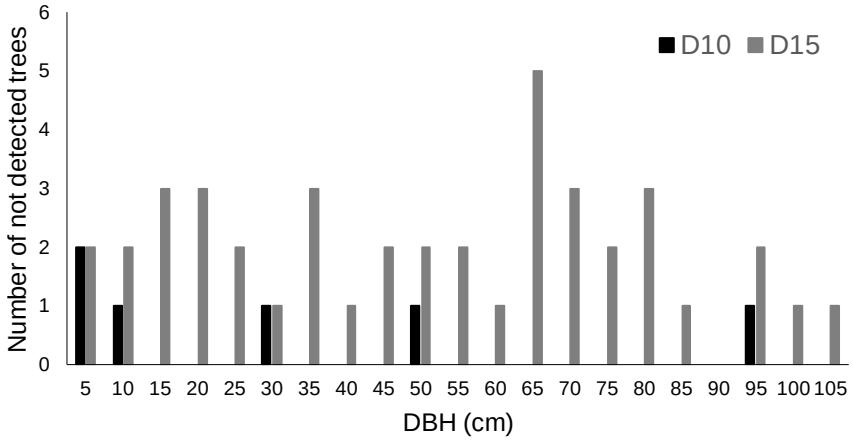

Figure 4. Stem number–diameter distribution of not detected trees by D10 and D15 scans. Data for all three areas are reported.

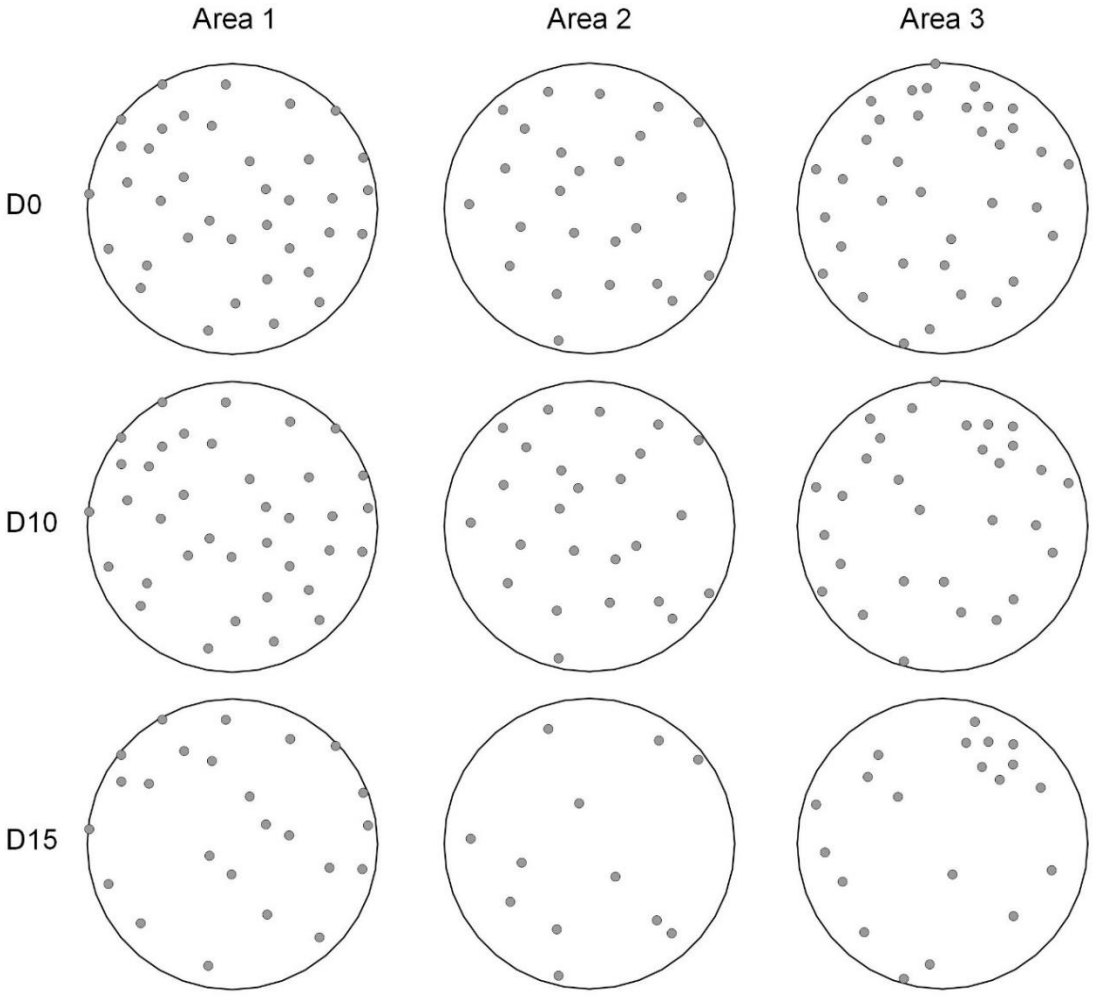

Figure 5. Single-tree position in the three areas estimated with D10 and D15 scans vs the reference data (D0 scan).

The accuracy of TP is reported in Table 4. The coefficient of determination for x and y coordinates was equal to 1 for both the D10 and D15 scans. The RMSE and bias across all the three areas were 0.091m and -0.001m for the D10 scan, and 0.139m and -0.003m for the D15 scan.

Area	RMSE		Bias	
	D10	D15	D10	D15
1	0.000	0.005	0.000	-0.001
2	0.139	0.244	-0.015	-0.024
3	0.097	0.136	0.009	0.007
All	0.091	0.139	-0.001	-0.003

Table 4. Summary statistics of single-tree position estimated by D10 and D15 scans. RMSE and Bias are reported in meters.

Table 5 shows the accuracy of the single-tree attributes (DBH, TH and CBH) estimated by D10 and D15 scans. For the DBH, the coefficient of determination across all three areas was higher than 0.98, revealing a good fit between the D10 and the D15 scans and the reference data. Similar results are provided by RMSE%, which was lower than 6% for both scans. For TH, the coefficient of determination across the areas was higher than 0.94, with an RMSE% lower than 8% for the D10 and D15 scans. For CBH, the coefficient of determination achieved was 0.91 and 0.87 and the RMSE% was 11% and 18% for the D10 and D15 scans, respectively.

Single-tree attribute	Area	R^2		RMSE		RMSE %		Bias	
		D10	D15	D10	D15	D10	D15	D10	D15
DBH (cm)	1	1.000	0.981	0.000	2.544	0.000	5.240	0.000	-0.100
	2	0.975	0.979	3.919	3.993	6.208	7.028	0.362	1.578
	3	0.995	0.994	2.381	2.589	5.032	5.445	-0.981	-0.430
	All	0.991	0.986	2.451	2.930	4.775	5.864	-0.222	0.142
TH (m)	1	1.000	0.945	0.000	0.644	0.000	5.359	0.000	0.309
	2	0.913	0.980	0.704	0.296	6.893	3.042	0.308	0.163
	3	0.879	0.929	0.984	1.143	11.544	12.639	0.259	0.777
	All	0.952	0.943	0.671	0.814	6.523	7.781	0.168	0.445
CBH (m)	1	1.000	0.958	0.000	0.272	0.000	9.762	0.000	-0.209
	2	0.917	0.660	0.255	0.804	8.771	26.280	-0.140	-0.463
	3	0.862	0.958	0.474	0.453	19.625	18.217	-0.298	-0.302
	All	0.915	0.872	0.302	0.494	11.126	18.016	-0.135	-0.297

Table 5. Summary statistics of single-tree attributes (DBH, TH and CBH) estimated by D10 and D15 scans.

4. Discussion

In this study we evaluated the performance of ZEB1 HMLS to assess single-tree attributes in pure sweet chestnut stands cultivated for fruit production. Two different survey paths (D10 and D15 scans) for data collection were tested to investigate the influence of scan density on estimation accuracies and acquisition costs. Scanning every tree by walking around the stem avoided the occlusion effect and allowed us to obtain the reference data (D0 scan) for the assessment.

TP was assessed with high accuracy across all the study areas, with slightly better results provided by the D10 scan (Table 4). The RMSE was 0.09m for the D10 scan and 0.14m for the D15 scan and the bias was -0.001m for the D10 scan and -0.003m for the D15 scan. For TP, using the ZEB1 HMLS, Giannetti et al. (2018) obtained an RMSE of 0.09m and a bias of 0.021m.

The DBH assessment provided good results with both scan densities. The RMSE was 2.5cm and 2.9cm and the bias was -0.22cm and 0.14cm for the D10 and D15 scans, respectively. However, the D10 scan had a slightly lower RMSE% compared to the D15 scan (Table 5). These results are similar to those reported for ZEB1 HMLS by Ryding et al. (2015) (RMSE = 2.9cm and bias = 0.30cm), Bauwens et al. (2016) (RMSE = 1.11cm and bias = -0.08cm), Giannetti et al. (2018) (RMSE = 1.28cm and bias = -0.38cm) and Oveland et al., (2018)(RMSE=3.1cm and bias=0.3cm).

For TH, the RMSE and bias were 0.67m and 0.168m for the D10 scan, which had slightly better performances compared to the D15 scan (Table 5). Our results for TH are better than those reported by Giannetti et al. (2018) (RMSE = 2.15m and bias = -4.61m) who tested the ZEB1 HMLS in a Mediterranean multi-layered forest stand. In fact, it is known that the direct measure of tree heights by terrestrial laser scanner is limited by the laser range when the range is similar to tree heights and/or by point occlusion within the point cloud due to dense vegetation layers (Liang and Hyypa, 2013; Kankare, 2015). For ZEB1 HMLS, Bauwens et al. (2016) found that an important part of the laser does not penetrate15-20 m in height. However, in the case of multi-layered forest stands, better results for the estimation of TH by HMLS can be obtained by integrating terrestrial and airborne laser scanning data (Giannetti et al., 2018). In our case studies, tree heights (Figure 3) were slightly smaller than the laser range (15-20 m) and no dense vegetation layers were present.

CBH was estimated with an RMSE% higher than the one obtained for DBH and TH. However, the D10 scan was able to provide assessment slightly better than the D15 scan (Table 5), with an RMSE of 0.30m and a bias of -0.14m. The complexity in estimating the CBH is also reported by Giannetti et al. (2018) who obtained a bias of 1.67m, an RMSE of 1.91m and an RMSE% of 40% due to the difficulties of recognizing dead branches on the basis of the ZEB1 HMLS cloud.

The assessment of the number of trees was influenced by scan density more than the other single-tree attributes. The D10 scan was not able to detect 6 out 96 trees across all the three areas, with an omission difference of 6%. Similar results were obtained by Ryding et al. (2015) who report an omission difference of 9%. Using the D15 scan data set, 42 trees were undetected, with an omission error of 43%. Half of the undetected trees in the D10 scan had a DBH in the range between 6cm and 8cm. For the D15 scan, a large number of not detected trees had a DBH higher than 10cm (Figure 4).

Other studies report that in the case of stems with a DBH < 10cm the small size of the target resulted in fewer point returns, which hindered the tree detection process in the point cloud (Ryding et al., 2015). For the ZEB1 HMLS, the manufacturer reports that the laser range outdoors is 15-20m around the instrument. Our study shows that collecting data with ZEB1 HMLS with the user walking with the instrument along straight lines 15m distant from each other provides a point cloud unsuitable to obtaining satisfying results for tree detection. With this scan density, we were not able to model several large stems in the cloud due to the few points returns available. Occlusion effects might have influenced the results of the D15 scan.

Regarding the time needed to collect the ZEB1 HMLS data (Table 2), we were able to scan a plot of 2827m^2 with an average time of 13.6min (48min ha^{-1}) and 10.3min (38min ha^{-1}) for the D10 and D15 scans, respectively. In a previous study, conducted in the same three areas, using conventional manual measurement instruments (e.g., calliper and hypsometer), the same single-tree attributes were collected with an average survey time of 100min ha^{-1} (Bertini et al., 2009). The survey time reported by other authors (Ryding et al., 2015, Bauwens et al., 2016, Giannetti et al., 2018), who collected the ZEB1 HMLS data in more complex forest structures with respect to our study areas, are in the range between 130 and 200min ha^{-1}. Analyzing the pre-processing cost of the data and the total time needed to acquire and extract single tree parameters from each plot cloud, we found that following the D10 path there is an average decrease in cost of € 14 to pre-processing data and an average decrease of 37 minutes to acquire and derive single tree data (Table 2). From these results, we can affirm that the use of D10, which allows the acquisition of single trees data that are in line with D0 and previous studies (Ryding et al., 2015, Bauwens et al., 2016, Oveland et al., 2018; Giannetti et al., 2018), could be efficient in terms of balance between accuracy/cost and times. In fact, if we assume the collection of 30 field plots with a size of 1256 m^2, which is usual for forest management plans of 240 ha chestnut stands, using D0 we can estimate from the results obtained in this work (Table 2) approximately 125 hours of work (field work and elaboration of point clouds), while with D10 the time of work decrease to 106,5 hours. Moreover, we can estimate, also, a reducing of the cost of pre-processing from € 2580 to €2160 thanks to the reduction of walk path length (Giannetti et al., 2017). We must clarify that the structure of the sweet chestnut stands cultivated for fruit production, which are characterized by a relatively low tree density, large stems and without an understory layer, has simplified our study in terms of time needed to collect the data, while other studies conduct in complex forest stands underline how the workload necessary for point cloud

segmentation and single-tree attribute extraction requires much more time compared to our results (Giannetti et al., 2018).

5. Conclusions

HMLS systems have been recognized as promising tools to collect the 3D structure of a forest with potential practical application in forest inventory and forest monitoring. With HMLS, accurate information on tree position and DBH can be obtained with lower survey times than those required by static terrestrial laser scanners and conventional field measurements. However, the accuracy of the estimations based on HMLS is influenced by the survey path followed by the user during data acquisition and thus new solutions to optimize the walking scan line should be tested. To maximize efficiency, during the survey it is fundamental that the user understand which areas have already been scanned.

On the basis of the results obtained in our study, which was carried out with ZEB1 HMLS in sweet chestnut stands with simplified forest structures, we can conclude that:

- walking around each tree (D0 scan) improves the detection of the trees with small diameters (DBH<10cm), but this solution is not feasible in dense and complex forest structures and requires high acquisition times;
- walking up and down along straight lines drawn at a distance of 10m (D10) from each other provides sufficient data to assess single-tree attributes such as tree position, DBH, tree height and crown base with results similar to those obtained walking around each tree; this survey scheme is simple to put into practice and produced an omission error (6%) similar to that reported in other studies;
- survey schemes based on straight lines drawn at a distance higher than 10m from each other are not recommended; using 15m distance between the walking scan lines, more than 40% of the trees were undetected independent of the stem size.
- The D10 scan enables the right balance between time of acquisition and extraction of accurate results reducing the cost of pre-processing data.

These findings can help in planning future HMLS surveys. However, further studies are necessary to take into account other survey schemes and other types of HMLS systems in different forest structures.

References

Bertini R., Faini A. Montaghi A., Puletti N., Travaglini D. (2009) Metodologia per il censimento e la mappatura dei castagneti da frutto. In: III Congresso Nazionale di Selvicoltura, Taormina, Italy, 16-19 ottobre 2008, Accademia Italiana di Scienze Forestali, vol. Atti del III Congresso Nazionale di Selvicoltura per il miglioramento e la conservazione dei boschi italiani, 16-19 ottobre 2008 – Taormina (Messina), Volume 3. Accademia Italiana di Scienze Forestali, Firenze 2009, pp. 1455-1461, ISBN:9788887553161

Bauwens S., Bartholomeus H., Calders K., Lejeune P. (2016) Forest Inventory with Terrestrial LiDAR: A Comparison of Static and Hand-Held Mobile Laser Scanning. Forests, 7(6), 127; doi:10.3390/f7060127

Bosse M., Zlot R., Flick P. (2012) Zebedee: Design of a spring-mounted 3-d range sensor with application to mobile mapping. IEEE Trans. Robot, 28, 1104–1119.

Bottalico F., Travaglini D., Chirici G., Marchetti M., Marchi E., Nocentini S., Corona P. (2014) Classifying silvicultural systems (coppices vs. high forests) in mediterranean oak forests by airborne laser scanning data. Eur J Remote Sens 47:437–460. doi: 10.5721/EuJRS20144725

Bottalico F., Chirici G., Giannini R., Mele S., Mura M., Puxeddu M., McRoberts R., Valbuena R., Travaglini D. (2017) Modeling Mediterranean forest structure using airborne laser scanning data International Journal of Applied Earth Observation and Geoinformation Volume 57, doi: 10.1016/j.jag.2016.12.013

Brosofske K.D., Froese R.E., Falkowski M.J., Banskota A. (2014) A review of methods for mapping and prediction of inventory attributes for operational forest management. For. Sci. 60, 733–756. https://doi.org/10.5849/forsci.12-134

Corona P., Chirici G., McRoberts R.E., Winter S., Barbati A. (2011) Contribution of large-scale forest inventories to biodiversity assessment and monitoring. For. Ecol. Manage. 262, 2061–2069. https://doi.org/10.1016/j.foreco.2011.08.044

Dassot M., Constant T., Fournier M. (2011) The use of terrestrial LiDAR technology in forest science: Application fields, benefits and challenges. Ann. For. Sci. 2011, 68, 959–974

GEOSLAM (2017) User Manual. GeoSLAM Ltd

Giannetti F., Chirici G., Travaglini D., Bottalico F., Marchi E., Cambi M. (2017) Assessment of Soil Disturbance Caused by Forest Operations by Means of Portable Laser Scanner and Soil Physical Parameters. Soil Science Society of America Journal 1–23. doi: 10.2136/sssaj2017.02.0051

Giannetti F., Puletti N., Quatrini V., Travaglini D., Bottalico F., Corona P., Chirici G. (2018) Integrating terrestrial and airborne laser scanning for the assessment of single tree attributes in Mediterranean forest stands. European Journal of Remote Sensing 51, 795–807. doi:10.1080/22797254.2018.1482733

Forsman M., Holmgren J., Olofsson K. (2016) Tree Stem Diameter Estimation from Mobile Laser Scanning Using Line-Wise Intensity-Based Clustering. Forests, 7, 206.

Hackenberg J., Spiecker H., Calders K., Disney M., Raumonen P. (2015) SimpleTree – An efficient open source tool to build tree models from TLS Clouds. Forests, 6: 4245–4294. doi:10.3390/f6114245.

Hyyppä J., Kelle O., Lehikoinen M., Inkinen M. (2001) A segmentation-based method to retrieve stem volume estimates from 3-D tree height models produced by laser scanners. IEEE Trans. Geosci. Remote Sens. 39, 969–975.

Holopainena M., Kankarea V., Vastarantaa M., Liangb X., Linb Y., Vaajac M., Yub X. (2013) Tree mapping using airborne, terrestrial and mobile laser scanning – A case study in a heterogeneous urban forest. Urban Forestry & Urban Greening V. 12, Issue 4, pp546–553

Hopkinson C., Chasmer L., Young-Pow C., Treitz P. (2004) Assessing forest metrics with a ground-based scanning LiDAR. Canadian Journal of Remote Sensing, 34, 573–583

Kangas A., Astrup R., Breidenbach J., Fridman J., Gobakken T., Korhonen K.T., Maltamo M., Nilsson M., Nord-Larsen T., Næsset E., Olsson H. (2018) Remote sensing and forest inventories in Nordic countries – roadmap for the future. Scand. J. For. Res. 7581, 1–16. https://doi.org/10.1080/02827581.2017.1416666

Kankare V., Liang X., Vastaranta M., Yu X., Holopainen M., Hyyppä J. (2015) Diameter distribution estimation with laser scanning based multisource single tree inventory. ISPRS J.

Liang X, Hyyppä J. (2013) Automatic stem mapping by merging several terrestrial laser scans at the feature and decision levels. SensorS, 13, 1614–1634.

Liang X., Kukko A., Kaartinen H. (2014) Possibilities of a personal laser scanning system for forest mapping and ecosystem services. Sensors, vol. 14, pp. 1228–1248

Liang X., Kankare V., Hyyppä J., Wang Y., Kukko A., Haggrén H., Yu X., Kaartinen H., Jaakkola A., Guan F., Holopainen M., Vastaranta M. (2016) Terrestrial laser scanning in forest inventories. ISPRS Journal of Photogrammetry and Remote Sensing 115, 63–77. Doi:10.1016/j.isprsjprs.2016.01.006

Maas H. G., Bienert A., Scheller S., Keane E. (2008) Automatic forest inventory parameter determination from terrestrial laser scanner data. International Journal of Remote Sensing, 29, 1579–1593. doi:10.1080/ 01431160701736406

Miller J., Morgenroth J., Gomez C. (2015) 3D modelling of individual trees using a handheld camera: Accuracy of height, diameter and volume estimates. Urban For. Urban Green. 14, 932–940. https://doi.org/10.1016/j.ufug.2015.09.001

Mura M., McRoberts R., Chirici G., Marchetti M. (2015) Estimating and mapping forest structural diversity using airborne laser scanning data. Remote Sensing of Environment, 170: 133–142. doi:10.1016/j.rse.2015.09.016.

Mura M., McRoberts R.E., Chirici G., Marchetti M. (2016) Statistical inference for forest structural diversity indices using airborne laser scanning data and the k-Nearest Neighbors technique. Remote Sens. Environ., 186 (2016), pp. 678-686, 10.1016/j.rse.2016.09.010

Næsset E., Gobakken T., Holmgren J., Hyyppä H., Hyyppä J., Maltamo M., Nilsson M., Olsson H., Persson Å., Söderman U. (2004) Laser scanning of forest resources: the nordic experience. Scand. J. For. Res. 19, 482–499. https://doi.org/10.1080/02827580410019553

Oveland I., Hauglin M., Giannetti F., Kjørsvik N.S., Gobakken T. (2018) Comparing three different ground based laser scanning methods for tree stem detection. Remote Sens. 10. https://doi.org/10.3390/rs10040538

Rahlf J., Breidenbach J., Solberg S., Næsset E., Astrup R. (2014) Comparison of four types of 3D data for timber volume estimation. Remote Sens. Environ. 155, 325–333. https://doi.org/10.1016/j.rse.2014.08.036

Ryding J., Williams E., Smith M., Eichhorn M. (2015) Assessing handheld mobile laser scanners for forest surveys. Remote Sens. 7

Solberg S., Naesset E., Bollandsas O. M. (2006) Single Tree Segmentation Using Airborne Laser Scanner Data in a Structurally Heterogeneous Spruce Forest. Photogramm. Eng. Remote Sens. 72, 1369–1378. https://doi.org/0099-1112/06/7212–1369

Talbot B., Pierzchała M., Astrup R. (2016) Applications of Remote and Proximal Sensing for Improved Precision in Forest Operations 327–336.

Thies M., Pfeifer N., Winterhalder D., Gorte B. G. H. (2004) Three-dimensional reconstruction of stems for assessment of taper, sweep, and lean based on laser scanning of standing trees. Scandinavian Journal of Forest Research, 19, 571–581. doi:10.1080/ 02827580410019562

Tomppo E., Olsson H., Ståhl G., Nilsson M., Hagner O., Katila M. (2008) Combining national forest

inventory field plots and remote sensing data for forest databases. Remote Sens. Environ. 112, 1982–1999. https://doi.org/10.1016/j.rse.2007.03.032

Wulder M. A., Bater C. W., Coops N. C., Hilker T., White J. (2008) The role of LiDAR in sustainable forest management. For. Chron. 84, 807–826.

Yang B., Dai W., Dong Z., Liu Y. (2016) Automatic Forest Mapping at Individual Tree Levels from Terrestrial Laser Scanning Point Clouds with a Hierarchical Minimum Cut Method. Remote Sens. 8, 372.

Zlot R., Bosse M., Greenop K., Jarzab Z., Juckes E., Roberts J. (2014) Efficiently capturing large, complex cultural heritage sites with a handheld mobile 3D laser mapping system. Journal of Cultural Heritage, 15(6), 670–678.

4. Other publication and contributions

4.1 Papers

1. **Del Perugia B.**, Gonzalez Aracil S., Herries D. (2018) Optimal acquisition specifications for the Riegl VUX-1LR over a Pinus radiata plantation - Optimising remotely acquired, dense point cloud data for plantation inventory. (PNC377-1516). Final Report for Forest & Wood Products Australia.
2. **Del Perugia B.,** Travaglini D., Bottalico F., Nocentini S., Rossi P., Salbitano F., Sanesi G. (2017) Are Italian stone pine forests (Pinus pinea L.) an endangered coastal landscape? A case study in Tuscany (Central Italy). L' ITALIA FORESTALE E MONTANA, vol. 72, pp. 103-121, ISSN:2036-3494
3. D'Amico G., **Del Perugia B.,** Chirici G., Giannetti F., Travaglini D. (2018) Caratterizzazione delle pinete litoranee di pino domestico della toscana con dati telerilevati a supporto della gestione forestale sostenibile. ATTI DEL SIMPOSIO IL MONITORAGGIO COSTIERO MEDITERRANEO: PROBLEMATICHE E TECNICHE DI MISURA (Livorno - Giugno 2018)
4. Chirici G., Bottalico F., Giannetti F., Rossi F., **Del Perugia B.**, Travaglini D., Nocentini S., Kutchartt E, Marchi E., Foderi C., Fioravanti F., Fattorini L., Guariglia A., Ciancio O., Bottai L., E. McRoberts R., Næsset E., Corona P., Gozzini B. (2017) Assessing forest windthrow damage using single-date, post-event airborne laser scanning data. Forestry: An International Journal of Forest Research. https://doi.org/10.1093/forestry/cpx029
5. Chirici, G., Bottalico, F., Giannetti, F., Rossi, P., **Del Perugia, B.**, Travaglini, D., Nocentini S., Kutchartt E, Marchi E., Foderi C., Fioravanti F., Fattorini L., Guariglia A., Ciancio O., Bottai L., E. McRoberts R., Næsset E., Corona P., Gozzini B. (2016) Stima dei danni da vento ai soprassuoli forestali in Regione Toscana a seguito dell'evento del 5 marzo 2015. L Italia Forestale e Montana 71(4):197-213 DOI: http://10.4129/ifm.2016.4.02
6. Härkönen, S., Neumann, M., Mues, V., Berninger, F., Bronisz, K., Cardellini, G., Chirici, G., Hasenauer, H., Koehl, M., Lang, M., Merganicova, K., Mohren, F., Moiseyev, A., Moreno, A., Mura, M., Muys, B., Olschofsky, K., **Del Perugia, B.**, Rørstad, P.K., Solberg, B., Thivolle-Cazat A., Trotsiuk, V., Mäkelä, A. (2014) Alternative forest management strategies (Project no. 311970)

Final Report for FORMIT (FORest management strategies to enhance the MITigation potential of European forests).

7. Härkönen, S., Neumann, M., Mues, V., Berninger, F., Bronisz, K., Cardellini, G., Chirici, G., Hasenauer, H., Koehl, M., Lang, M., Merganicova, K., Mohren, F., Moiseyev, A., Moreno, A., Mura, M., Muys, B., Olschofsky, K., **Del Perugia, B**., Rørstad, P.K., Solberg, B., Thivolle-Cazat A., Trotsiuk, V., Mäkelä, A. (2018) Climate-sensitive forest growth simulator for assessing impacts of forest management in Europe. Environmental Modelling and Software.

4.2 Conference talks and seminars

1. **Del Perugia B**., Travaglini D., Barbati A., Barzagli A., Giannetti F., Lasserre B., Nocentini S., Santopuoli, G., Chirici G. (2018) "*Classification of dominant forest tree species by multi-source very high spatial resolution remote sensing data*". In: ForestSAT 2018 (2-5 October 2018 College Park, MD USA.)
2. Krisanski S., **Del Perugia B**., Sadegh Taskhiria M., Turnera P. (2018) Below Canopy UAS Photogrammetry for Stem Measurement in a Radiata Pine Plantation. SPIE Remote Sensing conference in Berlin (10-13 September, 2018).
3. **Del Perugia B**., Travaglini D., Barbati A., Barzagli A., Giannetti F., Lasserre B., Nocentini S., Santopuoli, G., Chirici G. (2018) "*Classification of dominant forest tree species by multi-source very high spatial resolution remote sensing data*". In: AIT2018 ITALIAN SOCIETY OF REMOTE SENSING IX CONFERENCE. Florence (Italy, 4-6 July 2018. Abstract-book URL: https://aitonline.org/2018/07/10/download-the-abstract-book/)
4. **Del Perugia B.**, Herries D., Gonzalez S. (2018) "*Optimising Remotely Acquired, Dense Point Cloud Data".* In: GCFF Phenotyping Workshop - SCION. Rotorua (New Zealand - April 2018).
5. **Del Perugia B**., Travaglini D., Barbati A., Barzagli A., Giannetti F., Lasserre B., Nocentini S., Santopuoli, G., Chirici G. (2017) "*Classificazione delle specie forestali con dati multispettrali e laser scanning multipiattaforma".* In: Proceedings of the XI SISEF National Congress "La Foresta che Cambia: qualità della vita e opportunità in un paese che cambia" (Fares S, Alivernini, A, Ferrara C, Marchi M, Sallustio L, Chianucci F, Bucci G, eds). Rome (Italy, 10-13 Sept 2017. Abstract-book URL: http://www.sisef.it/sisef/xi-congresso/)

6. Travaglini D., Corona P., **Del Perugia B.**, Giannetti F., Chirici G. (2017). "Rilievi inventariali con laser scanner terrestre mobile: un confronto con rilievi classici in castagneti da frutto". In: Proceedings of the XI SISEF National Congress "La Foresta che Cambia: qualità della vita e opportunità in un paese che cambia" (Fares S, Alivernini, A, Ferrara C, Marchi M, Sallustio L, Chianucci F, Bucci G, eds). Rome (Italy, 10-13 Sept 2017. Abstract-book URL: http://www.sisef.it/sisef/xi-congresso/)
7. Giuliarelli D., Barbati A., **Del Perugia B.**, Ferrari B., Giannetti F., Lasserre B., Mattioli W., Oreti L., Santopuoli G., Tomao A., Travaglini D., Chirici G. (2017) "Mappatura degli European Forest Types da drone e applicazioni per la stima di indicatori di biodiversità forestale". In: Proceedings of the XI SISEF National Congress "La Foresta che Cambia: qualità della vita e opportunità in un paese che cambia" (Fares S, Alivernini, A, Ferrara C, Marchi M, Sallustio L, Chianucci F, Bucci G, eds). Rome (Italy, 10-13 Sept 2017. Abstract-book URL: http://www.sisef.it/sisef/xi-congresso/)
8. Travaglini D., Barbati A., Barzagli A., **Del Perugia B.**, Giannetti F., Giuliarelli D., Lasserre B., Marchetti M., Santopuoli G., Tomao A., Chirici G. (2017) Integrazione di dati inventariali e dati telerilevati con sistemi a pilotaggio remoto per la stima di indicatori della gestione forestale sostenibile. XIV ATTI CONVEGNO AISSA, Campobasso, 16-17 Febbraio 2017
9. Travaglini D., Chirici G., **Del Perugia B.**, Giannetti F., Bottai L., Gozzini B., Corona P. (2017) Metodologia per il rilievo dei castagneti da frutto IGP. Giornata di studio: metodologie innovative per l'aggiornamento dell'inventario castanicolo nazionale. Accademia dei Georgofili, Firenze, 6 Febbraio, 2017
10. **Del Perugia B**. (2017) Comparison of two remote sensing techniques (aerial and terrestrial) with traditional field-based method for forest inventory - Phd Day 8
11. **Del Perugia B.,** Aglietti C. (2017) Management and valorization of an historical chestnut forest for use as an urban park - Phd Day 8

Acknowledgements

First of all, I would like to thank my PhD supervisors and co-authors Prof. Davide Travaglini and Prof. Gherardo Chirici for their support and guidance and Prof. Susanna Nocentini coordinator of the PhD program. The works included in this thesis are the result of their support with financial and intellectual resources.

I would like to thanks Martin Isenburg and Anahita Khosravipour for helping me with my internship in New Zealand.

A special thanks to Interpine Group who hosted me for six months and provided useful knowledge about remote sensing and LiDAR analysis. Your advice and experience have been very helpful for me to realize what I can do and want do. I truly appreciate the opportunity to work on the FWPA project.
Thanks to Mike and Kaye, George and Polly, you are an amazing family; Elizabeth and Bruce for the good time in New Zealand and Australia; David, Sarah and Peter for welcoming me in the remote sensing team, it has been a pleasure to work with you; all the amazing person of Interpine, I had a great time.
Thanks to Susana, my tutor and friend, it has been invaluable to work with you and to learn many new things.

Thank you to all my co-authors and collegues at GEOLAB for their help in guiding me in the complex work of writing papers and understand the world of research.

Thanks to the reviewers of this thesis for their valuable comments.

Last but not the least, thanks to my friends: the ones met in the other emispher and the ones I know from a longer time... I would not have achieved this goal without you!